Doctoral Dissertations   Student Scholarship

Fall 2007

Modeling secondary organic aerosol formation from biogenic hydrocarbons

Jianjun Chen
University of New Hampshire, Durham

Follow this and additional works at: https://scholars.unh.edu/dissertation

MODELING SECONDARY ORGANIC AEROSOL FORMATION
FROM BIOGENIC HYDROCARBONS

BY

JIANJUN CHEN

Baccalaureate Degree, Tsinghua University, 2001
Master's Degree, North Carolina State University, 2003

DISSERTATION

Submitted to the University of New Hampshire
in Partial Fulfillment of
the Requirements for the Degree of

Doctor of Philosophy
in
Earth and Environmental Science

September, 2007

UMI Number: 3277136

INFORMATION TO USERS

The quality of this reproduction is dependent upon the quality of the copy submitted. Broken or indistinct print, colored or poor quality illustrations and photographs, print bleed-through, substandard margins, and improper alignment can adversely affect reproduction.

In the unlikely event that the author did not send a complete manuscript and there are missing pages, these will be noted. Also, if unauthorized copyright material had to be removed, a note will indicate the deletion.
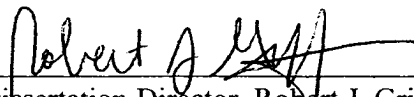
UMI®

UMI Microform 3277136

Copyright 2007 by ProQuest Information and Learning Company.

All rights reserved. This microform edition is protected against unauthorized copying under Title 17, United States Code.
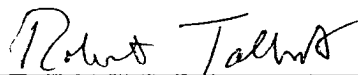
ProQuest Information and Learning Company
300 North Zeeb Road
P.O. Box 1346
Ann Arbor, MI 48106-1346

This dissertation has been examined and approved.
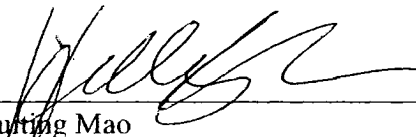
Dissertation Director, Robert J. Griffin,
Assistant Professor of Atmospheric
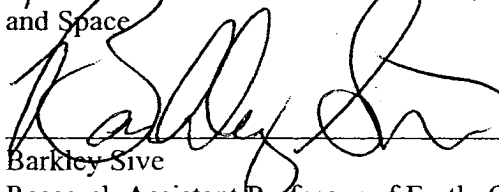Chemistry and Earth Science and Earth,
Oceans, and Space

Robert W. Talbot
Research Professor of Earth Sciences and Earth,
Oceans, and Space

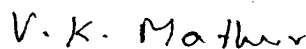Huiting Mao
Research Assistant Professor of Earth, Oceans,
and Space

Barkley Sive
Research Assistant Professor of Earth, Oceans,
and Space

V. K. Mathur
Virendra K. Mathur
Professor of Chemical/Environmental
Engineering

18 JULY 2007
Date

ACKNOWLEDGEMENTS

First, I want to thank my advisor, Dr. Robert Griffin for his guidance, support, and encouragement throughout the past four years. I feel extremely fortunate to pursue my Ph.D. under his guidance. I also want to thank my committee members: Dr. Robert Talbot, Dr. Huiting Mao, Dr. Barkley Sive, and Dr. Virendra Mathur for their guidance and valuable time. I owe special thanks to Mr. Tod Hagan for his tremendous help on computers, to Dr. Huiting Mao for providing three-dimensional air quality model inputs, and to Dr. Adrian Sandu at Virginia Polytechnic Institute and State University for making KPP software available. Thanks are also due to members of the AIRMAP program, who come from different disciplines and have unique expertise. I have learned a lot from them. Finally, I thank my families for their love and support.

iii

TABLE OF CONTENTS

iv

LIST OF TABLES

vii

LIST OF FIGURES

x

ABSTRACT

MODELING SECONDARY ORGANIC AEROSOL FORMATION
FROM BIOGENIC HYDROCARBONS

by

Jianjun Chen

University of New Hampshire, September, 2007

Secondary organic aerosol (SOA) is formed generally by the oxidation of gas-phase volatile organic compounds (VOCs) to form semi- or non-volatile products that then undergo gas to particle partitioning. In this work, the Caltech Atmospheric Chemistry Mechanism (CACM) and the Model to Predict the Multi-phase Partitioning of Organics (MPMPO) were updated with detailed chemistry associated with three monoterpene species — α-pinene, β-pinene, and d-limonene. The updated CACM and MPMPO modules were calibrated by ozone formation and SOA yield data for α-pinene, β-pinene, and d-limonene from chamber experiments. Then, the updated CACM and MPMPO were incorporated into the Community Multi-scale Air Quality Model v4.4 (CMAQ). CMAQ with the updated CACM and MPMPO was applied to the eastern United States (US) for August 3-4, 2004. It was found that SOA formation for this domain was dominated by monoterpenes. CMAQ with CACM and MPMPO predicted similar SOA formation when compared to CMAQ with the CB-IV gas-phase mechanism and the SORGAM SOA module. However, responses of SOA predictions at Thompson Farm, New Hampshire to domain NO_x emissions changes and temperature variations are different for CACM/MPMPO and CB-IV/SORGAM.

In addition, an aqueous-phase chemistry mechanism (AqChem) was developed to study the potential of SOA formation via irreversible cloud processing of organic compounds. AqChem considers irreversible organic reactions that lead mainly to the formation of carboxylic acids, which are usually less volatile than the corresponding aldehydes. AqChem was incorporated into CMAQ with CACM/MPMPO and applied to the eastern US for August 3-4, 2004. The CMAQ simulation indicates that the maximum contribution of SOA formation from irreversible reactions of organics in clouds is 0.28 $\mu g/m^3$ for 24-hour average concentrations and 0.60 $\mu g/m^3$ for one-hour average concentrations at certain locations. On average, domain-wide surface SOA predictions over the episode are increased by 8.6% when irreversible, in-cloud processing of organics is considered. For our modeling domain and episode, the increase of SOA predictions is due to the cloud processing of oxidation products from monoterpenes, while contribution from irreversible cloud processing of isoprene oxidation products is negligible.

CHAPTER I

INTRODUCTION

Motivation of the Thesis

Atmospheric particulate matter (PM) is associated with adverse human health effects, impaired visibility, and global climate change. Epidemiological studies show that elevated PM concentrations are linked with increased morbidity and mortality (Pope and Dockery, 2006). The United States (US) Environmental Protection Agency (EPA) has established air quality standards for 24-hour and annual average $PM_{2.5}$ (PM of aerodynamic diameter smaller than 2.5 micron) concentrations and 24-hour average PM_{10} (PM of aerodynamic diameter smaller than 10 micron) concentrations to protect human exposure to PM (40 CFR part 50). Atmospheric aerosols directly influence climate by affecting incoming solar radiation and outgoing thermal-infrared radiation through scattering and absorption of solar radiation (Charlson et al., 1992; Jacobson, 2001). Atmospheric aerosols indirectly affect climate by affecting the radiative properties, amount, and lifetime of clouds (Jones et al., 1994).

Atmospheric PM is composed of a variety of chemical species. The major chemical species are inorganic salts (e.g., sulfate, nitrate, and ammonium), siliceous crustal minerals, elemental carbon (EC), and organic aerosol (OA) (Seinfeld and Pankow, 2003). Among them, OA typically constitutes 20-60% of $PM_{2.5}$ by mass depending on location and time (Chow et al., 1994; NARSTO, 2004). OA consists of primary OA

1

(POA) and secondary OA (SOA). POA is emitted directly from emission sources (e.g, fossil fuel burning and biomass burning) (Liousse et al., 1996; Bond, et al., 2004). SOA is formed in the atmosphere from the oxidation of volatile organic compounds (VOCs) (Seinfeld and Pankow, 2003). The relative abundance of POA and SOA varies with location and time. Modeling studies have demonstrated that under certain circumstances, SOA constitutes a substantial fraction of OA (Kanakidou et al., 2000; Griffin et al., 2002a; Pun et al., 2003; Cabada et al., 2004; Yu et al., 2004).

Over the past decade, substantial work has been devoted to elucidation of SOA formation mechanisms in the atmosphere. Despite the fact that significant progress has been made, our knowledge on SOA formation is still far from being complete (Kanakidou et al., 2005).

Three-dimensional air quality models, which combine the representation of various processes governing the properties of PM in the atmosphere, have been developed and widely used for both research and regulatory purposes (Seigneur, 2001). Because of the complexity of SOA formation processes and the limited understanding of these processes, treatment of SOA formation is one of the most uncertain parts of current state-of-the-art three-dimensional PM models (Seigneur, 2001; Pun et al., 2003; NARSTO, 2004). The motivation of this thesis is to update and improve representation of SOA formation in three-dimensional air quality models applied to the eastern US.

Background on SOA Formation Mechanisms

SOA is formed when gas-phase VOCs are oxidized in the atmosphere to form higher polarity and lower volatility products which then partition to the aerosol phase (Seinfeld and Pankow, 2003). Over the last decade, much work has been devoted to

2

elucidate the gas-phase oxidation mechanisms of VOCs and the partitioning mechanism for semi-volatile organics.

VOCs are oxidized by various species in the atmosphere (e.g., hydroxyl radical (OH), ozone (O_3), and the nitrate radical (NO_3)). The oxidation processes typically lead to formation of semi-volatile organics, which typically exhibit lower vapor pressure and higher solubility because of the presence of functional groups. For the purpose of studying SOA formation, the investigation of oxidation of VOCs has been focused on the chemical identification and quantification of semi-volatile organics and elucidation of their mechanistic formation pathways. Because of the importance of SOA formation from monoterpenes, oxidation of monoterpenes (e.g., α-pinene) in the atmosphere has received substantial attention. For example, studies concerning the oxidation of α-pinene include reaction with OH (Arey et al., 1990; Hakola et al., 1994; Hallquist et al, 1997; Jaoui and Kamens, 2001; Winterhalter et al., 2003), reaction with NO_3 (Hallquist et al, 1997; Wangberg et al., 1997), and reaction with O_3 (Hakola et al, 1994; Kamens et al., 1999; Yu et al, 1999; Koch et al., 2000; Winterhalter et al., 2003). The reactions of α-pinene with OH, NO_3, and O_3 lead to the formation of a large number of semi-volatile organics, examples of which include aldehydes, oxo-aldehydes, carboxylic acids, oxy-carboxylic acids, hydroxy-carboxylic acids, dicarboxylic acids, and organic nitrates (Kanakidou et al., 2005). Mechanisms have been proposed for formation pathways of these products (Kamens et al, 1999; Winterhalter et al., 2003; Jenkin, 2004).

SOA is formed from the partitioning of semi-volatile organics (SVOCs) between gas and aerosol phases or full partitioning of non-volatile organics. The mostly widely accepted theory describing the partitioning of SVOCs is that proposed by Pankow (1994).

3

This theory states that SOA formation results from the absorption of semi-volatile organics into existing particle-phase organic material in a manner analogous to Henry's law. In an SOA system assumed to be free of any particle-phase water, a temperature-dependent partitioning coefficient, $K_{om,i}$ (m^3 μg^{-1}), for compound i is represented by (Pankow, 1994; Pankow et al., 2001)

$$K_{om,i} = \frac{A_i}{G_i M_o} = \frac{RT}{MW_{om} 10^6 \gamma_i p_{L,i}^o} \tag{1}$$

where A_i (μg m^{-3}) and G_i (μg m^{-3}) are the aerosol- and gas-phase concentrations of compound i, respectively, M_o (μg m^{-3}) is the total aerosol-phase organic mass concentration (including POA, if present), R is the ideal gas constant (8.206×10^{-5} m^3 atm mol^{-1} K^{-1}), T is temperature (K), MW_{om} is the average molecular weight of the organic phase (g mol^{-1}), γ_i is the activity coefficient of compound i, and $p_{L,i}^o$ is the sub-cooled liquid vapor pressure (atm) of compound i at temperature T. In this theory, the partitioning of organics is controlled mainly by vapor pressure, interaction with other organics (through activity coefficient), the total amount of organic material (M_o), and the temperature. The theory of Pankow (1994) has been used successfully to model SOA formation from various hydrocarbons in laboratory chambers (e.g., Kamens et al., 1999; Kamens et al., 2001).

A long standing puzzle surrounding the SOA formation mechanism is that many semi-volatile species partition to the aerosol phase to an extent beyond that determined by their vapor pressure according to Equation (1) (Kanakidou et al., 2005). Recent experiments revealed oligomer and/or polymer formation in the aerosol phase (Jang et al., 2002; Kalberer et al., 2004). Small molecules are oligomerized and/or polymerized in the aerosol phase to form larger and less volatile species. Although the exact mechanism for

4

oligomer and/or polymer formation in the aerosol phase remains to be determined, the oligomer and/or polymer formation processes partially solve the puzzle described above (Kanakidou et al., 2005).

An additional potential SOA formation pathway is through the cloud processing of organic compounds. Atmospheric organic species can dissolve into cloud and fog droplets. The dissolved species can undergo chemical transformations in the aqueous phase, which potentially leads to the formation of products that have lower vapor pressure. The less volatile products from the aqueous-phase processing may stay in the particle phase after evaporation of the cloud and fog droplets, leading to the addition of secondary particle mass to pre-existing particles. This process can lead to SOA formation (Blando and Turpin, 2000; Kanakidou et al., 2005). Recent atmospheric measurements and modeling studies have suggested the potential of SOA formation from this pathway (Blando et al., 1998; Yao et al., 2002; Warneck, 2003; Ervens et al., 2004; Lim et al., 2005).

Approaches

Two approaches have been used primarily for modeling SOA formation in the atmosphere. One is based on the empirical two-product model (Odum et al., 1996), which assumes that there are two hypothetical products formed from the oxidation of the parent VOCs and that these two hypothetical products partition to the aerosol phase by the absorption process. The parameters in two-product model are derived from chamber studies (Odum et al., 1996; Odum et al., 1997; Griffin et al., 1999). The second is a mechanistic approach. It simulates the probable semi-volatile products formed in the gas- phase oxidation process in contrast to the hypothetical products used in the two-

5

product model (Kamens et al., 1999; 2001; Griffin et al., 2002b; Jenkin, 2004). The SOA modeling approach used in this thesis is a mechanistic approach and is mainly based on the Caltech Atmospheric Chemistry Mechanism (CACM, Griffin et al., 2002b) and the Model to Predict the Multiphase Partitioning of Organics (MPMPO, Griffin et al., 2003).

CACM is a gas-phase chemistry mechanism. The main purpose of CACM is to predict the formation of semi-volatile organics and O_3 from the oxidation of parent VOCs (Griffin et al., 2002b). In CACM, the oxidation mechanism of VOCs is determined mainly based on relevant findings from laboratory experiments and the protocol regarding gas-phase oxidation of VOCs in the atmosphere established by Jenkin et al. (1997). In addition, the oxidation mechanism in CACM is described in moderate detail so that it remains computationally reasonable for three-dimensional simulations.

MPMPO simulates the thermodynamic equilibrium between gas and aerosol phases for semi-volatile organics predicted from CACM. MPMPO assumes that there are two phases in aerosols, an aqueous phase consisting of water and inorganic and organic species and an organic phase consisting of POA and SOA species (Griffin et al., 2003). The equilibrium between the gas and aqueous phases is governed by Henry's law, while the equilibrium between the gas and organic phases is based on Equation (1).

The host three-dimensional air quality model used in this thesis is the Community Multiscale Air Quality (CMAQ) model. CMAQ is a state-of-the-science three-dimensional air quality model developed by the US EPA (Dennis, et al., 1996; Byun and Ching, 1999). It simulates the processes, which include mainly emissions, dry and wet depositions, advection, diffusion, gas-phase chemistry, aqueous-phase chemistry, and secondary aerosol formation, which govern the spatial and temporal distributions for gas-

6

phase and aerosol-phase chemical species. CMAQ has been used widely in the US and internationally for both research and regulatory purposes (EPA, 2005; Mao et al., 2006; Morris et al., 2006; Streets et al., 2007).

In order to calibrate and evaluate the performance of the models in the thesis, a wide range of measurement data were obtained from various sources. Chamber experimental data were obtained from Hoffman et al. (1997), Griffin et al. (1999a), and Hallquist et al. (1999). Field experimental data are mainly from the AIRMAP Program (Talbot et al., 2005), EPA Air Quality System, the Southeastern Aerosol Research Characterization Study (SEARCH) (Hansen et al., 2003), and the Interagency Monitoring of Protected Visual Environments (IMPROVE) (Malm et al., 1994).

Outline of the Thesis

The thesis is organized in five chapters, with the first being this introduction.

Chapter II: **Modeling secondary organic aerosol formation from oxidation of α-pinene, β-pinene, and d-limonene.** This work involves updating CACM with explicit gas-phase oxidation mechanisms for α-pinene, β-pinene, and d-limonene. The gas-phase chemistry mechanism of these three species was linked to an absorption code to simulate SOA formation from these three species for experiments conducted in laboratory chambers. Simulated SOA yields for a series of experiments were compared with observed values. Results are described in Chen and Griffin (2005).

Chapter III: **Application of the CACM and MPMPO modules using the CMAQ model for the eastern United States.** This work involves incorporation of the updated CACM and MPMPO code from Chapter 2 into the CMAQ model. This version of CMAQ was applied to the eastern US for an episode in August 2004. Ozone and

7

$PM_{2.5}$ chemical components from model output were compared extensively with measured data from various sources. Special focus was placed on SOA prediction from the model. Results are described in Chen et al. (2006).

Chapter IV: **Modeling secondary organic aerosol formation through cloud processing of organic compounds**. This work evaluates the potential of SOA formation from the aqueous-phase chemistry of organic compounds in clouds. An aqueous-phase chemistry mechanism that describes the irreversible reactions of organic compounds with OH to form less volatile products was developed. The aqueous-phase chemistry mechanism was linked to CACM and MPMPO and incorporated into the CMAQ model. The new model was applied to the same August 2004 episode studied in Chapter 3 to determine the potential for SOA formation due to the proposed aqueous-phase chemistry in clouds. This work is described in Chen et al. (2007).

Chapter V: **Conclusions and future research**. This section summarizes the conclusions from the thesis and points out future research that is needed to better simulate SOA formation in the atmosphere.

CHAPTER II

MODELING SECONDARY ORGANIC AEROSOL FORMATION FROM OXIDATION OF A-PINENE, B-PINENE, AND D-LIMONENE

Abstract

The biogenic species α-pinene, β-pinene, and d-limonene are among the most abundant monoterpenes emitted globally. They are also important precursors to secondary organic aerosol (SOA) formation in the atmosphere. This study involves the development of proposed oxidation mechanisms for these three species. Semi- and non-volatile oxidation products with the potential to lead to SOA formation are predicted explicitly. Simulation code that describes the gas-phase oxidation mechanisms including reactions that lead to ozone (O_3) formation is coupled to an equilibrium absorptive partitioning code. The coupled model is used to simulate both gas-phase chemistry and SOA formation associated with oxidation of these three species in chamber experiments involving single as well as multiple oxidants. For the partitioning model, required molecular properties of the oxidation products are taken from the literature or estimated based on structural characteristics. The predicted O_3 and SOA concentrations are typically within ±50% of the reported measured values for most of the experiments except for the experiments with low initial hydrocarbon concentrations and the nitrate radical experiments with α-pinene. The developed model will be used to update a gas-phase chemical mechanism and a SOA formation module used in a three-dimensional air

9

quality model.

Introduction

Biogenic hydrocarbons play important roles in tropospheric ozone (O_3) production (Chameides et al., 1988) as well as secondary organic aerosol (SOA) formation (Hoffman et al., 1997; Griffin et al., 1999a; Griffin et al., 1999b). α-Pinene, with an endocyclic double bond, and β-pinene, with an exocyclic double bond, are the most representative and abundant monoterpenes emitted in North America (Guenther et al., 2000). d-Limonene is the most abundant monoterpene which has both an endocyclic and an exocyclic double bond (Guenther et al., 2000).

A mechanistic approach has been developed recently to model atmospheric SOA formation (Griffin et al., 2002; Pun et al., 2002; Griffin et al., 2003). The approach features a detailed gas-phase chemistry model (Caltech Atmospheric Chemistry Mechanism or CACM) to predict explicitly potential semi-volatile organic compounds (SVOCs) and an aerosol module (Model to Predict Multi-phase Partitioning of Organics or MPMPO) to simulate the gas/aerosol partitioning of SVOCs. The mechanistic approach for modeling SOA generated in laboratory chamber experiments has been demonstrated successfully (Barthelmie and Pryor, 1999; Kamens et al., 1999; Kamens et al., 2001; Colville and Griffin, 2004a; Colville and Griffin, 2004b; Jenkin, 2004). The primary purposes of this study are to develop detailed gas-phase oxidation mechanisms for α-pinene, β-pinene, and d-limonene under the framework of CACM and to simulate SOA formation in laboratory chambers by linking the gas-phase oxidation mechanism to an equilibrium absorptive model.

10

Gas-phase Oxidation Mechanism Development

α-Pinene, β-pinene, and d-limonene react with hydroxyl radicals (OH), O_3, nitrate radicals (NO_3), and oxygen atoms (O) in the atmosphere (Atkinson, 1997). Numerous experimental studies have been conducted to elucidate the kinetic and mechanistic parameters for the oxidations of these three species (Atkinson, 1997 and references therein; Atkinson and Arey, 2003 and references therein). The oxidation mechanisms proposed here for these three species are developed based on the organic degradation protocol established by Jenkin et al. (1997) and recently reported experimental results concerning the degradation of these three species and formation pathways for important SVOCs (Jenkin et al., 2000; Winterhalter et al., 2000). The host gas-phase chemistry model is CACM, which includes close to 200 species and over 360 reactions. CACM has been incorporated into three-dimensional air quality models and applied successfully to various areas (Griffin et al., 2002; Pun et al., 2003).

In developing the oxidation mechanisms for the monoterpenes discussed here, a number of simplifications are made in order to reduce the number of reactions and species that need to be considered. This is done with the goal of minimizing computational demand when these mechanisms are used in a three-dimensional atmospheric model. In most cases, only the dominant position is considered for attack of OH on hydrocarbons. Organic peroxy radical (RO_2) cross permutations and self reactions are treated by considering the reaction with an operator term, RO_2T, which is the sum of all organic peroxy radicals (Griffin et al., 2002). Reactions among the peroxy radicals potentially form multifunctional carbonyls. When the formed carbonyls are believed to be SVOCs, they are represented explicitly. Otherwise, it is assumed that the

11

products of an RO_2 + RO_2T reaction are the same as those of RO_2 + nitric oxide (NO) that are not alkyl nitrates. Criteria for whether or not a species is a SVOC include: 1) that it has at least 10 carbons and two functional groups; 2) that it has at least six carbon atoms and two functional groups, one of which is an acid; and 3) that it is trifunctional (Griffin et al., 2002). It is assumed that the RO_2 + hydroperoxy radical (HO_2) reaction forms carboxylic acid only in the case that RO_2 is an acyl radical (Griffin et al., 2002). Organic peroxides are not explicitly treated. Instead, when RO_2 is not an acyl radical, RO_2 + HO_2 reactions are assumed to form the same carbonyl products as RO_2 + NO reactions plus either an -OOH1 or -OOH2 operator, which is similar to the treatment of the SAPRC mechanism (Carter, 1990). The choice of -OOH1 or -OOH2 depends on whether a HO_2 radical is generated in the RO_2 + NO reaction. If HO_2 is formed in the RO_2 + NO reaction, -OOH1 is used; otherwise, -OOH2 is used. -OOH1 and -OOH2 are allowed to react as a hydroperoxide does. Upon photolysis, -OOH1 releases OH and HO_2, while -OOH2 releases OH. -OOH1 reacts with OH with one pathway forming H_2O and HO_2 and another reforming OH, while the -OOH2 operator reacts with OH with one pathway forming H_2O and another reforming OH.

In the following sections, detailed oxidation mechanisms for α-pinene, β-pinene, and d-limonene are described. These oxidation mechanisms are an intermediate approach between the non-specific SAPRC mechanism (Carter, 1990) and the fully explicit Master Chemical Mechanism (MCM, http://chmlin9.leeds.ac.uk/MCMframe.html). Such an approach allows for SOA prediction based on the chemical nature of secondary SVOCs while simultaneously limiting computational demand when the mechanism is associated with a three-dimensional atmospheric model.

12

Oxidation Mechanism for α-Pinene

A total of 50 reactions are used to represent the oxidation mechanism for α-pinene. They are shown in Table A.1 of the Appendix. Species involved in the oxidation mechanism are described in more detail in Table A.2 of the Appendix.

OH addition to the double bond of α-pinene forms a β-hydroxy peroxy radical, RO_2101. (See the Appendix for notation.) Upon reaction of RO_2101 with NO, it is assumed that 20% forms hydroxy nitrate, 60% forms pinonaldehyde, and the remaining 20% forms formaldehyde (HCHO) and another product that is lumped to the CACM long-chain ketone group. The yields for hydroxy nitrate, pinonaldehyde, and HCHO are in general agreement with the findings of Noziere et al. (1999). Pinonaldehyde undergoes photolysis and reactions with OH and NO_3. Upon photolysis, pinonaldehyde forms CO, HO_2, and RO_2103, a peroxy radical that reacts with NO to form norpinonaldehyde. Absorption cross sections for pinonaldehyde are assigned to be the same as other aldehydes in CACM. Based on Noziere and Barnes (1999), 80% of OH attack on pinonaldehyde occurs on the aldehydic H-atom, such that an acyl peroxy radical (RO_2106) is formed. Upon reaction with NO, RO_2106 decomposes to form RO_2103. By reacting with HO_2, RO_2106 also forms pinonic acid, a SVOC which has been identified in the aerosol phase (Yu, et al., 1998; Kamens et al., 2001). The remaining OH attack occurs on other positions to form peroxy radicals that are lumped to a single α-carbonyl peroxy radical, RO_2104, which further decomposes to the acetyl peroxy radical (RO_28) treated in CACM, and another peroxy radical, RO_2108, further reaction of which leads to formation of the CACM long-chain ketone. Reaction of pinonaldehyde with NO_3 is assumed to proceed via abstraction of the aldehydic H-atom, leading to the acyl radical

13

RO_2106. The reactions of norpinonaldehyde are treated similarly to those of pinonaldehyde.

The O_3 oxidation chemistry for α-pinene is adapted from Jenkin et al. (2000). Upon reaction of α-pinene with O_3, pinonaldehyde, pinonic acid, RO_2103, RO_2104, and RO_2105 are formed. RO_2105, a C_{10} α-carbonyl peroxy radical, is of particular importance. Jenkin et al. (2000) propose an H-atom isomerization mechanism so that reaction of RO_2105 with RO_2T partly leads to 10-hydroxy-pinonic acid. RO_2105 also decomposes to RO_2109, a C_9 acyl peroxy radical. Upon reaction with RO_2T, RO_2109 also forms pinic acid through 1,7 H-atom isomerization (Jenkin et al., 2000). These hydroxy-pinonic acid and pinic acid formation processes are parameterized empirically without complete treatment of intermediate radicals. Another pinic acid formation pathway involving intramolecular rearrangement of perpinalic acid (product of RO_2109 + HO_2) is also incorporated based on Winterhalter et al. (2000). Overall, the O_3 scheme ensures that pinonic acid, 10-hydroxy-pinonic acid, pinic acid, and pinalic-3 acid, which are found in significant amounts in the SOA formed in α-pinene ozonolysis experiments (Kamens et al., 1999; Yu et al., 1999), are produced and that their yields are comparable to measured values from Yu et al. (1999).

The reaction of NO_3 with α-pinene involves addition of NO_3 into the double bond (65% adds to the less-substituted carbon and 35% to the other carbon, based on Jenkin et al. (1997)), forming a β-nitrato peroxy radical, RO_2102. Upon reaction with NO, 60% of RO_2102 forms pinonaldehyde, 17.5% leads to formation of keto-nitrate, and the remainder forms HCHO and another product lumped to the CACM long-chain ketone group. Organic nitrate yields in dark experiments with NO_3 have been determined to be

14

about 14–20% (Wangberg et al. 1997; Hallquist et al., 1999). In this work, it is assumed that 13.5% hydroxy-nitrate and 7% keto-nitrate are formed upon reaction of RO_2102 with RO_2T. The O/α-pinene reaction is assumed to form an epoxide and a ketone that is lumped to nopinone, which is described in the β-pinene oxidation mechanism below. No further reaction is considered for epoxide.

Oxidation Mechanism for β-Pinene

A total of 16 reactions are used for the β-pinene oxidation mechanism; they are shown in Table A.3 of the Appendix. Descriptions of species involved in the mechanism are given in more detail in Table A.4 of the Appendix.

OH reacts with β-pinene by adding to the double bond, leading to a β-hydroxy peroxy radical, RO_2201. Upon reaction of RO_2201 with NO, a portion forms organic nitrate, while the remainder undergoes decomposition to form nopinone and HCHO. The stoichiometric coefficient for organic nitrate is determined using the formula of Arey et al. (2001). Nopinone is assumed only to react with OH. Photolysis of nopinone is not included because photolysis of ketones is usually considered of minor importance for large molecules (Seinfeld and Pandis, 1998). Reaction of nopinone with OH involves H-atom abstraction, leading to a peroxy radical, assumed to be 3-peroxy nopinone, RO_2203. Upon reaction with NO, RO_2203 breaks down to RO_2109, an acyl peroxy radical treated in the α-pinene oxidation mechanism.

The chemistry scheme for β-pinene and O_3 is adapted from the work of Winterhalter et al. (2000). Upon reaction of β-pinene with O_3, 16% leads to nopinone and a C_1 Criegee intermediate (C1_CI), while the remaining 84% forms HCHO and a C_9 Criegee intermediate (C9_CI). The C1_CI further forms formic acid (HCOOH), CO, and

15

H₂O. Part of C9_CI (33% of the reacted β-pinene) follows a hydroperoxide channel to form RO_2203 and OH, and another portion (16% of the reacted β-pinene) proceeds by the ester channel to form CO_2 and a product lumped to the CACM long-chain alkane group. The remaining C9_CI stabilizes and forms nopinone and H_2O_2 if it reacts with H_2O. Under ambient conditions, Winterhalter et al. (2000) suggest that reaction with H_2O is the dominant pathway for the stabilized C9_CI. However, in chamber experiments, other reactions for stabilized C9_CI could be as important. For example, Bonn et al. (2002) propose that secondary organic ozonides formed by combination of stabilized C9_CI with nopinone act as nucleating agents during β-pinene ozonolysis experiments. Kinetic data for the reaction between stabilized Criegee intermediates and ketones are generally not available. For the model presented here, incorporation of reactions of the stabilized C9_CI with HCHO, HCOOH, NO, and NO_2 is found to have only minor effect on O_3 and SOA modeling. Thus, only reaction with H_2O is considered for C9_CI. The O_3 chemistry of β-pinene ensures that pinic acid and pinalic-3-acid, which are the major carboxylic acids observed in the SOA of β-pinene ozonolysis experiments (Yu et al., 1999), are produced.

Dark experiments in which β-pinene is oxidized by NO_3 have been found to generate significant SOA (Griffin et al., 1999a; Hallquist et al., 1999). NO_3 adds to the double bond of β-pinene, forming β-nitrato peroxy radical RO_2202 (80% of nitrate adds to the less substituted carbon, based on Jenkin et al. (1997)). Upon reaction with NO, RO_2202 leads to formation of nopinone, dinitrate, and carbonyl nitrate. Conversely, the reaction of RO_2202 with RO_2T forms nopinone, dinitrate, hydroxy nitrate, and carbonyl nitrate. The yields of carbonyl and hydroxy nitrate are determined based on the protocol

16

of Jenkin et al. (1997), while the yield of dinitrate is assigned so that reaction between RO_2202 and RO_2T leads to a yield of organic nitrates of approximately 70%, which is close to that measured by Hallquist et al. (1999) for the β-pinene reaction with NO_3. Although the protocol of Jenkin et al. (1997) does not call for the formation of dinitrate for reaction of β-nitrato peroxy radical with NO, it has been incorporated here to model SOA formation, as in Barthelmie and Pryor (1999). The O/β-pinene reaction leads to formation of epoxide and a second carbonyl product lumped to nopinone. No further reactions are considered for epoxide.

Oxidation Mechanism for d-Limonene

Experimental studies aimed at elucidating the oxidation mechanism for d-limonene are less numerous compared to α-pinene and β-pinene. However, studies have been performed to quantify the yield of specific compounds (Hakola et al., 1994; Hallquist el al., 1999; Larsen et al., 2001). A total of 84 reactions are considered for d-limonene; these are shown in Table A.5 of the Appendix. Species involved in the mechanism are described in more detail in Table A.6 of the Appendix.

d-Limonene features both an endocyclic and an exocyclic double bond. 60% of OH addition is assumed to occur on the endocyclic double bond to form a β-hydroxy peroxy radical, RO_2301, with the remaining 40% assumed to occur on the exocyclic bond to form a different β-hydroxy peroxy radical, RO_2302. The ratio for oxidation probability of 3 to 2 is assumed based on the yield of limonaldehyde and limona ketone formed in d-limonene/OH experiments, which were found to be 0.3 and 0.2, respectively, by Hakola et al. (1994). Upon reaction with NO, RO_2301 leads to organic nitrate and limonaldehyde, and RO_2302 leads to organic nitrate and limona ketone. Organic nitrate

17

yields are determined based on Arey et al. (2001). Limonaldehyde, which contains an aldehydic group and a double bond, undergoes photolysis and reaction with OH, O_3, and NO_3. Reaction of limonaldehyde with OH and NO_3 is assumed to proceed completely by addition to the double bond to form RO_2310 and RO_2311, respectively. Further reaction of RO_2310 and RO_2311 forms primarily keto-limonaldehyde. Further treatment of detailed reactions for keto-limonaldehyde would result in significant expansion of the oxidation mechanism. For the purpose of modeling SOA, keto-limononic acid and O_3 are formed directly upon reaction of keto-limonaldehyde with OH, omitting other intermediate processes, similar to the treatment used in Griffin et al. (2002) for second or third generation aldehyde products. Reaction of limonaldehyde with O_3 is based on the protocol of Jenkin et al. (1997). Limona ketone, which contains a ketone group and an exocyclic double bond, is assumed to undergo photolysis and reaction with OH, O_3, NO_3 and O. The treatment of these processes is similar to the treatment of the chemistry of the parent species and is not discussed further.

Reaction between d-limonene and O_3 proceeds with 60% addition to the endocyclic double bond and 40% addition to the exocyclic double bond to form ozonides, with these fractions also based on the work of Hakola et al. (1994). Further treatment of the formed ozonides is based on the protocol of Jenkin et al. (1997). Detailed descriptions are not given. However, a peroxy radical that merits special attention is RO_2306. RO_2306 is a C_{10} α-carbonyl peroxy radical similar to RO_2105 in the α-pinene oxidation mechanism. Adopting the chemistry of RO_2105 to RO_2306 enables the production of 7-hydroxy-limononic acid, limonalic acid, and limonic acid, which have been identified in the aerosol phase of d-limonene/OH and d-limonene/O_3 experiments

18

(Glasius et al., 2000; Larsen et al., 2001). A similar treatment is used for RO$_2$317, formed in the limona ketone reaction with O$_3$, which enables the formation of 7-hydroxy keto-limonic acid, keto-limonalic acid, and keto-limonic acid, which are SVOCs found in the aerosol resulting from d-limonene reaction with O$_3$ (Glasius et al., 2000). Reactions of d-limonene with NO$_3$ and O are based on the protocol of Jenkin et al. (1997) and are not further described.

Equilibrium Absorptive Model

It has been demonstrated that an equilibrium absorptive mechanism is able to describe the gas/particle partitioning of SVOCs during the formation of SOA (Pankow, 1994a; Pankow, 1994b; Odum et al., 1996; Hoffman et al., 1997; Griffin et al., 1999a; Kamens et al., 1999; Kamens et al., 2001; Pankow et al., 2001). In a SOA system assumed to be free of any particle-phase water, a temperature-dependent partitioning coefficient, $K_{om,i}$ (m^3 µg^{-1}), for compound i is represented by (Pankow, 1994a; Pankow et al., 2001)

$$K_{om,i} = \frac{A_i}{G_i M_o} = \frac{RT}{MW_{om} 10^6 \gamma_i p_{L,i}^o} \tag{1}$$

where A_i (µg m^{-3}) and G_i (µg m^{-3}) are the aerosol- and gas-phase concentrations of compound i, respectively, M_o (µg m^{-3}) is the total aerosol-phase organic mass concentration (including primary organic aerosol, or POA, if present), R is the ideal gas constant (8.206 × 10^{-5} m^3 atm mol^{-1} K^{-1}), T is temperature (K), MW_{om} is the average molecular weight of the organic phase (g mol^{-1}), γ_i is the activity coefficient of compound i, and $p^o_{L,i}$ is the sub-cooled liquid vapor pressure (atm) of compound i at the temperature T. For the chamber experiments simulated in this study, no POA is present. Therefore,

19

$$M_o = \sum_{i=1}^{N} A_i \qquad (2)$$

where N is the total number of the organic components partitioning between the gas and aerosol phases. If C_i ($\mu g\ m^{-3}$) is defined as the total concentration of compound i, by a mass balance

$$C_i = G_i + A_i \qquad (3)$$

Combining Equations (1) to (3), M_o can be found by solving (Colville and Griffin, 2004b)

$$\sum_{i=1}^{N} \frac{K_{om,i} C_i}{1 + K_{om,i} M_o} - 1 = 0 \qquad (4)$$

Given the temperature and the total concentration of each partitioning compound predicted using the gas-phase model, the calculation of SOA is performed as follows: initial values for γ_i and MW_{om} are assumed, $K_{om,i}$ values are calculated by Equation (1), and Equation (4) is solved for M_o. Once M_o is determined, the value of A_i of each compound is calculated according to

$$A_i = \frac{K_{om,i} M_o C_i}{1 + K_{om,i} M_o} \qquad (5)$$

Equation (5) is derived by simple manipulation of Equations (1) and (3). Based on the calculated value of A_i and the known T, the values of the γ_i and MW_{om} are updated. This process is repeated until γ_i and MW_{om} converge. If γ_i is assumed to be one for all organic compounds, it is only necessary to iterate on MW_{om}.

The chamber experiments to be simulated in this study are typically conducted under low humidity. Therefore, it is assumed that the SOA formed in these experiments is purely organic. Water potentially affects SOA formation by shifting the organic mixture to an aqueous-inorganic-organic mixture because of the inorganic seed used.

20

Furthermore, the activity coefficients are assumed to be one for all compounds in this study. It has been confirmed that such an assumption is reasonable for many compounds making up the SOA mixture in chamber situations (Seinfeld et al., 2001). These assumptions substantially simplify the modeling of SOA for the experiments to be simulated.

The remaining parameter to be estimated is the sub-cooled liquid vapor pressure. The sub-cooled liquid vapor pressures of many organic compounds involved in SOA formation are not known. In this study, the group contribution method of Cordes and Rarey (2002) is used to estimate the boiling point of the organics, and the method proposed by Myrdal and Yalkowsky (1997) is used to calculate the sub-cooled liquid vapor pressure. However, the estimated values are typically adjusted by a factor of 0.001, while the temperature dependence of vapor pressure is retained. A similar method was employed by Colville and Griffin (2004b). Jenkin (2004) also applied a uniform adjustment factor of 120 for partitioning coefficients that are based on the estimated vapor pressures. Such a corrective approach is limited in use because of its uncertainty, but it is probably necessary at this time given the fact that heterogeneous and particle-phase reactions are not fully understood and therefore not considered completely in current SOA models. By doing this, the adjusted vapor pressures better match literature values if such values are available, or partitioning coefficients calculated according to Equation (1) are in closer agreement with those measured. For example, the adjusted vapor pressure for cis-pinic acid is 6.10×10^{-7} Torr at 298K. The upper limit for vapor pressures of C_9 carboxylic acids has been derived experimentally to be on the order of 10^{-8} Torr (Koch et al., 2000). The estimated vapor pressure for pinonaldehyde is

21

1.35×10^{-1} Torr at 308K. The partitioning coefficient based on the estimated vapor pressure is much lower than the one measured in O_3-initiated oxidation experiments (Yu et al., 1999). Thus, the vapor pressure for pinonaldehyde is adjusted so that the partitioning coefficient for pinonaldehyde is 0.0008 ($m^3 \mu g^{-1}$) at 308K, which is at the low end of the range measured by Yu et al. (1999).

Results

Gas-phase Chemistry

The developed oxidation mechanisms for α-pinene, β-pinene, and d-limonene are evaluated by simulating gas species profiles for chamber experiments. Unfortunately, detailed gas-species profiles are available only for photooxidation experiments of β-pinene and d-limonene from Griffin et al. (1999a). Detailed comparisons are thus made only for these species. Initial conditions for these experiments are included in Table II.1. However, only specific cases will be discussed below. For α-pinene, qualitative evaluations are made for two experiments modeled by Saunders et al. (2003). The simulated gas-species profiles are qualitatively comparable to the observed patterns.

During photooxidation experiments, temperature and solar intensity typically vary with time. However, a constant temperature and UV factor are used for the simulations. The average temperature during the individual experiment usually is used. In certain cases, the lowest temperature during the course of the experiments is used in order to model SOA more accurately. The UV factor is adjusted from 0.0 to 1.0 to minimize the differences between measured and simulated mixing ratios of NO and O_3. A UV factor of 1.0 represents clear sky at the top of the boundary layer at noon during the summer time in Los Angeles. For β-pinene photooxidation experiments, the simulated O_3 values

22

Table II.1. Summary of initial conditions for all experiments simulated.

	α-pinene					β-pinene					d-limonene			
						Photooxidation experiments								
expr.	avg. temp.	HC	NO_X	Ref	expr.	avg. temp.	HC	NO/NO_2	Ref	expr.	avg. temp.	HC	NO/NO_2	Ref
09/22/95a	318.7	94.5	135	1	07/15/97a	313.6	33.7	49.2/62.5	2	08/19/95a	319.2	159.0	134[*]	1
09/22/95b	318.7	87.4	125	1	07/15/97b	313.6	62.2	87.0/79.7	2	08/21/95b	317.2	95.0	205[*]	1
09/25/95a	315.2	95.5	124	1	07/17/97a	316.2	42.0	15.6/43.4	2	08/25/95a	317.7	89.2	174[*]	1
09/25/95b	315.2	94.6	122	1	07/21/97a	313.5	85.5	93.7/63.6	2	08/17/97a	309.4	49.5	75.7/64.4	2
8/14/95a	-	136.0	240	1	07/21/97b	313.5	96.5	93.0/67.0	2	08/17/97b	309.4	65.1	73.6/65.8	2
8/14/95b	-	144.0	240	1	07/27/97a	313.3	45.0	53.1/58.6	2	08/26/97a	312.7	35.2	17.4/62.8	2
9/15/95b	320.2	53.0	206	1	08/15/97a	308.8	32.3	81.4/53.4	2	08/26/97b	312.7	20.6	43.1/61.8	2
8/17/95a	312.2	72.0	203	1	08/19/97a	312.0	79.0	88.8/64.8	2					
8/17/95b	312.2	19.5	113	1	10/06/95b	312.2	95.0	204	1					
						Ozone experiments								
expr.	avg. temp.	HC	O_3	Ref	expr.	avg. temp.	HC	O_3	Ref	expr.	avg. temp.	HC	O_3	Ref
06/05/98a	309.9	16.7	67	2	06/11/98a	306.9	57.6	230	2					
06/05/98b	309.9	18.2	73	2	06/11/98b	306.9	80.1	320	2					
06/07/98a	303.3	31.0	124	2	06/13/98b	308.4	35.2	140	2					
06/07/98b	303.3	45.5	182	2										
06/09/98a	308.0	57.0	228	2										
06/09/98b	308.0	65.0	260	2										
						Nitrate experiments								
expr.	avg. temp.	HC	N_2O_5	Ref	expr.	avg. temp.	HC	N_2O_5	Ref	expr.	avg. temp.	HC	N_2O_5	Ref
	293.2	420	278	3	05/13/98b	302.0	96.4	123	2		286.2	18	10.2	3
	288.2	140	99	3	06/01/98a	309.0	18.8	55	2					
					06/01/98b	309.0	54.7	99	2					

Temperature in K, initial mixing ratios in ppb. Ref.: 1. Hoffman et al. (1997); 2. Griffin et al. (1999a); 3. Hallquist et al. (1999). If one value is given for NO/NO_2, it represents total NO_X with a desired initial NO/NO_2 ratio of 2 to 1.

23
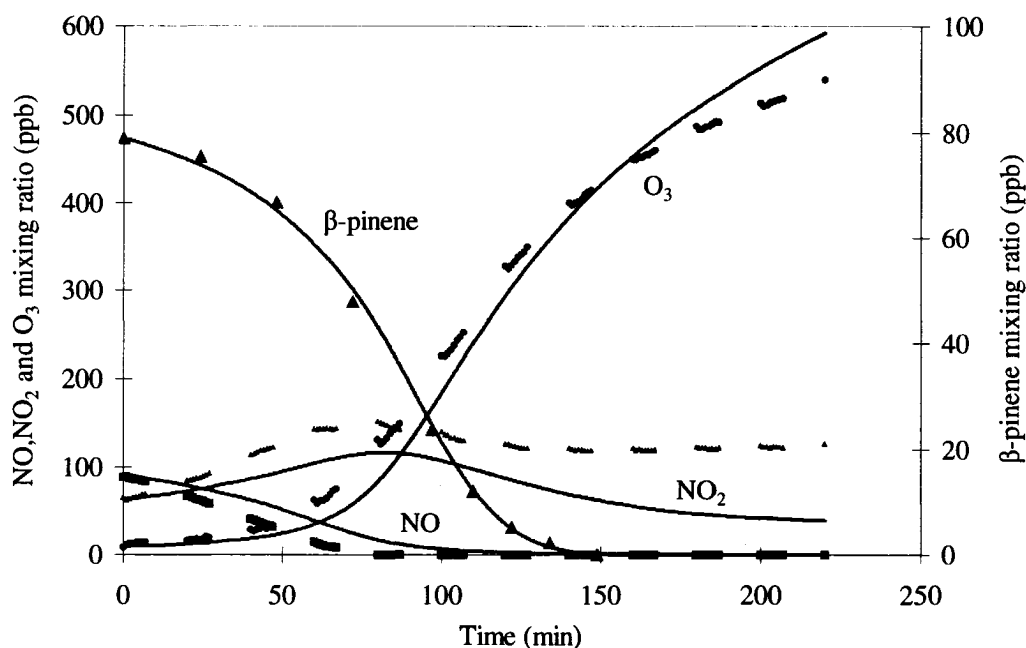
Figure II.1. Observed (points) and predicted (lines) mixing ratios of NO, NO_2, O_3, and β-pinene for photooxidation experiment 8/19/97a from Griffin et al. (1999a). Experimentally measured NO_2 is NO_y – NO.

are typically within ±50% of the measured values. For d-limonene, the simulated O_3 values are within ±30% of the measured values. Figure II.1 shows the simulated and measured NO, NO_2, O_3, and β-pinene profiles during the photooxidation experiment 08/19/97a. For this experiment, the simulated O_3 values are within ±30% of the measured values. The simulated NO, NO_2, and β-pinene mixing ratios adequately follow the trends of the measured ones. Figure II.2 shows the simulated and measured profiles for d-limonene photooxidation experiment 08/17/97a. The simulated values are typically within ±20% of the measured values, except for NO_2. The measured NO_2 is likely to be closer to the difference between total active nitrogen (NO_y) and NO because peroxyacyl nitrate and other nitrogen containing compounds interfere with the measurement.

24
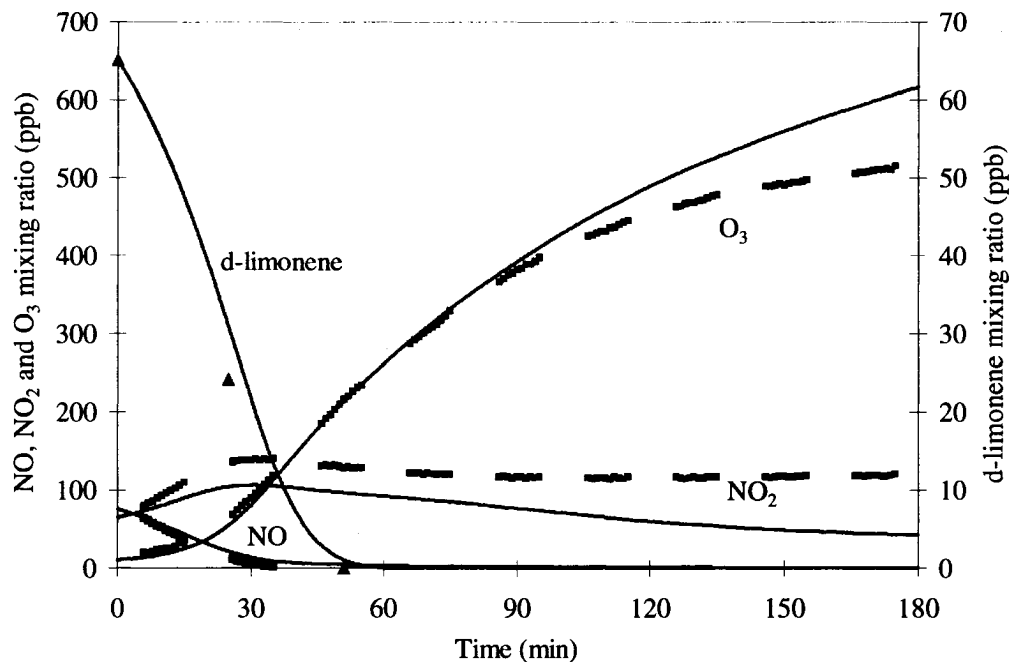
Figure II.2. Observed (points) and predicted (lines) mixing ratios of NO, NO_2, O_3, and d-limonene for photooxidation experiment 8/17/97a from Griffin et al. (1999a). Experimentally measured NO_2 is NO_y – NO.

SOA Modeling for α-Pinene

A total of seventeen separate chamber experiments with α-pinene as the parent hydrocarbon are simulated using the mechanism and partitioning module described previously. These include nine photooxidation experiments, six O_3 experiments, and two NO_3 experiments. Initial conditions for these experiments are summarized in Table II.1.

Figure II.3 shows the comparison of observed and predicted SOA concentration for the experiments simulated. These concentrations represent those at the end of both a simulation and the corresponding experiment. The ranges of predicted SOA are also shown if the partitioning coefficients of all compounds are adjusted by ±20%. Nitrate experiments are simulated with a vapor pressure for pinonaldehyde that is different from

25
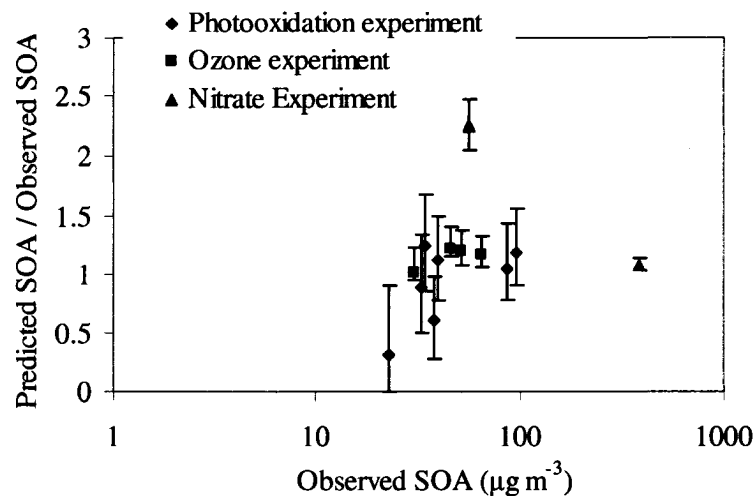
Figure II.3. Comparison between final observed and model predicted SOA concentrations for a series of α-pinene experiments (photooxidation experiments from Hoffman et al. (1997); O_3 experiments from Griffin et al. (1999a); NO_3 experiments from Hallquist et al. (1999)). The nitrate experiments were modeled using a different assumption about the vapor pressure of pinonaldehyde than the other experiments. See text for detailed discussions. The range of the predicted SOA/observed SOA is assessed by adjusting the partitioning coefficients of all partitioning compounds by ±20%.

that used in the simulation of photooxidation and O_3 experiments as discussed subsequently. Results of four cases (photooxidation experiments 08/17/95b and 09/15/95b and O_3 experiments 06/05/98a and 06/05/98b, for which the final measured SOA concentration is less than 10 μg m^{-3}) are not shown in Figure II.3 because no SOA is predicted to form in the model. Observed and predicted SOA concentrations are typically within ±50% for most experiments. The model underpredicts SOA formation when the initial α-pinene concentration, and hence the final observed SOA formation, is low. A potential explanation is ignorance of other processes that may lead to formation of SOA, such as association reactions of aldehydes (e.g., pinonaldehyde) with stabilized Criegee biradicals produced in the O_3 reaction to form very low vapor pressure secondary ozonides (Kamens et al., 1999, 2001) or dimer formation by pinic acid (Hoffman et al.,

26
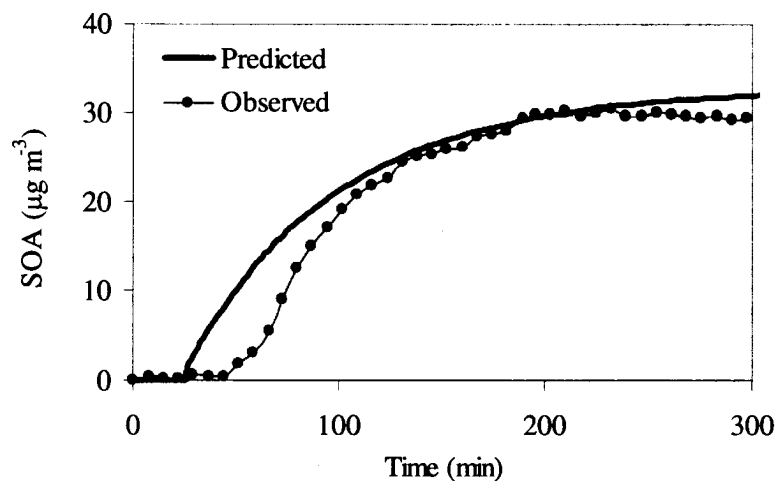
Figure II.4. Observed and predicted SOA concentration as a function of time for experiment 06/07/97a (α-pinene + O₃) from Griffin et al. (1999a).

1998; Kamens et al., 1999, 2001). However, for the model presented here, adding these processes with kinetic data from Kamens et al. (1999, 2001) yielded only minor improvement. Expanding dimer formation by pinic acid, Jenkin (2004) introduced an "acid chaperone" mechanism involving dimer formation among bi- and multifunctional acid species. This approach was not tested.

For several O₃ experiments, data on the temporal evolution of SOA over the course of the experiment are also available, enabling a direct comparison of simulated and measured SOA temporal profiles. Figure II.4 shows measured and simulated SOA mass concentration during the O₃ experiment 06/07/97a. The final predicted SOA concentration is within 10% of the measured one. Generally, the evolution of SOA over time is characterized adequately, although the predicted onset of SOA formation occurs earlier than that observed, which is most likely due to uncertainties associated with gas-phase mechanistic parameters as well as gas/aerosol partitioning coefficients.

27

Table II.2. Partitioning coefficients for major predicted semi-volatile α-pinene oxidation products.

Term	Description	Partitioning coefficients ($m^3 \mu g^{-1}$) at 308K*	Partitioning coefficients ($m^3 \mu g^{-1}$) from Yu et al. (1999)**
PINA	pinonaldehyde	0.00079	0.0012
NRPA	norpinonaldehyde	0.00064	0.0019
RP101	pinalic-3-acid	0.028	0.013
RP102	1-hydroxy-pinonaldehyde	0.0013	0.019
RP103	10-hydroxy-pinonaldehyde	0.0042	0.019
UR101	pinonic acid	0.045	0.028
UR102	norpinonic acid	0.019	0.013
UR104	pinic acid	0.056	0.028
UR105	10-hydroxy-pinonic acid	0.078	0.040
UR106	1-hydroxy-pinonic acid	0.046	0.040
AP101	2-nitrato-3-hydroxy-pinane	0.0031	-
AP102	2-nitrato-3-oxo-pinane	0.0030	-
PAN101	peroxy 2,2-dimethyl-3-acetyl-cyclobutyl acetyl nitrate	0.0031	-
PAN102	peroxy 2,2-dimethyl-3-acetyl-cyclobutyl formyl nitrate	0.0026	-
PAN103	peroxy 2,2-dimethyl-3-formylmethyl-cyclobutyl formyl nitrate	0.0035	-

*Because MW_{om} varies among photooxidation experiments, ozone experiments, and nitrate experiments, the partitioning coefficients here for illustrative purposes are calculated based on a MW_{om} of 180 g mol^{-1}.

** Based on three ozonolysis experiments conducted at 306-308K.

Table II.2 shows the partitioning coefficients at 308K for predicted major SVOCs involved in the simulation of SOA for α-pinene experiments. For comparison, experimentally determined partitioning coefficients for a number of compounds from Yu et al. (1999) are also shown. For illustrative purposes, these partitioning coefficients are calculated for a MW_{om} of 180 g mol^{-1}. Partitioning coefficients for carboxylic acids (e.g., pinic acid) and aldehydes (e.g., pinonaldehyde) are generally comparable to those measured by Yu et al. (1999) at 308K, while partitioning coefficients for organic nitrates (e.g., 2-hydroxy-3-nitrato-pinane) are of the same order of magnitude as those used in the

28

model of Barthelmie and Pryor (1999) at 313K. To assess the effect of uncertainties in partitioning coefficients on SOA predictions, sensitivity analysis was performed by adjusting the partitioning coefficients of all species by ±20%. As shown in Figure II.3, the magnitudes of predicted SOA variations differ by each individual experiment. On average, the predicted SOA vary by ±35%, indicating strong dependence of predicted SOA on partitioning coefficients. In general, simulation of α-pinene photooxidation experiments depends more strongly on partitioning coefficients than does simulation of O_3 and NO_3 experiments.

With these partitioning coefficients, final SOA concentrations are overpredicted for NO_3 experiments by more than a factor of five compared to those observed. SOA contributions from pinonaldehyde are especially high. The parameterization of gas-phase nitrate chemistry for α-pinene leads to production of approximately 79% pinonaldehyde, 14% 2-hydroxy-3-nitrato-pinane, and 7% 2-nitrato-3-oxo-pinane. Wangberg et al. (1997) identified approximately 80% of the products of the α-pinene/NO_3 reaction and measured the formation yield for pinonaldehyde, 2-hydroxy-3-nitrato-pinane, and 2-nitrato-3-oxo-pinane to be 62%, 5%, and 3%, respectively. Total alkyl nitrate yield was measured to be approximately 14%. Hallquist et al. (1999) reported an approximate 70% yield of pinonaldehyde and an approximate 20% yield of organic nitrates for the α-pinene reaction with NO_3. Because of the qualitative agreement between observations and the gas-phase mechanism, it is believed that the gas-phase chemistry parameterization is not the cause of such high over prediction of SOA. As seen in Table II.2, based on an adjusted vapor pressure, the partitioning coefficient for pinonaldehyde is 0.0008 $m^3 \mu g^{-1}$ at 308K, in accord with measured values in O_3 experiments. This partitioning coefficient

29

requires an adjustment factor of 0.001 for the estimated vapor pressure of pinonaldehyde. If the adjustment factor of 0.001 for the estimated vapor pressure of pinonaldehyde is not used, reasonable predictions of SOA formation for the two NO_3 experiments are achieved, as shown in Figure II.3. Indeed, the vapor pressure of pinonaldehyde was measured to be approximately 5.1 Pa at 298K (Hallquist et al., 1997). The estimated vapor pressure for pinonaldehyde without using the adjustment factor is 7.8 Pa at the same temperature. Other processes, such as particle-phase reactions (Jang et al., 2002; Ziemann, 2002; Kalberer et al., 2004), potentially cause the partitioning coefficient of pinonaldehyde in O_3 experiments to be much higher than that based on absorptive theory. Thus, different vapor pressures for pinonaldehyde are used under O_3 experiments (An adjustment of 0.001 is applied to the estimated vapor pressure.) and NO_3 experiments. (No adjustment factor is used for the estimated vapor pressure.) This discrepancy potentially indicates that heterogeneous or particle-phase reactions leading to SOA formation may not be as significant in NO_3 experiments as they are in O_3 experiments, as organic acids, such as pinonic acid and pinic acid, have been determined experimentally to be important components of SOA formed in O_3 experiments. These species are not predicted to be important in the NO_3 system. When modeling photooxidation experiments, the adjustment factor is used; contributions of pinonaldehyde to SOA typically are minor in photooxidation simulations.

In terms of SOA composition, pinonic acid, norpinonic acid, pinic acid, and hydroxy-pinonic acid, together with nitrogen containing organics (peroxyacyl nitrogen, and hydroxyl- or keto- nitrates) are the main constituents during photooxidation experiments. During O_3 experiments, pinonic acid, pinalic-3 acid, pinic acid, and

30

hydroxy-pinonic acid are major SOA components, with smaller contributions from pinonaldehyde, hydroxy-pinonaldehyde, and norpinonaldehyde. During NO_3 experiments, SOA is predicted to be comprised almost exclusively of nitrogen-containing organics. Many of the predicted SOA constituents have been identified experimentally in the SOA formed from α-pinene oxidation (Hallquist et al., 1999; Kamens et al., 1999; Yu et al., 1999; Kamens et al., 2001).

SOA Modeling for β-Pinene

Simulations of experiments with β-pinene include nine photooxidation experiments, three O_3 experiments, and three NO_3 experiments. Initial conditions for these experiments are summarized in Table II.1.

Figure II.5 shows the final observed and predicted SOA mass concentration for the fifteen experiments simulated, as well as the ranges of predicted SOA if the partitioning coefficients for all compounds are adjusted by ±20%. Observed SOA concentrations range from around 10 μg m^{-3} to approximately 500 μg m^{-3}, except for in one O_3 experiment that will be discussed below. Predicted SOA concentrations are typically within ±30% of the observed SOA concentrations. Figure II.6 shows the temporal profiles of observed and predicted SOA formation for photooxidation experiment 10/06/95b from Hoffman et al. (1997). Although the final SOA formation is under predicted by approximately 20%, the evolution of SOA formation is well simulated. The SOA composition for this experiment is predicted to be composed mainly of dinitrates, hydroxy nitrate, and peroxyacyl nitrate, with a smaller contribution from nopinone and pinic acid, which is similar to the modeling results of Barthelmie and Pryor (1999).

31
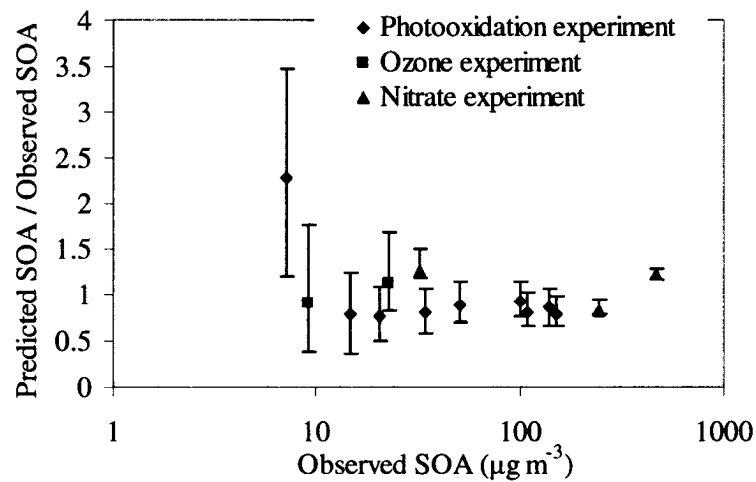
Figure II.5. Comparison between final observed and model predicted SOA concentrations for a series of β-pinene experiments (photooxidation experiments from Hoffman et al. (1997) and Griffin et al. (1999a); O_3 and NO_3 experiments from Griffin et al. (1999a)). The range of the predicted SOA/observed SOA is assessed by adjusting the partitioning coefficients of all partitioning compounds by ±20%.
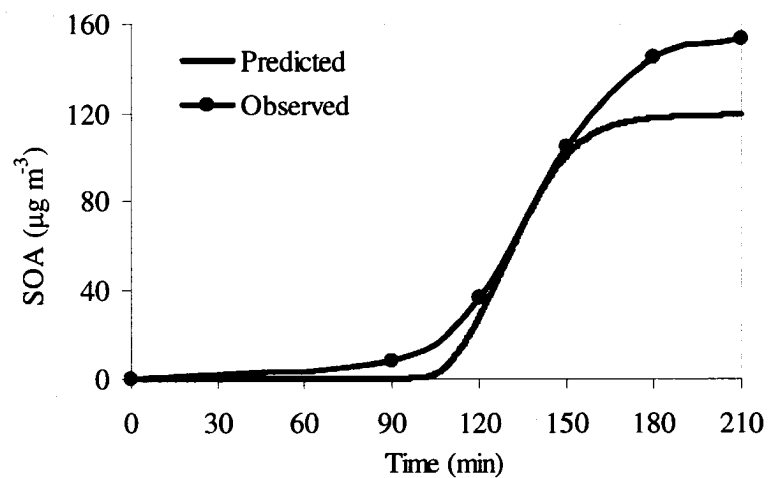
Figure II.6. Observed and predicted SOA concentration as a function of time for experiment 10/06/95 (β-pinene photooxidation) from Hoffman et al. (1997).

32

SOA formation is predicted reasonably for O_3 experiments 06/11/98a and 06/11/98b, for which final measured SOA concentrations are 10-30 μg m^{-3}. SOA formation is not predicted for experiment 06/13/98b, for which final measured SOA concentration is 1.8 μg m^{-3}. Processes in addition to absorption potentially need to be considered at such a low level of SOA. For example, Bonn et al. (2002) suggest that the secondary ozonide formed by the stabilized C9_CI reaction with nopinone is responsible for new particle formation during β-pinene/O_3 experiments. Docherty and Ziemann (2003) hypothesize that particle nucleation and growth following β-pinene ozonolysis is probably controlled by unidentified, low volatility products. The low volatility products are not pinic acid or compounds that are more volatile. Though the exact mechanism remains unclear, such products are speculated to be produced through radical-mediated decomposition of the excited C9_CI (Docherty and Ziemann, 2003).

Table II.3 shows the partitioning coefficients for major predicted SVOCs involved in β-pinene experiments at 308K. For comparison, the experimentally determined partitioning coefficients for a number of products from Yu et al. (1999) are also given. The partitioning coefficients are comparable to those adopted for α-pinene experiments and are also in general agreement with measured values (e.g., ring retaining carboxylic acids from Yu et al., (1999)) or values used in modeling studies by other researchers (e.g., organic nitrates from Barthelmie and Pryor, (1999)). The sensitivity of SOA predictions to the uncertainties in the partitioning coefficients is also shown in Figure II.5. On average, the predicted SOA varies by ±30% if the partitioning coefficients of all species are adjusted by ±20%. For simulations with β-pinene, it appears that smaller predicted

33

Table II.3. Partitioning coefficients for major predicted semi-volatile β-pinene oxidation products.

Term	Description	Partitioning coefficient ($m^3 \mu g^{-1}$) at 308K*	Partitioning coefficient ($m^3 \mu g^{-1}$) from Yu et al. (1999)**
NOPI	nopinone	0.00076	-
UR204	3-hydroxy-nopinone	0.0015	0.0094
RP101	Pinalic-3-acid	0.028	0.014
UR104	pinic acid	0.056	0.035
UR203	2,10-dinitrato-pinane	0.11	-
AP201	2-nitrato-10-hydroxy-pinane	0.0045	-
AP202	2-formyl-2-nitrato-6-dimethyl-norpinane	0.0038	-
PAN103	peroxy 2,2-dimethyl-3-formylmethyl-cyclobutyl formyl nitrate	0.0035	-

*Based on a MW_{om} of 180 g mol^{-1} for aerosol-phase organics; see note on Table II.2.
** Based on two ozonolysis experiments conducted at 306-308K.

concentrations of SOA are much more sensitive to the values used for partitioning coefficients.

SOA Modeling for d-Limonene

Eight experiments with d-limonene as the parent species are simulated. These include seven photooxidation experiments from Hoffman et al. (1997) and Griffin et al. (1999a) and one NO_3 experiment from Hallquist et al. (1999). The initial conditions for these experiments are summarized in Table II.1.

Figure II.7 shows the comparison of observed and predicted SOA formation for the simulated experiments. The ranges of predicted SOA if the partitioning coefficients for all compounds are adjusted by ±20% are also shown. (Photooxidation experiment 09/26/97b, for which final SOA concentration is less than 10 μg m^{-3} is not included; no SOA is predicted for this experiment.) A simplification made in the gas-phase chemistry concerns the treatment of keto-limonaldehyde, as discussed previously. Keto-

34
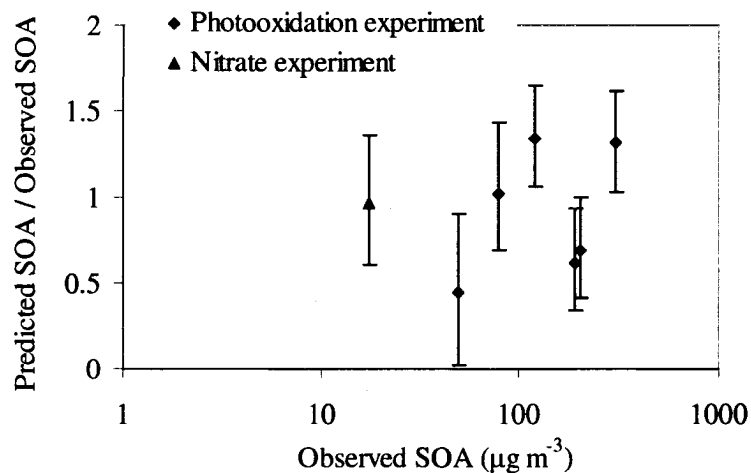
Figure II.7. Comparison between final observed and model predicted SOA concentrations for a series of d-limonene experiments (photooxidation experiments from Hoffman et al. (1997) and Griffin et al. (1999a); NO_3 experiment from Hallquist et al. (1999)). The range of the predicted SOA/observed SOA is assessed by adjusting the partitioning coefficients of all partitioning compounds by $\pm 20\%$.

limonaldehyde is the main oxidation product of limonaldehyde and limona ketone, which are in turn the main oxidation products of d-limonene. Generation of keto-limononic acid from keto-limonaldehyde is represented by a single reaction without detailed treatment of intermediate steps, as done by Griffin et al. (2002) for second or third generation aldehyde products. However, complete transformation of keto-limonaldehyde to keto-limononic acid yields too much simulated SOA formation during photooxidation experiments. When a 10% transformation ratio is used, reasonable agreement between observed and predicted SOA formation is achieved. The remaining 90% is degraded to an aldehyde, which is lumped back to keto-limonaldehyde by considering carbon conservation.

Experimental yield and temporal data on SOA formation from the d-limonene reaction with O_3 are not available. A hypothetical simulation is performed with an initial

35

d-limonene mixing ratio of 57 ppb, an initial O_3 mixing ratio of 228 ppb, and a temperature of 308 K (same initial conditions as α-pinene O_3 experiment 06/09/98a). SOA formation is predicted to be 89.6 μg m^{-3}, in comparison to SOA formation of 52.3 μg m^{-3} observed in the α-pinene experiment (Griffin et al., 1999a). This is reasonable because d-limonene, like α-pinene, includes an endocyclic double bond and a methyl group on the endocyclic double bond, a structure that is found to increase SOA yields in cycloalkene/O_3 system (Keywood et al., 2004). In addition, a higher yield is expected for d-limonene because of its second double bond.

The partitioning coefficients at 308K of major predicted SVOCs in d-limonene experiments are shown in Table II.4. Quantitative information about the partitioning coefficients of d-limonene oxidation products is not found in the literature, although oxidation products that partition to the aerosol phase have been identified in several studies (Glasius, et al., 2000; Larsen et al., 2001). Most of the products identified in these studies have been represented explicitly in the gas-phase chemistry developed in this study. In photooxidation experiments, SOA is predicted to be composed mainly of keto-limononic acid, keto-limonaldehyde, organic nitrates, and several other acids, such as limononic acid. Partitioning coefficients for major predicted SOA constituents in photooxidation experiments range from 0.001 m^3 μg^{-1} to 0.025 m^3 μg^{-1}, comparable to values of 0.0053 m^3 μg^{-1} and 0.055 m^3 μg^{-1}, which were derived through application of a two-product model (Griffin et al., 1999a). The sensitivity of predicted SOA to the uncertainties in partitioning coefficients is shown in Figure II.7. On average, predicted SOA vary by ±40% if the partitioning coefficients of all species are adjusted by ±20%. In O_3 experiments, SOA is predicted to consist of carboxylic acids (e.g., limononic acid,

36

Table II.4. Partitioning coefficients for major predicted semi-volatile d-limonene oxidation products.

Term	Description	Partitioning coefficient ($m^3 \mu g^{-1}$) at 308K*
EDLM	limonaldehyde (3-isopropenyl-6-keto-heptanal)	0.00073
RP301	keto-limonaldehyde (3-acetyl-6-keto-heptanal)	0.0037
RP302	3,6-dioxo-heptanal	0.0010
RP303	3-acetyl-pentadial	0.00087
UR301	limononic acid	0.022
UR304	keto-limononic acid	0.025
UR307	7-hydroxy-limononic acid	0.089
UR308	limonalic acid	0.011
UR309	limonic acid	0.031
UR310	7-hydroxy-keto-limononic acid	0.10
UR311	keto-limonalic acid	0.017
UR312	keto-limonic acid	0.074
UR315	5-keto-limonaldehyde	0.0049
UR316	5-hydroxy-limonaldehyde	0.011
UR319	3-acetyl-5-hydroxy-6-keto-heptanal	0.016
UR321	3-hydroxymethyl-2,6-heptanedione	0.0083
UR323	3-acetyl-5,6-dioxo-heptanal	0.0097
UR324	3-acetyl-4-formyl-butanoic acid	0.019
AP301	1-methyl-1-nitrato-2-hydroxy-4-isopropenyl-cyclohexane	0.0042
AP302	1-methyl-4-(1-methyl-1-nitrato-2-hydroxy-ethyl)-cyclohexene	0.0065
AP303	1-methyl-1-nitrato-2-keto-4-isopropenyl-cyclohexane	0.0019
AP304	2-methyl-2-nitrato-2-(4-methyl-4-cyclohexenyl)-acetaldehyde	0.0028
AP306	1-hydroxy-2-methyl-2-nitrato-3-formylmethyl-6-keto-heptane	0.015
AP307	2-methyl-2-nitrato-3-formylmethyl-6-keto-heptanal	0.014
AP308	1-methyl-1-nitrato-2-hydroxy-4-acetyl-cyclohexane	0.0075
AP309	1-methyl-1-nitrato-2-keto-4-acetyl-cyclohexane	0.0082

*Based on a MW_{om} of 180 g mol^{-1} for aerosol-phase organics; see note on Table II.2.

37

limonic acid, and hydroxy-limononic acid) and multifunctional aldehydes. In the NO_3 experiment, organic nitrates are predicted to constitute most of the formed SOA.

Conclusions

Gas–phase oxidation mechanisms have been developed for α-pinene, β-pinene, and d-limonene within the CACM framework. SVOCs are predicted explicitly in the gas-phase oxidation mechanisms and are allowed to partition to the aerosol phase to form SOA via an absorption process. Reasonable agreement between simulated and measured SOA concentrations is achieved for a series of chamber experiments involving single as well as multiple oxidants, except for the α-pinene reactions with NO_3, for which a different partitioning coefficient for pinonaldehyde has to be used in order to match the observed SOA levels. The heterogeneous-heteromolecular nucleation process was not treated in the model. This could potentially explain the underprediction of SOA for experiments with low initial hydrocarbon concentrations, as well as the underprediction of SOA onset times for certain experiments. In addition, the size dependence of partitioning coefficients is ignored (Cai and Griffin, 2005). SVOCs from α-pinene, β-pinene, and d-limonene oxidation will be lumped into one of the surrogate organics treated in the MPMPO module, or new surrogate organics will be created in future work (Griffin et al., 2003). The updated CACM model and the updated MPMPO module will be incorporated into a three-dimensional air quality model and applied to the New England region, which is influenced heavily by biogenic hydrocarbons (Lamb et al., 1993). Development and application of the mechanisms described here indicate clearly that the approach that is intermediate between SAPRC and the MCM is capable of accurate SOA prediction for biogenic compounds.

38

A significant uncertainty associated with the approach used in this study is the determination of partitioning coefficients. While experimentally derived $K_{om,i}$ values are available for a number of ozonolysis products, such values for nitrate containing organics are scarce. Uncertainties associated with the estimated $K_{om,i}$ values could result from inaccurate estimates of sub-cooled liquid vapor pressure, as well as potential influences from other chemical processes that cause the partitioning of organics to deviate from a strict absorption mechanism (e.g., heterogeneous or particle-phase reactions).

CHAPTER III

APPLICATION OF THE CACM AND MPMPO MODULES USING THE
CMAQ MODEL FOR THE EASTERN UNITED STATES

Abstract

The Caltech Atmospheric Chemistry Mechanism (CACM) and the Model to
Predict the Multi-phase Partitioning of Organics (MPMPO) have been updated with a
detailed treatment of the oxidation mechanisms and secondary organic aerosol (SOA)
formation potentials of α-pinene, β-pinene, and d-limonene. The updated CACM and
MPMPO modules have been incorporated into the Community Multi-scale Air Quality
(CMAQ) model. The revised CMAQ model was used to simulate air quality over the
eastern United States, with a particular focus on New England (NE) for the period August
3-4, 2004, which was part of the International Consortium for Atmospheric Research on
Transport and Transformation (ICARTT) campaign. On August 3, 24-hour-average
organic aerosol (OA) and $PM_{2.5}$ concentrations were approximately 7.0 μg m^{-3} and 13.0
μg m^{-3}, respectively, at Thompson Farm (TF), a rural site in southeastern New
Hampshire. The model results (e.g., ozone (O_3), $PM_{2.5}$, and individual $PM_{2.5}$ chemical
components) were compared against various observational datasets (e.g., AIRMAP,
IMPROVE, SEARCH, and AIRNOW), as well as CMAQ model predictions using the
CB-IV gas-phase mechanism and the SORGAM SOA module. Both CMAQ model
simulations with CACM/MPMPO and with CB-IV/SORGAM predicted O_3, $PM_{2.5}$,

40

sulfate, and ammonium reasonably well but underestimated elemental and organic carbon aerosol. SOA predictions from CACM/MPMPO and from CB-IV/SORGAM were very close for the sites where OA concentrations were available on August 4, though sensitivity of SOA predictions at TF to domain-wide NO_x emissions and temperature variations differed significantly. Additionally, based on the predicted chemical composition of OA from CMAQ with CACM/MPMPO, 24-hour averages of the ratio of the organic mass to organic carbon were determined to be in the range of 1.1 to 1.9, depending on the relative abundance of SOA and primary organics.

Introduction

Organic mass (OM) is an important component of atmospheric aerosols, generally accounting for 30-60% of fine particle mass (Chow et al., 1994; Tanner et al., 2004). A substantial fraction of OM is secondary organic aerosol (SOA), which is formed in the atmosphere from the gas-to-particle partitioning of the oxidation products of gas-phase hydrocarbons. Examples of SOA formation mechanisms include absorption into existing aerosol-phase organics (Pankow, 1994), dissolution into aerosol-phase water (Saxena and Hildemann, 1996; Aumont et al., 2000), heterogeneous or particle-phase reactions (Jang et al., 2002; Kalberer et al., 2004), and cloud-phase reactions (Ervens et al., 2004; Lim et al., 2005).

Because of the complexity of SOA formation processes, treatment of SOA formation is a major source of uncertainty in three-dimensional particulate matter (PM) models (Seigneur, 2001; Pun et al., 2003). Typical three-dimensional air quality models use empirical approaches based on environmental chamber data to simulate SOA formation (Schell et al., 2001; Pun et al., 2003). Recently, mechanistic or semi-

41

mechanistic approaches for modeling SOA have emerged in the literature and are considered to be the future direction of more realistic SOA modeling (Griffin et al., 2005; Kanakidou et al., 2005; Johnson et al., 2006).

An example of such a mechanistic approach that has been used in three-dimensional air quality models is the Caltech Atmospheric Chemistry Mechanism (CACM) and the Model to Predict the Multi-phase Partitioning of Organics (MPMPO) (Griffin et al., 2002a; Pun et al., 2002; Griffin et al., 2002b; Griffin et al., 2003). CACM predicts the products of gas-phase oxidation of volatile organic compounds (VOCs), and MPMPO simulates the phase partitioning of those that are semi- or non-volatile. The CACM and MPMPO were incorporated originally into the California Institute of Technology urban-scale air quality model and applied to the South Coast Air Basin (SoCAB) of California (Griffin et al., 2002b; Griffin et al., 2003). Griffin et al. (2005) updated the CACM and MPMPO to mimic SOA yields from laboratory chambers. Chen and Griffin (2005) further updated the CACM mechanism with a detailed treatment of chemistry for α-pinene, β-pinene, and d-limonene.

In this study, the CACM and MPMPO with the updates of Griffin et al. (2005) and Chen and Griffin (2005) have been incorporated into a state-of-the-science regional air quality model, the Community Multi-scale Air Quality (CMAQ) model (Byun and Ching, 1999), and have been applied over the eastern United States. Focus is placed on the New England (NE) region, which is heavily influenced by biogenic hydrocarbons (Lamb et al., 1993). The objectives of the study are: to evaluate the performance of the updated CACM/MPMPO in simulating ambient SOA formation; to compare the updated CACM/MPMPO with default gas-phase chemistry and SOA modules in the CMAQ

42

model; to evaluate the sensitivity of the different SOA modules to variations in temperature and emissions of oxides of nitrogen (NO_x) and VOCs; to quantify aqueous-phase SOA concentrations relative to the total in the MPMPO module; and to investigate the OM to organic carbon (OC) ratio predicted by the MPMPO module. For the first of these objectives, CACM/MPMPO output will be compared to high-time-resolution aerosol mass spectrometer (AMS) data for the first time.

Models and Measurement Data

CACM and MPMPO

CACM is designed to characterize the formation of O_3 and products that could potentially contribute to SOA from the oxidation of VOCs (Griffin et al., 2002a). CACM lumps parent VOCs into categories based on their SOA formation potentials, reactivity, and structure. Examples of such lumped species are aromatic low and aromatic high, where low and high represent relative SOA formation potentials. CACM is an intermediate approach between the non-specific SAPRC mechanism (Carter, 1990) and the fully explicit Master Chemical Mechanism (MCM) (Jenkin et al., 2003; Saunders et al., 2003). It allows for an increased level of detail while still maintaining reasonable computational demands.

The MPMPO calculates the partitioning of CACM-predicted semi-volatile oxidation products between the gas- and aerosol phases using ten surrogate species (Griffin et al., 2003). Two processes that are responsible for SOA formation are treated simultaneously, in contrast to only one process that is typically treated in other SOA modules. The first is absorption into existing aerosol OM (i.e., primary organic aerosol,

43

POA, or preexisting SOA). This is characterized by an absorption coefficient, $K_{om,i}$ (m^3 μg^{-1}) (Pankow, 1994):

$$K_{om,i} = \frac{O_i}{G_i M_o} = \frac{RT}{MW_{om} 10^6 \gamma_i p_{L,i}^o}$$ (1)

where O_i ($\mu g\ m^{-3}$) and G_i ($\mu g\ m^{-3}$) are the organic aerosol- and gas-phase concentrations of compound i, respectively, M_o ($\mu g\ m^{-3}$) is the total aerosol-phase OM concentration (including POA, if present), R is the ideal gas constant (8.206×10^{-5} $m^3\ atm\ mol^{-1}\ K^{-1}$), T is temperature (K), MW_{om} is the average molecular weight of the organic phase (g mol^{-1}), γ_i is the activity coefficient of compound i, and $p_{L,i}^o$ is the sub-cooled liquid vapor pressure (atm) of compound i at temperature T.

The second process is dissolution into aerosol-phase water, which is represented by Henry's Law:

$$A_i = \frac{G_i (\text{LWC}) HL_i}{\gamma_{aq,i}}$$ (2)

where A_i is the aqueous aerosol-phase concentration of species i ($\mu g\ m^{-3}$), HL_i is its Henry's Law coefficient (($\mu g\ \mu g^{-1}\ H_2O$) / ($\mu g\ m^{-3}$ air)), LWC is the aerosol liquid water content ($\mu g\ H_2O\ m^{-3}$ air), and $\gamma_{aq,i}$ is the activity coefficient of species i in the aqueous aerosol phase, normalized by that at infinite dilution. Further dissolution of the oxidation products into organic ions is also considered.

44

Chen and Griffin (2005) updated the CACM with detailed oxidation mechanisms for α-pinene, β-pinene, and d-limonene and used an absorption module based on Pankow (1994) to simulate SOA formation from oxidation of these three compounds in laboratory experiments. For application in three dimension, over forty simulated oxidation products for α-pinene, β-pinene, and d-limonene are lumped into the three original biogenic surrogate species in the MPMPO module plus a newly created surrogate species (2,10-dinitrato-pinane).

To improve the model performance for the experiments with low initial VOC concentrations in the simulations of Chen and Griffin (2005), a mechanism involving dimer formation of di- and multifunctional acid species proposed by Jenkin (2004) has also been adopted. This is represented by inclusion of a pseudo-unimolecular reaction

$$\text{acid (gas)} \rightarrow \text{acid (aerosol)} \tag{3}$$

for each of the 15 multifunctional acid species generated from oxidation of the monoterpenes. The reaction was assigned a rate coefficient $k = k'\Sigma[\text{acid(gas)}]$ (Jenkin, 2004), where $\Sigma[\text{acid(gas)}]$ is the sum of the gas-phase concentrations of all multifunctional acids generated from α-pinene, β-pinene, and d-limonene and $k' = 1.5e\text{-}35\times\exp(14770/T)$ cm^3 molecule^{-1} s^{-1}, a value decreased by three orders of magnitude compared to that used in Jenkin (2004), in order to fit experimental data. Reaction (3) is treated as a gas-phase reaction in CACM, leading to an assumed nonvolatile dimer (Jenkin, 2004). The mass of the dimer is added to the SOA mass, with the corresponding monomer acid mass no longer available for partitioning using MPMPO.

45
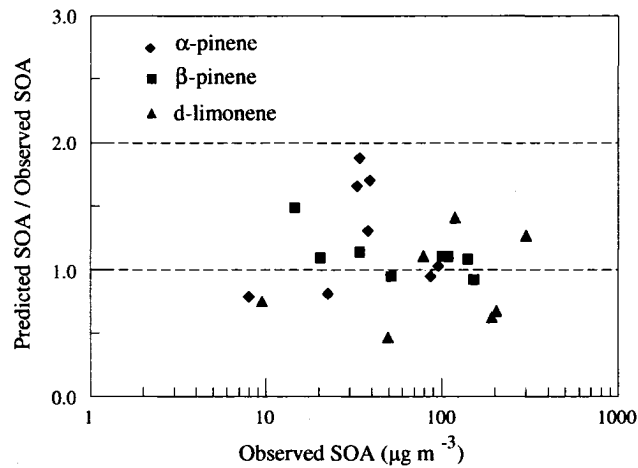
Figure III.1. Comparison of observed SOA during photooxidation experiments with those predicted by CACM and an absorption module based on four surrogate species (Observed data from Hoffman et al. (1997) and Griffin et al. (1999)).

Simulation based on the four MPMPO surrogate species with the additional acid gas-to-particle transfer process were evaluated using the photooxidation experimental data from Hoffman et al. (1997) and Griffin et al. (1999). Figure III.1 shows the comparison of observed and predicted final SOA for these experiments. Reasonable agreement is achieved, indicating that use of the four surrogate species is appropriate. After the update, five individual monoterpene species (i.e., α-pinene, β-pinene, d-limonene, α-terpineol, and γ-terpinene) and their products are now treated explicitly in CACM and accounted for in the surrogates used in MPMPO.

Within CMAQ, CACM was coupled to a general Rosenbrock ordinary differential equation solver (Sandu et al., 1997). Existing gas-phase chemistry mechanisms in CMAQ include CB-IV (Gery et al., 1989), RADM (Stockwell et al., 1990), and SAPRC99. In CMAQ, inorganic aerosol formation is simulated with ISORROPIA (Nenes et al., 1998), and organic aerosols are simulated using SORGAM (Schell et al.,

46

2001). Because MPMPO interacts with the inorganic aerosol module in order to treat the effect of additional water uptake by SOA and dissociated SOA ions on the inorganic partitioning, the ISORROPIA module from the MADRID model that has that capability (Zhang et al., 2004a) was used in this study.

Measurement Data

Measurement data were taken from a wide range of sources. Hourly O_3, 24-hour average PM with diameters less than 2.5 micron ($PM_{2.5}$), and 24-hour average speciated $PM_{2.5}$ were taken from a variety of programs, including the AIRMAP program (Talbot et al., 2005), EPA Air Quality System (AQS), the Southeastern Aerosol Research Characterization Study (SEARCH) (Hansen et al., 2003), and the Interagency Monitoring of Protected Visual Environments (IMPROVE) (Malm et al., 1994). Highly time-resolved chemical mass concentrations for speciated $PM_{2.5}$ were drawn from an Aerodyne AMS (Jayne et al., 2000) deployed at the Thompson Farm (TF), a rural site in southeastern New Hampshire, as part of International Consortium for Atmospheric Research on Transport and Transformation (ICARTT). The TF site is part of the AIRMAP network of atmospheric observatories operated by the University of New Hampshire (Talbot et al., 2005). Additionally, observed PM from a particle-into-liquid sampler (PILS) measurement (Sullivan et al., 2004) on board the NOAA P3 aircraft was used to evaluate vertical predictions of PM.

47

Model Applications

The CMAQ model implemented with CACM/MPMPO was used to simulate air quality for the eastern United States. While an earlier version of CACM was applied to a similar spatial domain previously using CMAQ (Pun et al., 2003), this is the first application of the full MPMPO and the updated CACM (Chen and Griffin, 2005; Griffin et al., 2005) within this framework. For comparison purposes, simulations were also performed using the default CB-IV/SORGAM modules. The model domain is shown in Figure III.2. It has a 62×66 horizontal grid with a resolution of 36 km. Vertically, 21 layers are specified with a σ-pressure coordinate extending from the surface to 10,000 Pa.

The MPMPO module uses the UNIFAC method to calculate activity coefficients for the surrogate species in the aerosol organic and aqueous phases (Fredenslund et al., 1977), which dramatically increases the computational time. It was found to be computationally too intensive to simulate the entire modeling domain while including the UNIFAC calculation. Therefore, the smaller domain shown in Figure III.2 was selected to evaluate whether assuming unity for all activity coefficients yields results similar to those from the full UNIFAC calculation. In order to focus on those areas where SOA formation was most significant, only those cells in which predicted SOA concentrations were greater than 0.5 μg m^{-3} were considered in this analysis. Simulation within this small domain for these cells shows that SOA predictions while assuming unity for activity coefficients were within ±5% of the base predictions. This is largely due to the fact that the majority of simulated SOA formation results from biogenic sources. Therefore, activity coefficients do not deviate significantly from unity because of the molecular similarity of the species. Thus, when the MPMPO-incorporated CMAQ model

48
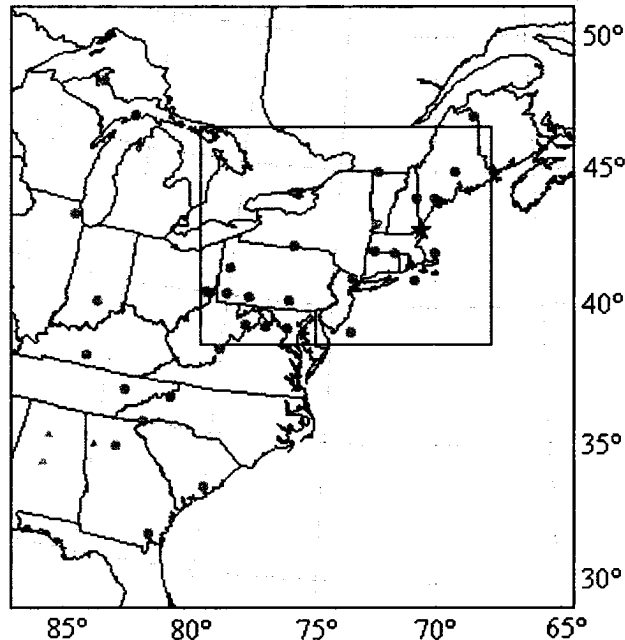
Figure III.2. Modeling domain for this study. The small domain was used for a sensitivity analysis with activity coefficient calculation on or off. AIRMAP sites are stars, SEARCH sites are triangles, and IMPROVE sites are circles.

was applied to the entire modeling domain, the activity coefficients of all organic species in the condensed phases were assumed to be one.

The episode of August 3-4, 2004 (UTC) is chosen for simulation, as August 3 experienced one of the highest OM concentrations measured during ICARTT using filters at TF (Ziemba et al., 2007). Much of NE featured clear or partly cloudy skies with high temperatures in the range of 27 to 32°C during the daytime of August 3, 2004. A cold front pushed through NE during August 4, 2004. Twenty-four-hour average OM and $PM_{2.5}$ concentrations were approximately 7.0 μg m^{-3} and 13.0 μg m^{-3}, respectively, at TF on August 3. The maximum one-hour O_3 mixing ratio during August 3, 2004 reached 95 parts per billion (ppb) at Appledore Island (AI), which is one of the Isles of Shoals in the Gulf of Maine and is host to another AIRMAP observatory.

49

Emission profiles have been processed with the Sparse Matrix Operator Kernel Emissions (SMOKE1.0) system, as in Mao et al. (2006). Anthropogenic emissions are based on the U.S. National Emissions Inventory 99 Version 2, while biogenic emissions are calculated with the Biogenic Emissions Inventory System (BEIS3.09) model. Because the VOCs emissions data processed by SMOKE were formatted for the CB-IV mechanism, they had to be transformed for use with CACM. This was done using the VOC speciation profile for the SoCAB, as was done by Pun et al. (2003). The monoterpene speciation was based on annual emission estimates for individual monoterpenes for North America from Guenther et al. (2000). Meteorological fields were simulated with the PSU/NCAR Mesoscale Modeling System Generation 5 version 3.4 (MM5). Additional details of model set-up and configuration also can be found in Mao et al. (2006).

Model Results

In this study, model results are compared with measured values for O_3, $PM_{2.5}$, and $PM_{2.5}$ composition at various surface locations. Vertical profiles are also considered. Only species with lifetimes in excess of a few hours are shown due to the spatial resolution of the host model.

O_3 Predictions

Figure III.3 shows the simulated and observed hourly average O_3 mixing ratios at the surface at TF and AI. Simulations with both CACM and CB-IV generally are able to capture the temporal variations of O_3 mixing ratios at AI, but not at TF. For August 3, 2004, at TF, CACM accurately predicts the O_3 peak, while CB-IV underpredicts the O_3 peak by 11%. For the same day at AI, CACM and CB-IV overpredict the O_3 peak by

50

36% and 23%, respectively. The only difference between the simulations is the gas-phase chemical mechanism used. Disparities in their VOC aggregation scheme, reaction rate constants, product yields, etc. likely lead to the discrepancies in modeled O_3 mixing ratios.

An interesting feature in the O_3 profiles at TF is the depletion of O_3 at night, which occurs frequently at this site (Talbot et al., 2005). This was not captured by the model. This is potentially caused by use of a minimum vertical diffusion coefficient, K_{zz}, of 1.0 m^2/sec. If the minimum K_{zz} is assigned to be 0.1 m^2/sec (Zhang et al., 2004b), the O_3 predictions at night from the CB-IV mechanism could be decreased to 20 ppb, still significantly higher than observed values. The model probably underestimates dry deposition losses, which were found to be responsible for night time O_3 depletion at this site (Talbot et al., 2005).

The modeled one-hour average O_3 mixing ratios for August 3-4, 2004 (EST) are compared to observations for approximately 400 EPA AQS sites across the modeling domain. Table III.1 summarizes the model performance statistics for the CACM and CB-IV applications for one-hour average O_3 mixing ratios when the observed O_3 mixing ratios exceed 60 ppb (Zhang et al., 2004b). The model performance in terms of mean normalized gross error (MNGE) and mean normalized bias (MNB) for both CACM and CB-IV is comparable to those reported in other studies (Zhang et al., 2004b).
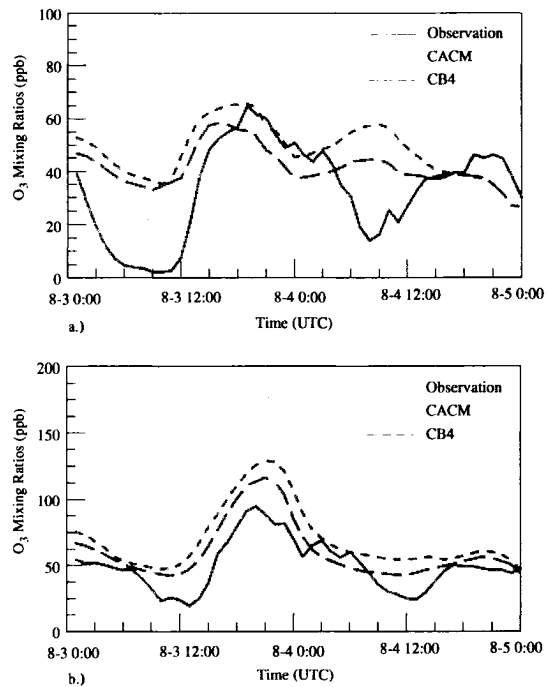
Figure III.3. Measured and modeled O_3 mixing ratios: a.) TF; b.) AI.

PM2.5 Predictions

　　　Model-simulated, 24-hour average $PM_{2.5}$ concentrations are evaluated against measurements at 117 EPA AQS sites across the modeling domain. The model performance statistics are summarized in Table III.2 for CACM/MPMPO and CB-IV/SORGAM. Model predictions from CACM/MPMPO are only slightly different than those from CB-IV/SORGAM. The differences are due solely to differences in the gas-phase chemical mechanism and the SOA module. The gas-phase chemical mechanism affects inorganic aerosol formation by providing gas-phase concentration fields (e.g., hydroxyl radical (OH), hydrogen peroxide (H_2O_2), and O_3). Predictions of the concentrations of primary species (e.g., elemental carbon (EC), POA, and other $PM_{2.5}$

52

species) are independent of the gas-phase chemical mechanism and SOA modules. For both CACM/MPMPO and CB-IV/SORGAM for 24-hour average $PM_{2.5}$, the MNGE and MNB are approximately 38% and -24%, respectively, which are values comparable to other studies (Zhang et al., 2004b).

Model-predicted, 24-hour average compositions are also compared to speciation measurements from the AIRMAP, SEARCH, and IMPROVE programs. A summary of model performance statistics is given in Table III.3. Among the 45 data pairs, 43 data points are for August 4, 2004 (EST) because the SEARCH and IMPROVE programs did not sample on August 3, 2004. The remaining two pairs are from TF from AIRMAP and Jefferson Street, Atlanta, GA, from SEARCH on August 3, 2004. For these sites, the performance of total $PM_{2.5}$ mass predictions is consistent with that for the EPA AQS sites given in Table III.2. Model simulations using CACM/MPMPO and CB-IV/SORGAM show only minor differences in percentage for sulfate, nitrate, ammonium, EC, and OM predictions. For the predictions of individual chemical species, MNGE is largest for nitrate and smallest for ammonium. Based on MNE, both OM and EC are underestimated significantly. The underprediction of EC may reflect underestimation of EC emissions because EC is purely a primary, non-reactive species in the model. OM, however, consists of both primary and secondary material. The slight difference in terms of OM predictions reflects the difference in SOA predictions, as will be discussed subsequently.

53

Table III.1. Performance summary for one-hour average O_3 mixing ratios on August 3-4, 2004, for CACM and CB-IV. Data are from EPA AQS.

Date (EST)	Data points	Mean observation (ppb)	Mean prediction (ppb)		MNGE		MNB	
			CACM	CB-IV	CACM	CB-IV	CACM	CB-IV
08/03/2004	1870	69.7	70.0	58.6	0.21	0.22	0.01	-0.16
08/04/2004	929	69.7	75.8	60.7	0.23	0.18	0.09	-0.12

Table III.2. Performance summary for 24-hour average $PM_{2.5}$ concentrations on August 3-4, 2004, for CACM/MPMPO and CB-IV/SORGAM. Data are from EPA AQS.

Date (EST)	Mean observation ($\mu g\ m^{-3}$)	Mean prediction ($\mu g\ m^{-3}$)		MNGE		MNB	
		CACM /MPMPO	CB-IV /SORGAM	CACM /MPMPO	CB-IV /SORGAM	CACM /MPMPO	CB-IV /SORGAM
08/03/2004	20.1	14.6	14.7	0.37	0.37	-0.23	-0.22
08/04/2004	21.0	15.1	15.3	0.38	0.39	-0.25	-0.24

54

Table III.3. Performance summary for 24-hour average concentrations of $PM_{2.5}$ and individual $PM_{2.5}$ species for CACM/MPMPO and CB-IV/SORGAM. Data are from the SEARCH, IMPROVE, and AIRMAP programs. Ammonium concentrations for most sites from the IMPROVE program are missing.

Species	Data points	Mean observation ($\mu g\ m^{-3}$)	Mean prediction ($\mu g\ m^{-3}$)		Mean normalized gross error (MNGE)		Mean normalized bias (MNB)	
			CACM /MPMPO	CB-IV /SORGAM	CACM /MPMPO	CB-IV /SORGAM	CACM /MPMPO	CB-IV /SORGAM
$PM_{2.5}$	45	16.70	13.70	14.10	0.33	0.36	-0.17	-0.15
Sulfate	44	7.13	7.98	8.55	0.52	0.60	0.32	0.39
Nitrate	44	0.28	0.19	0.18	1.34	1.23	-0.06	-0.03
Ammonium	15	2.73	2.74	2.71	0.14	0.15	0.03	0.02
EC	44	0.80	0.39	0.39	0.52	0.52	-0.45	-0.45
OC	44	3.82	1.26	1.18	0.66	0.69	-0.66	-0.69

55
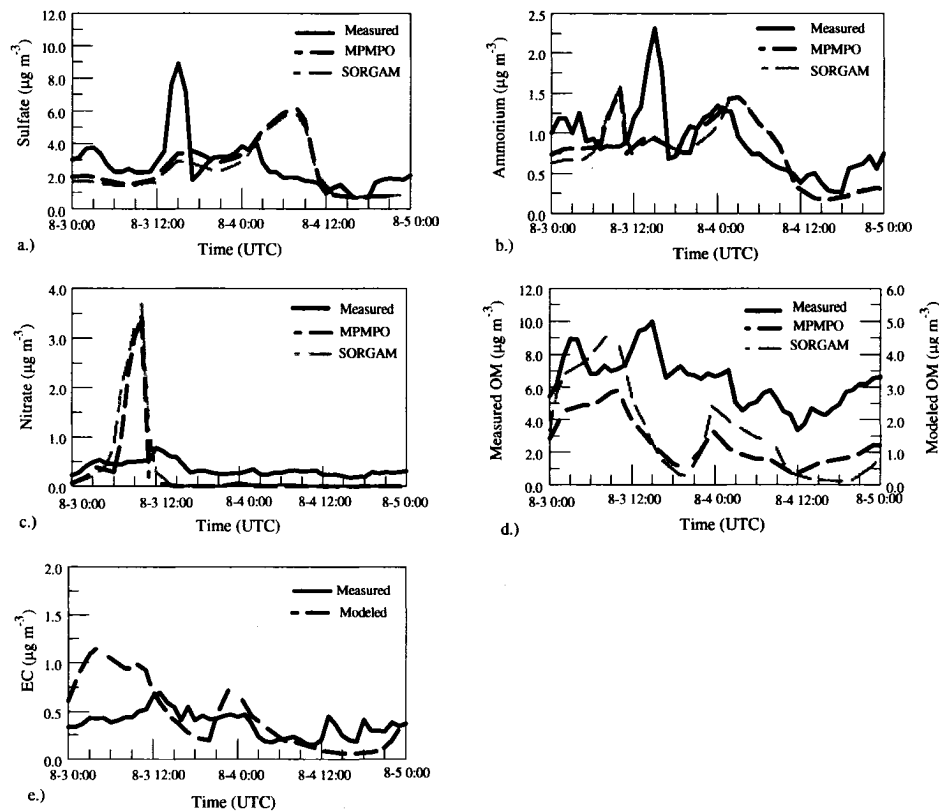
Figure III.4. Comparisons of AMS-measured temporal profiles for a.) sulfate, b.) ammonium, c.) nitrate, and d.) OM and e.) aethalometer-measured EC with model simulations with CACM/MPMPO and CB-IV/SORGAM at TF. Note the difference in scale between measured and modeled OM. In the case of EC, simulations with CACM/MPMPO and with CB-IV/SORGAM produce the same modeled value.

Figure III.4 shows the AMS-measured and model-predicted temporal profiles for major aerosol species at TF. The AMS is able to produce highly time-resolved chemical mass concentrations for sulfate, ammonium, nitrate, and OM in aerosols with aerodynamic diameter less than approximately 1 μm. However, a study in Mexico City (Salcedo et al., 2005) shows that AMS-measured species plus black carbon and soils are a

56

good approximation for $PM_{2.5}$. For this reason, model-predicted concentrations of $PM_{2.5}$ species are compared to AMS-measured values.

Model simulations with CACM/MPMPO and with CB-IV/SORGAM produce very similar temporal profiles for ammonium, nitrate, and sulfate because the same basic inorganic aerosol module is used. Besides missing one significant short-lived observed peak in both ammonium and sulfate, observed temporal profiles for ammonium and sulfate are followed adequately by the model output. The model predicts a nitrate peak that is not evident from observations.

Simulations significantly underpredict the OM concentrations at this site. However, the correlations between modeled hourly OM concentrations and those measured with the AMS are 0.61 for CACM/MPMPO and 0.51 for CB-IV/SORGAM, indicating that the temporal variations of AMS-measured OM were characterized by the model to a certain extent, with slightly better performance for CACM/MPMPO. The differences in the comparisons for the high-time resolution data indicate that comparison of model output using 24-hour filter data should be done with caution. Figure III.4 indicates significant differences between CACM/MPMPO and CB-IV/SORGAM despite similar predicted 24-hour average SOA concentrations.

Figure III.4 also shows the model predicted EC concentrations at this site compared to the measurement from an aethalometer. Modeled EC shows diurnal cycles that are not obvious from the observations. Averaged over the 48-hour period, modeled EC is actually approximately 20% higher than observed EC at this site, in contrast to the overall EC performance in the model domain, as indicated in Table III.3.

57

Model predictions of vertical profiles have been compared to observed values from a PILS measurement onboard the NOAA P3 aircraft. PILS measures water-soluble aerosol species at a time resolution of 60-90 seconds. The position of the NOAA P3 aircraft is averaged over the PILS measurement time to yield the average position for that measurement. The average position of the aircraft is then mapped onto the modeling cells. To construct the vertical profiles, the observational points and the corresponding model predictions are averaged for every 200 meters extending from the surface to an altitude of three kilometers. The modeled vertical profiles for sulfate and ammonium follow the observed ones reasonably well. Therefore, only the vertical profile for OM is discussed here. Measured water-soluble OC is multiplied by 2.25 to yield approximate total OM concentrations [R.J. Weber, Georgia Institute of Technology, personal communication].

Figure III.5 shows the comparison between observed and model-predicted vertical profiles for OM. As with the AMS, the PILS collected particles with diameters smaller than approximately one micron; model predicted $PM_{2.5}$ OM concentrations are again shown in Figure III.5. The vertical OM profile is very similar for CACM/MPMPO and CB-IV/SORGRAM. OM concentrations are significantly underestimated. The relative bias is approximately -70% at the surface and approximately -97% at the altitude of three kilometers, indicating poorer model performance at greater height. Heald et al. (2005) found that observed OM concentrations in the free troposphere were also 10-100 times higher than model values computed using a standard two-product simulation of SOA formation based on chamber data. They suggest that a large, sustained source of SOA in

58
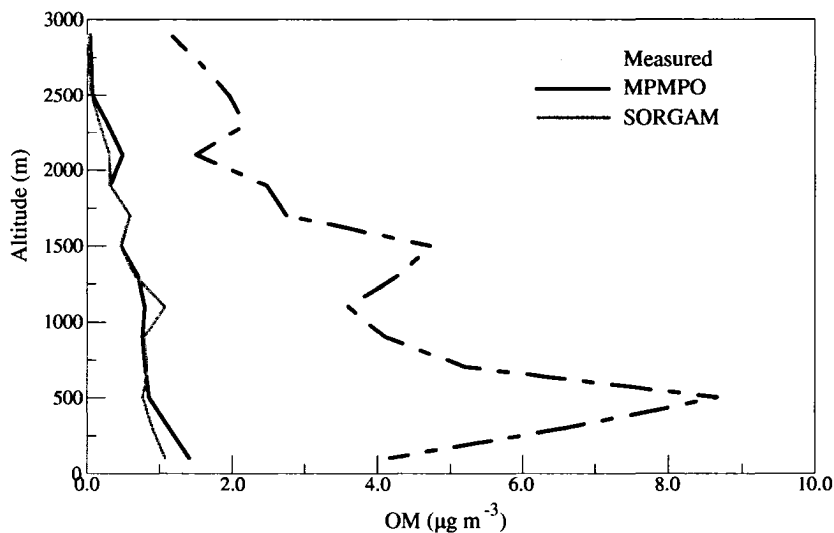
Figure III.5. Comparison of observed vertical profiles for OM from a PILS measurement onboard the NOAA P3 aircraft with those predicted by CACM/MPMPO and CB-IV/SORGAM.

the free troposphere is the oxidation of long-lived organic compounds that are not

captured by current SOA modules.

SOA Predictions

Figure III.6 shows the predicted 24-hour average SOA on August 3-4, 2004 from

CACM/MPMPO and CB-IV/SORGAM. The modeled SOA within this domain is

derived mainly from monoterpenes. The spatial distributions of SOA are coincident with

biogenic VOC emissions. For August 3, 2004, CB-IV/SORGAM predicts high SOA

formation in the northeastern United States, particularly in Maine, as well as in places

around Lake Superior. Peak 24-hour SOA concentrations occurring in Maine and

Minnesota reach approximately 4.1 μg m^{-3}.

59
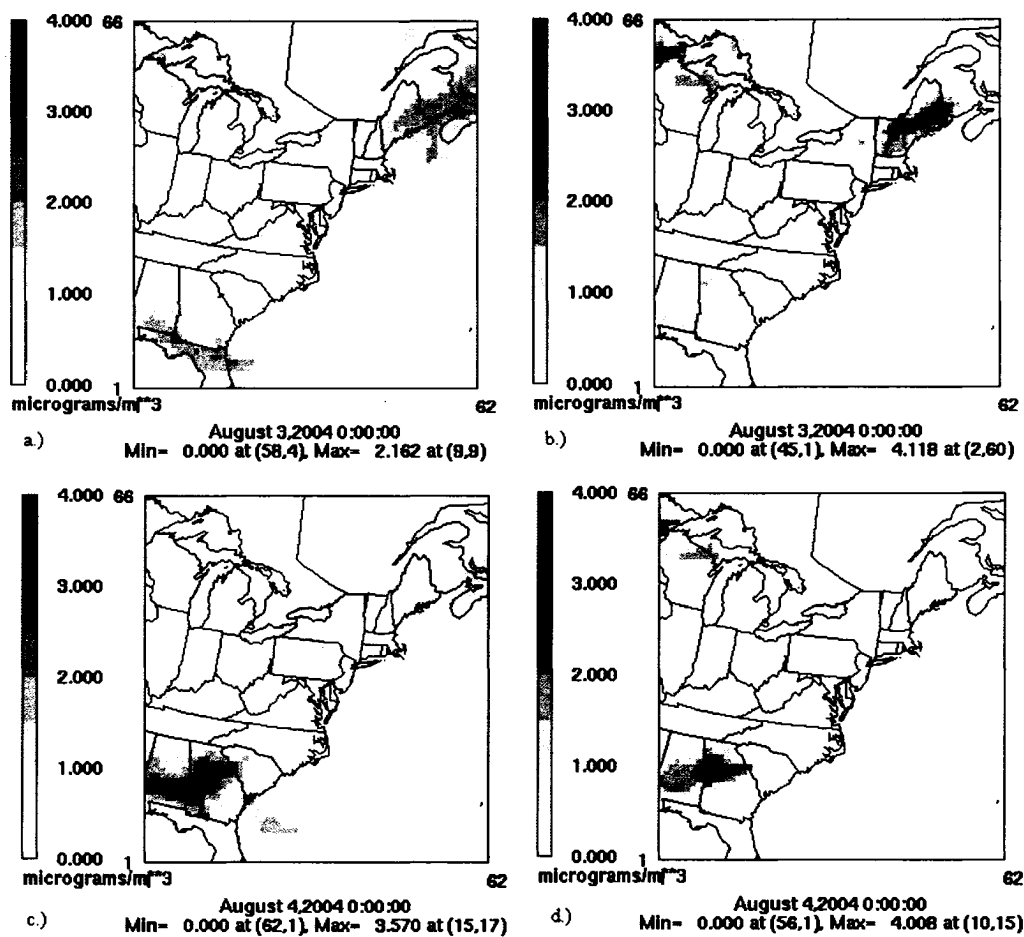
Figure III.6. Predictions of 24-hour average SOA: a.) CACM/MPMPO on August 3, 2004 (UTC); b.) CB-IV/SORGAM on August 3, 2004 (UTC); c.) CACM/MPMPO on August 4, 2004 (UTC); d.) CB-IV/SORGAM on August 4, 2004 (UTC).

For the same day, CACM/MPMPO yields high SOA predictions in the northeastern United States, New Brunswick, the southeastern United States, and places around the Great Lakes. Maximum 24-hour SOA concentrations are approximately 2.2 $\mu g\ m^{-3}$. For August 4, 2004, CB-IV/SORGAM produces high SOA formation in the southeastern United States, with peak values of 3.9 $\mu g\ m^{-3}$ occurring in Georgia. CACM/MPMPO

60

also produces strong SOA formation in the southeastern United States, with peak values of 3.6 μg m^{-3} in Georgia. The differences in predicted SOA from CACM/MPMPO and CB-IV/SORGAM mainly reflect differences in their predictions of biogenic SOA. Averaged over the entire modeling domain and throughout the modeling episode, however, SOA prediction from CACM/MPMPO is 51% higher than that from CB-IV/SORGAM. This indicates that the SOA predictions from CACM/MPMPO are spatially more spread than predictions from CB-IV/SORGAM. This is likely because CACM/MPMPO also tracks SOA formation from oxidation of the first and second generation products, while CB-IV/SORGAM assumes instantaneous SOA formation upon oxidation of parent hydrocarbons. This again underscores why use of 24-hour filter data for model comparison of simulated OM concentrations is not the most appropriate technique.

CACM/MPMPO and CB-IV/SORGAM both underestimate OM concentrations at TF. One potential reason is the inaccuracy of fine POA emissions. The AMS-measured, 24-hour average OM concentration was 7.5 μg m^{-3}. Following the approach of deGouw et al. (2005), the ratio of the AMS signal at m/z = 44 to the total organic signal suggests that on August 3, 2004, 35-65% of OM at TF was secondary in nature (Cottrell et al., 2007). Assuming that 50% of OM at TF is SOA on that day, the resulting POA concentration would be 3.75 μg m^{-3}, approximately five times the modeled value of 0.77 μg m^{-3}. On the same day, the EC concentration is predicted by the model reasonably well, as shown in Figure III.4. However, this does not suggest that POA should also be reasonably predicted by the model because the current emission inventory is not able to

61

capture substantial variations of the ratio of OC to EC in emissions from various sources (McDonald et al., 2000; Shah et al., 2004).

Although this factor of five under prediction is unlikely to be applicable to the entire modeling domain, a sensitivity analysis has been performed to investigate the response of SOA predictions if the POA concentration is increased by a factor of five. For TF, CB-IV/SORGAM yields a 24-hour average SOA prediction of 2.3 μg m^{-3} on August 3, 2004, which is 0.61 μg m^{-3}, or 37%, higher than the base-case SOA prediction. This also increases the total modeled OM concentration to 6.0 μg m^{-3}. CACM/MPMPO predicts a SOA concentration of 1.4 μg m^{-3}, an increase of 0.4 μg m^{-3}, or 43%, compared to the base case, and increases the total modeled OM to 5.2 μg m^{-3}. With the five fold increase in POA levels, SOA only increases by approximately 40%, indicating that simulated SOA formation in this scenario is limited by the availability of condensing material. With the increase of POA levels, modeled OM is still smaller than that observed, indicating that additional SOA formation is needed. Reasons for underestimation of SOA at this site may include: uncertainties associated with the gas-phase mechanism and SOA formation module (e.g., vapor pressure values used for SOA products); the underestimation of parent hydrocarbons that are responsible for SOA formation; lack of a detailed treatment of polymerization processes (Jang et al., 2002; Kalberer et al., 2004) and potential cloud-phase SOA formation processes (Ervens et al., 2004; Lim et al., 2005); lack of consideration of SOA formation from isoprene and sesquiterpenes (Vizuete et al., 2004; Kroll et al., 2005a); and lack of consideration of

62

reactive uptake of carbonyl compounds, such as glyoxal (Kroll et al., 2005b; Hastings, et al., 2005; Liggio et al., 2005).

SOA Sensitivity Study. The sensitivity of SOA predictions to NO_x, VOC, and temperature variations is also studied for comparison to recent experimental results and to recent modeling results for the SoCAB performed using similar techniques (Vutukuru et al., 2006). Figure III.7 shows the SOA predictions at TF for August 3, 2004, for a series of sensitivity analysis studies. Twenty-four-hour average SOA prediction at TF from CACM/MPMPO is 17.2% lower when domain-wide NO_x emissions are increased by 40% from the base case compared to the case when domain-wide NO_x emissions are decreased by 40% from the base case. However, the simulation with CB-IV/SORGAM exhibits a much weaker opposite trend. TF is located in a semi-rural area and is probably NO_x-limited during summer (Griffin et al., 2004). NO and HO_2 compete for the reaction with organic peroxy radicals (RO_2). When NO_x increases, a smaller amount of organic acids that participate in SOA formation is formed from RO_2 + HO_2 reactions in the CACM mechanism, leading to less SOA formation, which is consistent with a simulation done by Jenkin et al. (2000) using MCM. Presto et al. (2005) and Song et al. (2005) report decreased SOA formation with increases in the NO_x to VOC ratio for α-pinene and m-xylene, respectively, in chamber studies. The NO_x-dependence of SOA formation predicted by CACM/MPMPO in the eastern United States is much stronger than that predicted by Vutukuru et al. (2006) for the SoCAB, probably because of the NO_x-saturated atmosphere in the SoCAB (Kelly and Gunst, 1990).

63
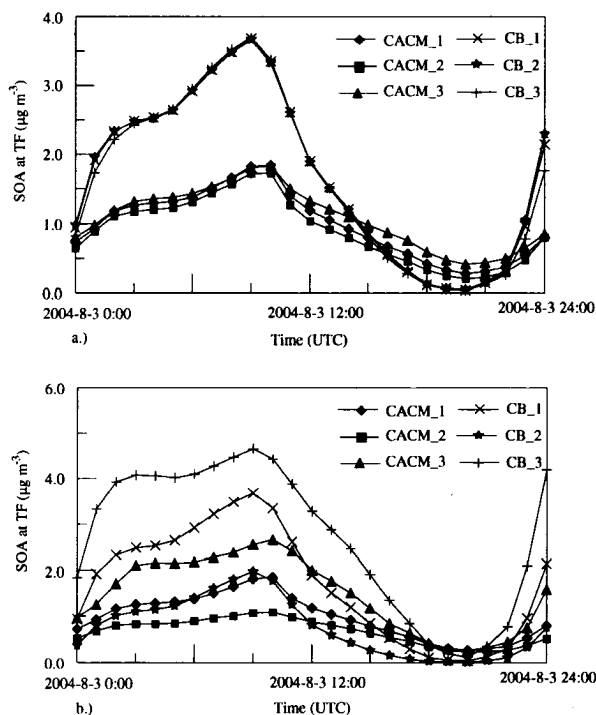
Figure III.7. SOA predictions on August 3, 2004 at TF: a.) domain-wide NO_x emissions were varied by ±40% from base case; b.) temperature used in gas-phase chemistry and aerosol modules was varied by ±5 K from base case. Notation: _1 represents the base case, _2 represents the case with 40% increase of emissions for a.) or the case with increase of temperature by 5K for b.), and _3 represents the case with 40% decrease of emissions for a.) or the case with decrease of temperature by 5K for b.).

On the contrary, an increase of NO_x emissions increases the oxidation power of the atmosphere at TF by leading to more O_3 and increased consumption of monoterpenes. This explains the very slight increase of SOA predicted by the simulation with CB-IV/SORGAM. Simulations with CACM/MPMPO and with CB-IV/SORGAM both predict higher SOA formation when domain-wide VOC emissions are increased, as would be expected.

64

The sensitivity of SOA predictions to the temperature was conducted by adjusting by ±5 K the temperature that is fed into the gas-phase chemistry mechanism and the aerosol module. In this way, the temperature dependence of other processes such as emissions was not included. The dependence of SOA predictions on temperature (T) is stronger for CB-IV/SORGAM than for CACM/MPMPO. Twenty-four-hour average SOA prediction at TF in the (T – 5 K) case is 3.4 times that in the (T + 5 K) case for CB-IV/SORGAM, while for CACM/MPMPO, 24-hour average SOA prediction in the (T – 5 K) case is 2.1 times that in the (T + 5 K) case. The temperature dependence of SOA predictions is due mainly to the value used for enthalpy of vaporization of the SOA constituents. SORGAM uses 156.0 kJ mol^{-1} for all molecules, while MPMPO uses an average of approximately 73.0 kJ mol^{-1} depending on individual surrogate species. The values used in MPMPO are based on a molecular structure prediction technique (Myrdal and Yalkowsky, 1997). Increases in the value of enthalpy of vaporization typically lead to greater predicted SOA (Pun et al., 2003). Takekawa et al. (2003) measured SOA yields from the photooxidation of toluene at different temperatures and found that the SOA yield at 283 K is approximately twice that at 303 K. Thus, the temperature dependence predicted by both CACM/MPMPO and CB-IV/SORGAM is stronger than that measured experimentally. Temperature sensitivity in the eastern United States is similar to that observed for simulations in the SoCAB performed by Vutukuru et al. (2006).

Aqueous SOA. A unique feature of the MPMPO module is that it simulates the simultaneous partitioning of semi-volatile organics into both the organic and the aqueous

65

a.) August 3,2004 0:00:00
Min= 0.000 at (1,1) Max= 0.430 at (16,29)

b.) August 4,2004 0:00:00
Min= 0.000 at (2,1) Max= 0.764 at (2,19)
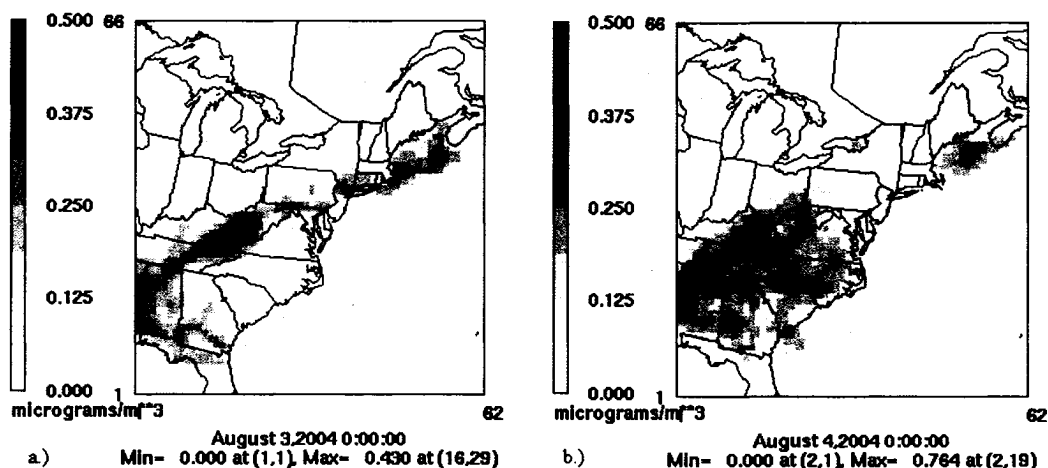
Figure III.8. Predictions of 24-hour average aqueous-phase SOA from CACM/MPMPO: a.) August 3, 2004 (UTC); b.) August 4, 2004 (UTC).

phases, while other SOA modeling approaches typically only simulate the partitioning of semi-volatile organics into one phase, usually organic. To evaluate the significance of partitioning of organics into the aqueous phase, the portion of SOA that resides in the aqueous phase was quantified. Figure III.8 shows the predictions of 24-hour average aqueous-phase SOA from CACM/MPMPO for August 3-4, 2004. The maximum 24-hour average aqueous- phase SOA concentration is 0.43 μg m^{-3} for August 3, 2004, and 0.76 μg m^{-3} for August 4, 2004. However, these maxima are not spatially coincident with the maximum 24-hour average SOA concentration predictions from CACM/MPMPO shown in Figure III.6. The aqueous-phase SOA can constitute from 0% to approximately 90% of the total SOA predictions from the MPMPO module. The relative importance of aqueous-phase SOA formation depends on multiple factors, among which are the LWC of aerosols, the aqueous-phase hydrogen ion concentration, and the competition with the partitioning to the organic phase. The MPMPO module does not treat potential further

irreversible or reversible reactions (except ionization for carboxylic acids) for the organics in the aqueous phase despite observations of polymerization for certain compounds in the aqueous phase (Hastings et al., 2005). This suggests the current MPMPO module underestimates the importance of aqueous-phase SOA.

OM to OC Ratio. Another strength of CACM/MPMPO is its ability to simulate organic composition. This enables calculation of the OM to OC ratio, which is used typically to convert measured aerosol OC content to aerosol OM (Turpin and Lim, 2001). Figure III.9 shows the spatial distributions of 24-hour average values for the average OM to OC ratio for the modeling domain. The average ratio varies from 1.10 to 1.90 in continental areas. In this study, the average OM to OC ratio is 1.16 for POA. The OM to OC ratio for surrogate species in the MPMPO module varies from 1.13 to 3.75, depending on the specific compound. The spatial distributions of average OM to OC show the spatial patterns of relative contributions of SOA and POA. In the northern part of the modeling domain, the average OM to OC ratio reaches 1.80 to 1.90 because of the dominant contributions of SOA to total OM. For areas where SOA formation is minor or where POA dominates over SOA formation, the average OM to OC ratio is in the range of 1.10 to 1.30. Turpin and Lim (2001) suggested that the average OM to OC ratio was 1.6 ± 0.2 for urban aerosols and 2.1 ± 0.2 for non-urban aerosols. The slightly lower OM to OC ratio from this study may be due to two reasons: a value of the OM to OC ratio used for POA that is too low and the potential under prediction of organic functionality for SOA from CACM/MPMPO.

67
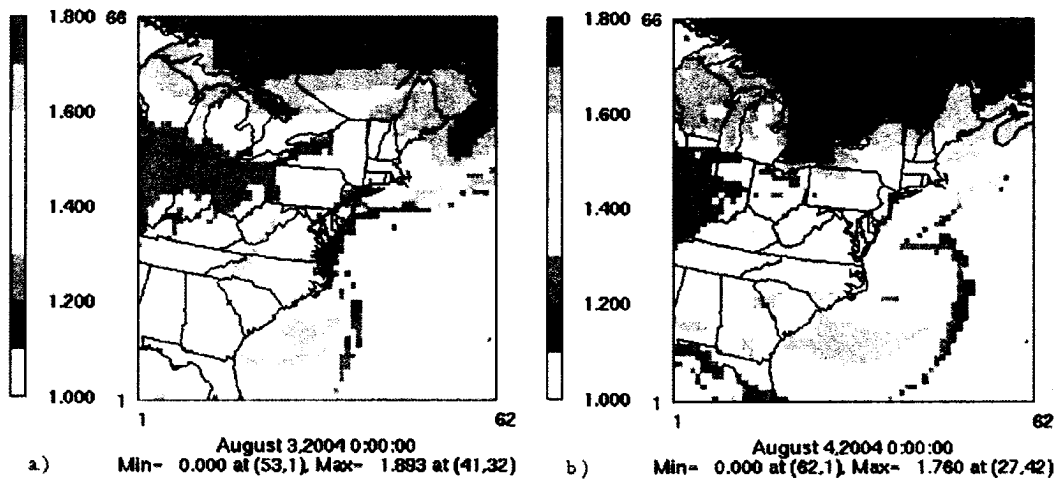
Figure III.9. Spatial distributions for the 24-hour average values of the ratio of OM to OC from CACM/MPMPO: a.) August 3, 2004 (UTC); b.) August 4, 2004 (UTC).

Conclusions

CACM and MPMPO have been incorporated into the CMAQ model and applied to the eastern United States for an August 2004 episode. Simulations with CACM/MPMPO were compared to simulations using CB-IV/SORGAM, as well as a number of observational datasets. Model simulations produce reasonable predictions for O_3, $PM_{2.5}$, sulfate, and ammonium but yield substantial underestimates for EC and OM. The underestimation of EC is probably due to the underestimation of emissions for EC. Reasons for the underestimation of OM may include uncertainties in the gas-phase mechanism and SOA modules used, the neglect of SOA formation from sesquiterpenes, isoprene, and additional formation pathways, and the potential underestimation of emissions of POA and parent hydrocarbons that are responsible for SOA formation.

Simulations with CACM/MPMPO and with CB-IV/SORGAM produce similar SOA predictions for the nearly 40 sites where OM concentrations are available on August 4, 2004, based on 24-hour filter samples. Again, comparison to 24-hour filter samples is not the best method for discussion of SOA model output discrepancies. However, responses of SOA predictions at TF to NO_x emissions changes and temperature variations are different for the two modeling approaches. This may lead to different results if both modeling approaches are used to examine the effect of NO_x emissions reductions on SOA concentrations or to study how climate change affects ambient SOA levels.

CHAPTER IV

MODELING SECONDARY ORGANIC AREOSOL FORMATION THROUGH
CLOUD PROCESSING OF ORGANIC COMPOUNDS

Abstract

Interest in the potential formation of secondary organic aerosol (SOA) through reactions of organic compounds in condensed aqueous phases is growing. In this study, the potential formation of SOA from irreversible aqueous-phase reactions of organic species in clouds was investigated. A new proposed aqueous-phase chemistry mechanism (AqChem) is coupled with the existing gas-phase Caltech Atmospheric Chemistry Mechanism (CACM) and the Model to Predict the Multiphase Partitioning of Organics (MPMPO) that simulate SOA formation. AqChem treats irreversible organic reactions that lead mainly to the formation of carboxylic acids, which are usually less volatile than the corresponding aldehydic compounds. Zero-dimensional model simulations were performed for tropospheric conditions with clouds present for three consecutive hours per day. Zero-dimensional model simulations show that 48-hour averaged SOA formation are increased by 27% for a rural scenario with strong monoterpene emissions and 7% for an urban scenario with strong emissions of aromatic compounds, respectively, when irreversible organic reactions in clouds are considered. AqChem was also incorporated into the Community Multiscale Air Quality Model (CMAQ) version 4.4 with CACM/MPMPO and applied to a previously studied photochemical episode (August 3-4, 2004) focusing on the eastern United States. The

70

CMAQ study indicates that the maximum contribution of SOA formation from irreversible reactions of organics in clouds is 0.28 μg m^{-3} for 24-hour average concentrations and 0.60 μg m^{-3} for one-hour average concentrations at certain locations. On average, domain-wide surface SOA predictions for the episode are increased by 8.6% when irreversible, in-cloud processing of organics is considered.

Introduction

Atmospheric particulate matter (PM) is associated with adverse human health effects (Pope and Dockery, 2006), decreases in visibility (Malm, 1989), and global climate forcing (Charlson et al., 1992, Jones et al., 1994). Organic aerosol (OA) is a ubiquitous and important constituent of atmospheric PM (Murphy et al., 1998; Turpin et al., 2000). OA consists of primary OA (POA), which is directly emitted from various sources, and secondary OA (SOA), which is formed in the atmosphere from the oxidation of volatile organic compounds (VOCs).

The processes leading to SOA formation typically are viewed as gas-phase oxidation of VOCs followed by nucleation/gas-particle partitioning of low-volatility products (Pankow, 1994; Odum et al., 1996; Griffin et al., 1999). Oligomer and/or polymer formation in the aerosol phase has also been shown to be important with regard to SOA formation (Jang et al., 2002; Kalberer et al., 2004). Besides these processes, it has also been hypothesized that fog/cloud processing, which leads to substantial sulfate formation, could also be a source for SOA (Blando and Turpin, 2000). The process of SOA formation from aqueous-phase processing of organic compounds in clouds involves formation of potential low-volatility products through aqueous-phase reactions of organics, followed by subsequent gas-particle partitioning of the low-volatility products

71

post evaporation of the hydrometeor (Blando and Turpin, 2000; Kanakidou et al., 2005). Recent experimental and modeling studies indeed demonstrated that SOA potentially can be formed from aqueous-phase processing of organic compounds in clouds (Carlton et al., 2006; Loeffler et al., 2006). Ambient particle size distribution measurements also showed the occurrence of droplet-mode organics (Blando et al., 1998; Yao et al., 2002), which, similarly to droplet-mode sulfate, are most likely formed from cloud processing of organic materials (Blando and Turpin, 2000). Several modeling studies (Warneck, 2003; Ervens et al., 2004; Lim et al., 2005) have demonstrated the formation of low-molecular weight dicarboxylic acid from cloud processing of organics. Such dicarboxylic acids have been found in atmospheric aerosols in various regions (Kawamura and Ikushima, 1993; Decesari et al., 2000). In addition, Claeys et al. (2004) showed that multiphase acid-catalyzed organic reactions with hydrogen peroxide provided a new route for SOA formation from isoprene and hypothesized that such a mechanism could also provide a pathway for SOA formation from monoterpenes and their oxidation products. Most recently, Heald et al. (2006) analyzed the covariance of water soluble particulate organics with other species in the free troposphere over the eastern United States, with the results suggesting aqueous-phase SOA generation involving biogenic precursors.

Given the increasing interest in potential SOA formation through the aqueous-phase processing of organic compounds, this paper evaluates the significance of SOA formation from aqueous-phase reactions of organics in cloud droplets through a modeling study. The study involves the development of an aqueous-phase chemistry mechanism (AqChem) that specifically includes treatment of potential organic reactions that lead to production of semi-volatile organic compounds. Because of our incomplete knowledge

72

on the aqueous-phase chemistry for organics (Kanakidou et al., 2005; Gelencser and Varga, 2005), AqChem treats organic reactions based on previous work by Ervens et al. (2004) and Lim et al. (2005) for organics of carbon number up to four and the simple protocol used by Aumont et al. (2000) for organics of carbon number greater than four. Potential reversible oligomerization reactions (Hastings et al., 2005; Loeffler et al., 2006) are not included because of a current lack of a quantitative description of these phenomena. AqChem utilizes an existing gas-phase chemistry mechanism, the Caltech Atmospheric Chemistry Mechanism (CACM) (Griffin et al., 2002) that provides the prediction of gas-phase production of organic compounds. It is also linked with a SOA module, the Model to Predict the Multi-phase Partitioning of Organics (MPMPO) (Griffin et al., 2003), such that the partitioning between gas and aerosol phases of semi-volatile organic products from aqueous-phase reactions is determined thermodynamically. AqChem was used in a zero-dimensional model as well as a three-dimensional model to study the magnitude of potential SOA formation in clouds.

Methods

Development of the AqChem Mechanism

AqChem was developed based on previous work (Aumont et al., 2000; Warneck et al., 2003; Ervens et al., 2004; Lim et al., 2005) and to work specifically with the CACM mechanism and the MPMPO module. The main purpose of AqChem is to treat the irreversible organic reactions that could potentially lead to the production of semi-volatile organic compounds in clouds.

In AqChem, the reactions for organics of carbon number up to four that are treated in the CACM mechanism were adopted from previous work by Ervens et al.

73

(2004) and Lim et al. (2005) and are shown schematically in Figure IV.1a. The main

purpose of the reaction scheme for organics of carbon number up to four is to provide

formation routes for oxalic and pyruvic acids. Briefly, organics in the cloud phase are

assumed to be oxidized only by hydroxyl radical (OH). Glycoladehyde and glyoxal are

converted to oxalic acid via glyoxylic acid (Ervens et al., 2004, Lim et al., 2005).

Methylglyoxal is converted to pyruvic acid, which decomposes to form acetic acid.

Ethanol and acetaldehyde are converted to acetic acid as well. A portion of acetic acid is

converted to oxalic acid, while the rest decomposes to formaldehyde (Lim et al., 2005).

No reactions are treated for methyl vinyl ketone and methacrolein in the aqueous phase

because of their low solubility in water (Ervens et al., 2004).

Within CACM, there are approximately 140 semi-volatile organic compounds of

carbon number greater than four (Griffin et al., 2002; Chen and Griffin, 2005). Instead of

treating potential aqueous-phase chemistry for these organic compounds individually, an

organic surrogate approach similar to that used in MPMPO was adopted here. In the

MPMPO module, each semi-volatile organic compound is lumped into one of 11 organic

surrogate species (Griffin et al., 2003; Griffin et al., 2005; Chen et al., 2006). MPMPO

calculates the partitioning between the gas and aerosol phases for these 11 surrogate

species. Similarly, AqChem treats the aqueous-phase chemistry for four of the 11

surrogates because of their potential to lead to less volatile organic products (e.g.,

carboxylic acids). These four surrogate species are surrogate 3 (S3, 3-hydroxy-2, 4-

dimethyl-2, 4-hexadiendial), surrogate 5 (S5, 2-hydroxyl-3-isopropyl-6-keto-heptanal),

74

CH₃CH₂OH → represented as CH_3CH_2OH (ethanol)

CH_2OHCHO (glycolaldehyde) CH_3CHO (acetaldehyde) CH_3COCHO (methylglyoxal)

$(OH)_2CH_2CH_2(OH)_2$ (glyoxal) CH_3COOH (acetic acid) ← $CH_3COCOOH$ (pyruvic acid)

0.85   0.15

$CHOCOOH$ (glyoxylic acid) → $HOOCCOOH$ (oxalic acid) $CH_2(OH)_2$ (formaldehyde)

CO_2 ← $HCOOH$ (formic acid) CH_3OH (methanol)

a.)

b.)

Figure IV.1. Schematic of organic reactions in clouds: a.) organics of carbon number less than four (based on Ervens et al. (2004) and Lim et al. (2005)); b.) organics of carbon number greater than four (based on Aumont et al. (2000)) (S2–S7 and S10 are surrogates in the MPMPO module).

surrogate 7 (S7, 2,4-dimethyl-3-formyl-benzoic acid), and surrogate 10 (S10, 1-methyl-1-hydroxy-2-nitrato-4-isopropyl-cyclohexane) in the MPMPO module (Griffin et al., 2003; Griffin et al., 2005). In this way, although only four aqueous-phase chemical reactions

75

were added for organic compounds of carbon number greater than four, 58 organic compounds that are lumped into these four surrogates in the MPMPO undergo further reactions in the aqueous phase. The products of aqueous-phase reactions for these four MPMPO surrogates were based on the protocol used by Aumont et al. (2000). Aumont et al. (2000) assumed that (1) OH is the only oxidant; (2) an aldehyde moiety is converted to a carboxylic acid moiety; and (3) the carbon skeleton is not changed during oxidation. Following the protocol of Aumont et al. (2000), the oxidation of S3 by OH leads to the formation of 3-hydroxy-2, 4-dimethyl-2, 4-hexadienalic acid (S3PD). The oxidation product of S5 is 2-hydroxyl-3-isopropyl-6-keto-heptanoic acid (S5PD). S7 is converted to 3, 5-dimethyl-1, 4-dibenzoic acid (S7PD). Oxidation of S10 by OH in the aqueous phase leads to a product (S10PD, 1-methyl-1-hydroxy-2-nitrato-3-oxo-4-isopropyl-cyclohexane) that has one more ketone group than surrogate 10. The aqueous-phase oxidation rates by OH for these surrogate species were estimated based on the method of Dutot et al. (2003). The reaction scheme for these surrogate species is shown in Figure IV.1b.

AqChem also includes a compact treatment of aqueous-phase hydrogen-oxygen and sulfur chemistry mainly based on Ervens et al. (2003) and Ervens et al. (2004). Such a compact treatment includes the important reactions for determining aqueous OH levels and aqueous sulfate formation but is computationally less demanding than detailed treatments, which is especially important for three-dimensional air quality simulations. Tables IV.1 and IV.2 list the irreversible and equilibrium reactions, respectively, that are

Table IV.1. Aqueous-phase irreversible reactions included in AqChem

Num	Reactions	k^a	E/R (K)	Ref.[b]
1	$O_3 + O_2^- \rightarrow 2O_2 + OH + OH^-$	1.5e9	2200	2
2	$H_2O_2 + OH \rightarrow HO_2 + H_2O$	3.0e7	1680	1
3	$H_2O_2 + h\nu \rightarrow 2OH$			1
4	$HO_2 + O_2^- \rightarrow H_2O_2 + O_2 + OH^-$	9.7e7	1060	1
5	$HO_2 + HO_2 \rightarrow H_2O_2 + O_2$	8.3e5	2720	1
6	$OH + HO_2 \rightarrow H_2O + O_2$	1.0e10		1
7	$OH + O_2^- \rightarrow OH^- + O_2$	1.1e10	2120	1
8	$O_3 + OH \rightarrow HO_2 + O_2$	1.0e8		1
9	$NO_3^- + h\nu \rightarrow NO_2 + OH + OH^-$			1
10	$S(IV) + O_2 \xrightarrow{Fe^{3+}, Mn^{2+}} S(VI)$	$2.6e3[Fe^{3+}]$ + $7.5e2[Mn^{2+}]$ $+1.0e10[Fe^{3+}][Mn^{2+}]$ (if PH $\leq$ 5.0) $7.5e2[Mn^{2+}]$ + $2.0e10[Fe^{3+}][Mn^{2+}]$ (if PH > 5.0)		5,6
11	$HSO_3^- + H_2O_2 + H^+ \rightarrow SO_4^{2-} + H_2O + 2 H^+$	6.9e7	4000	1,4
12	$HSO_3^- + O_3 \rightarrow HSO_4^- + O_2$	3.7e5	5530	1,4
13	$SO_2 \cdot H_2O + O_3 \rightarrow HSO_4^- + O_2 + H^+$	2.4e4		1,4
14	$SO_3^{2-} + O_3 \rightarrow SO_4^{2-} + O_2$	1.5e9	5280	1,4
15	$HCHO + HSO_3^- \rightarrow HOCH_2SO_3^-$	4.5e2	2660	4
16	$HCHO + SO_3^{2-} \rightarrow HOCH_2SO_3^- + OH^-$	5.4e6	2530	4
17	$HOCH_2SO_3^- + OH^- \rightarrow CH_2(OH)_2 + SO_3^{2-}$	4.6e3	4880	4
18	$HOCH_2SO_3^- + OH \rightarrow HOCHSO_3^- + H_2O$	3.0e8		4
19	$HOCHSO_3^- + O_2 \rightarrow HCOOH + HSO_3^- + HO_2$	2.5e9		4
20	$CH_3OH + OH \rightarrow HCHO + HO_2$	1.0e9	580	1
21	$CH_2(OH)_2 + OH \rightarrow HCOOH + HO_2 + H_2O$	1.1e9	1020	1
22	$CH_3OO + HO_2 \rightarrow CH_3OOH + O_2$	4.3e5		4
23	$CH_3OO + O_2^- \rightarrow CH_3OOH + OH^- + O_2$	5.0e7		4
24	$CH_3OOH + OH \rightarrow CH_3OO + H_2O$	3.0e7	1680	1
25	$CH_3OOH + OH \rightarrow HO_2 + HCOOH$	6.0e6	1680	1
26	$HCOOH + OH \rightarrow CO_2 + HO_2 + H_2O$	1.3e8	1000	1
27	$HCOO^- + OH \rightarrow CO_2 + H_2O$	1.0e9	1000	1
28	$CH_3CHO + OH \rightarrow CH_3COOH + HO_2$	3.6e9		1
29	$CH_3CH(OH)_2 + OH \rightarrow CH_3COOH + HO_2$	1.2e9		1
30	$CH_3CH_2OH + OH \rightarrow CH_3CHO + HO_2$	1.9e9		1
31	$CH_2OHCHO + OH \rightarrow (CH_2(OH)_2)_2 + HO_2$	1.2e9		2
32	$(CH_2(OH)_2)_2 + OH \rightarrow CHOCOOH + HO_2$	1.1e9	1516	1
33	$CHOCOOH + OH \rightarrow (COOH)_2 + HO_2$	3.6e8	1000	2
34	$CH_3COO^- + OH \rightarrow 0.85CHOCOOH + 0.15 CH_2(OH)_2$	8.5e7		3
35	$CH_3COOH + OH \rightarrow 0.85CHOCOOH + 0.15 CH_2(OH)_2$	1.6e7		3

77

Table IV.1 Continued

36	$CHOCOO^- + OH \rightarrow (COOH)_2 + HO_2$	2.9e9	4300	2
37	$(COOH)_2 + OH \rightarrow HO_2 + 2CO_2 + H_2O$	1.4e6		2
38	$HC_2O_4^- + OH \rightarrow HO_2 + 2CO_2 + H_2O$	1.9e8	2800	2
39	$C_2O_4^{2-} + OH \rightarrow HO_2 + 2CO_2 + H_2O$	1.6e8	4300	2
40	$CH_3COCHO + OH \rightarrow CH_3COCOOH + HO_2$	1.1e9	1600	2
41	$CH_3COCOOH + OH \rightarrow CH_3COOH + HO_2 + CO_2$	6.0e7		3
42	$CH_3COCOO^- + OH \rightarrow CH_3COO^- + HO_2 + CO_2$	6.0e7		3
43[c]	$S3 + OH \rightarrow S3PD + HO_2$	4.98e9		7
44[c]	$S5 + OH \rightarrow S5PD + HO_2$	5.76e9		7
45[c]	$S7 + OH \rightarrow S7PD + HO_2$	4.26e9		7
46[c]	$S7^- + OH \rightarrow S7PD + HO_2$	4.08e9		7
47[c]	$S10 + OH \rightarrow S10PD$	1.23e10		7

[a]: in appropriate units of M and s^{-1}

[b]: References: 1: Ervens et al. (2003); 2: Ervens et al. (2004); 3: Lim et al (2005); 4: Warneck (1999); 5. Martin and Good (1991); 6: Zaveri (1999); 7: Dutot et al. (2003).

[c]: S3: 3-hydroxy-2, 4-dimethyl-2, 4-hexadiendial; S3PD: 3-hydroxy-2, 4-dimethyl-2, 4-hexadienalic acid; S5: 2-hydroxyl-3-isopropyl-6-keto-heptanal; S5PD: 2-hydroxyl-3-isopropyl-6-keto-heptanoic acid; S7: 2,4-dimethyl-3-formyl-benzoic acid; S7PD: 3, 5-dimethyl-1, 4-dibenzoic acid; S10: 1-methyl-1-hydroxy-2-nitrato-4-isopropyl-cyclohexane; S10PD: 1-methyl-1, 3-dihydroxy-2-nitrato-4-isopropyl-cyclohexane.

included in AqChem. Gas and aqueous-phase mass transfer was treated according to the resistance model of Schwartz (1986) by considering mass accommodation coefficient (α), gas-phase diffusion constants (D_g), and Henry's law constants (K_H) for each soluble species, values of which are shown in Table IV.3.

After the evaporation of cloud droplets, the partitioning between the gas and aerosol phases for the oxidation products formed from the aqueous-phase reactions is computed by the MPMPO module. This is shown schematically in Figure IV.2. If clouds are not present, the amounts of semi-volatile organic compounds computed from the CACM mechanism are used directly as input to the MPMPO module to compute SOA formation, as in previous applications (Chen et al., 2006). If clouds are present, AqChem is first called to simulate the cloud processing of organics, followed by a call to

78

Table IV.2. Aqueous-phase equilibrium reactions included in AqChem

Num.	Equilibrium reactions	K (M)	E/R (K)	Ref.[a]
1	$H_2O \leftrightarrow H^+ + OH^-$	1.8e-16	6800	1
2	$CO_2 \cdot H_2O \leftrightarrow HCO_3^+ + H^-$	7.7e-7	-1000	2
3	$HCO_3^+ \leftrightarrow CO_3^{2-} + H^-$	4.84e-11	-1760	2
4	$HO_2 \leftrightarrow H^+ + O_2^-$	1.6e-5		1
5	$HNO_4 \leftrightarrow H^+ + NO_4^-$	1.0e-5		1
6	$HNO_3 \leftrightarrow H^+ + NO_3^-$	22.0	-1800	1
7	$HONO \leftrightarrow H^+ + NO_2^-$	5.3e-4	1760	1
8	$NH_3 \cdot H_2O \leftrightarrow NH4^+ + OH^-$	1.75e-5	560	1
9	$SO_2 \cdot H_2O \leftrightarrow HSO_3^- + H^+$	1.73e-2	-1940	1
10	$HSO_3^- \leftrightarrow SO_3^{2-} + H^+$	6.22e-8	-1960	1
11	$H_2SO_4 \leftrightarrow HSO_4^- + H^+$	1000		1
12	$HSO_4^- \leftrightarrow SO_4^{2-} + H^+$	1.02e-2	-2700	1
13	$HCHO + H_2O \leftrightarrow CH_2 (OH)_2$	36.0	-4030	1
14	$HCOOH \leftrightarrow HCOO^- + H^+$	1.77e-4	-12	1
15	$CH_3CHO + H_2O \leftrightarrow CH_3CH(OH)_2$	2.46e-2	-2500	1
16	$CH_3COOH \leftrightarrow H^+ + CH_3COO^-$	1.75e-5	-46	1
17	$CHOCOOH \leftrightarrow CHOCOO^- + H^+$	6.6e-4		2
18	$COOHCOOH \leftrightarrow HC_2O_4^- + H^+$	6.4e-2		1
19	$HC_2O_4^- \leftrightarrow C_2O_4^{2-} + H^+$	5.25e-5		1
20	$CH_3COCOOH \leftrightarrow CH_3COCOO^- + H^+$	4.07e-3		2
21	$S7 \leftrightarrow S7^- + H^+$	7.335e-5		3
22[b]	$S3PD \leftrightarrow S3PD^- + H^+$	3.7e-5		3
23[b]	$S5PD \leftrightarrow S5PD^- + H^+$	6.52e-4		3
24[b]	$S7PD \leftrightarrow S7PD^- + H^+$	1.7e-3		3

[a]: References: 1: Ervens et al. (2003); 2: Ervens et al. (2004); 3: Pun et al. (2002)

[b]: See Table IV.1 for molecular definition of S7, S3PD, S5PD, and S7PD

MPMPO to calculate SOA formation. The organic oxidation products in clouds were lumped into existing surrogates in the MPMPO module. Oxalic and pyruvic acids were lumped into surrogate 1 (oxalic acid) of MPMPO. S3PD, S5PD, S7PD, and S10PD were lumped into surrogate 2 (S2, 2-methyl-5-formyl-2, 4-hexadiendioic acid), surrogate 4 (S4, 2-hydroxy-3-isopropyl-5-keto-3-hexenoic acid), surrogate 6 (S6, 3, 5-dimethyl-2-nitro-4-hydroxy-benzoic acid), and surrogate 5 (S5, 2-hydroxy-3-isopropyl-6-keto-heptanal) of MPMPO, respectively. Overall, the aqueous products S3PD, S5PD, S7PD,

79

Table IV.3. Uptake parameters for gas-phase species in AqChem

Species[a]	$K_{H, 298K}$ (M atm^{-1})	$\Delta H/R$ (K)	α	D_g (m^2 s^{-1})	Ref.[b]
CO$_2$	3.11e-2	-2423	2.0e-4	1.55e-5	1
NH$_3$	60.7	-3920	0.04	2.3e-5	1
O$_3$	1.14e-2	-2300	0.05	1.48e-5	1
HO$_2$	9.0e3		0.01	1.04-5	1
OH	25.0	-5280	0.05	1.53e-5	1
H$_2$O$_2$	1.02e5	-6340	0.11	1.46e-5	1
HNO$_3$	2.1e5	-8700	0.054	1.32e-5	1
HONO	49.0	-4880	0.5	1.30e-5	1
HNO$_4$	3.0e4		0.1	1.30e-5	1
SO$_2$	1.24	-3247	3.5e-2	1.28e-5	1
H$_2$SO$_4$	2.1e5		0.07	1.30e-5	1
HCHO	2.5		0.02	1.64e-5	1
CH$_3$OH	220	-5390	0.015	1.16e-5	1
CH$_3$OO	310		3.8e-3	1.35e-5	1
CH$_3$OOH	310		3.8e-3	1.31e-5	1
HCOOH	5530	5630	0.10	1.0e-5	2
CH$_3$CHO	11.4	-6254	0.03	1.22e-5	1
CH$_3$CH$_2$OH	190	-6290	8.2e-3	0.95e-5	1
CH$_2$OHCHO	4.14e4		0.03	1.95e-5	2
CH$_3$COOH	5500	-5890	0.019	1.24e-5	2
COOHCOOH	3.26e6		0.019	1.24e-5	3
CHOCHO	3.0e5		3.8e-3	1.31e-5	2
CHOCOOH	9000		0.1	1.0e-5	2
CH$_3$COCHO	3710		0.023	1.15e-5	2
CH$_3$COCOOH	3.11e5	5100	0.1	1.0e-5	2
S3[c]	6.01e6		0.05	1.0e-5	4,5
S5[c]	3.90e7	.	0.05	1.0e-5	4,5
S7[c]	4.91e6		0.05	1.0e-5	4,5
S10[c]	1.18e6		0.05	1.0e-5	4,5

[a]: N$_2$O$_5$ is assumed to be completely dissolved in water and to form two moles of HNO$_3$.
[b]: References: 1: Ervens et al. (2003); 2: Ervens et al. (2004); 3: Lim et al. (2005); 4: Pun et al. (2002); 5: Aumont et al. (2000).
[c]: See Table IV.1 for molecular definition of S3, S5, S7, and S10.

and S10PD are less volatile than their precursors, as in the treatment used by Gelencser

and Varga (2005). Vapor pressure and K_H estimates for the surrogate species in MPMPO

can be found in Pun et al. (2002) and Griffin et al. (2005).

80
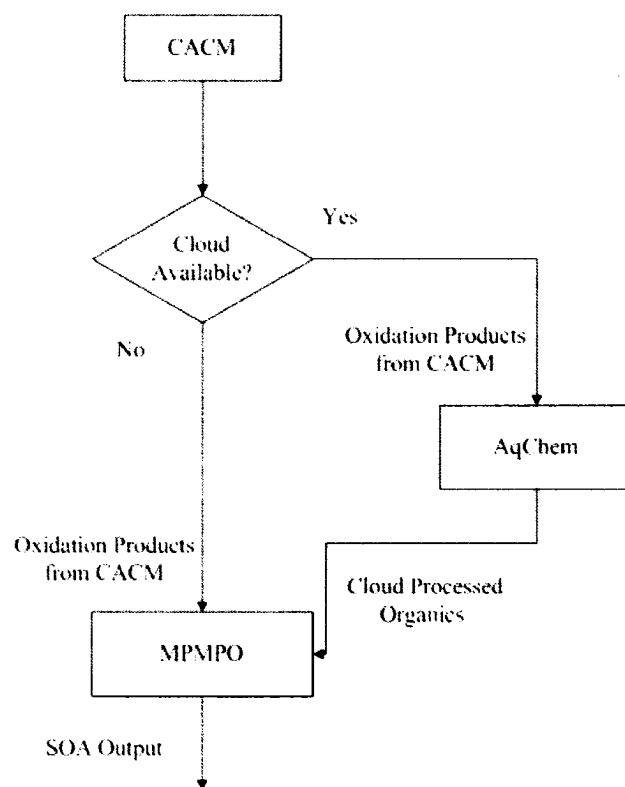
Figure IV.2. Flow diagram for SOA modeling with/without consideration of the aqueous-phase chemistry in clouds.

The kinetic processor KPP2.1 (Damian et al., 2002; Daescu et al., 2003; Sandu et al., 2003) was used to process AqChem and generate the associated numerical codes. A Rosenbrock solver in KPP2.1 was used to solve the differential equations associated with the mechanism (Sandu et al., 1997).

Zero-dimensional Model Simulations

A zero-dimensional model was constructed to investigate potential SOA formation due to irreversible aqueous-phase organic chemistry under scenarios for which cloud is present for three consecutive hours per day (Lim et al., 2005). The zero-dimensional model considers emissions, dry deposition, and gas- and aqueous-phase

81

chemistry for chemical species. The mass balance of the gas- and aqueous-phase species is described by (Pandis and Seinfeld, 1989; Lim et al., 2005)

$$\frac{dC_g}{dt} = Q_g - S_g + \frac{E}{Z} - \frac{vC_g}{Z} - LkC_g + \frac{LkC_a}{K_H RT} \tag{1}$$

$$\frac{dC_a}{dt} = Q_a - S_a + kC_g - \frac{kC_a}{K_H RT} \tag{2}$$

where C_g is the gas-phase concentration (mole L^{-1} of air), C_a is the aqueous-phase concentration (M), Q_g (mole L^{-1} of air sec^{-1}) and Q_a (M sec^{-1}) are the gas-phase and aqueous-phase production rate, respectively, S_g (mole L^{-1} of air sec^{-1}) and S_a (M sec^{-1}) are the gas-phase and aqueous-phase loss rate, respectively, E (mole dm^{-2} sec^{-1}) is the emission rate of the gas-phase species, Z (dm) is the boundary layer height, v (dm sec^{-1}) is the dry deposition velocity, L is the cloud liquid water volume fraction, K_H (M atm^{-1}) is the effective Henry's law constant, R (L atm $mole^{-1}$ K^{-1}) is the ideal gas constant, T (K) is the temperature, and k (sec^{-1}) is the mass transfer coefficient,

$$k = (\frac{a^2}{3D_g} + \frac{4a}{3v\alpha})^{-1} \tag{3}$$

where α is the mass accommodation coefficient, D_g (cm^2 s^{-1}) is the gas-phase diffusion constant, a is the cloud droplet radius (cm), and v is the mean molecular speed (cm s^{-1}).

The zero-dimensional model couples CACM, AqChem, and MPMPO. Emissions and dry deposition of gas-phase species were implemented within the gas-phase chemistry mechanism. As with AqChem, the latest version of CACM with emissions and dry deposition of species was processed by KPP2.1, and a Rosenbrock solver was used for solving the differential equations. If clouds are present, the simulations of gas-phase and aqueous-phase chemistry processes are split every 12 minutes, following the

82

treatment in the three-dimensional model that will be discussed subsequently. If clouds are not present, only gas-phase chemistry is simulated every 12 minutes. At the end of every 12 minutes, MPMPO is called to simulate SOA formation.

For the zero-dimensional model simulation, conditions are based on the study of Lim et al. (2005). The boundary layer height was assumed to be fixed at 1000 meters. Temperature and relative humidity (RH) are 298 K and 75%, respectively, if clouds are not present. Clouds are assumed to be present through the entire boundary layer for hours 13-16 of each day. Cloud water content was assumed to be 0.5 g m^{-3}, with a uniform cloud droplet diameter of 10 μm. Temperature and RH are assumed to be 288 K and 100%, respectively, when clouds are present. In addition, a constant cloud pH of 4.5 was assumed. Photolysis rates were assumed to vary semisinusoidally between hour 6 and hour 18 of each day, with a peak at hour 12.

Two emissions scenarios were studied. Scenario 1 features strong biogenic monoterpene emissions for a rural area, and Scenario 2 features strong anthropogenic emissions of aromatic compounds for an urban area. Emission rates and deposition velocities of gas-phase hydrocarbons were extracted from previous three-dimensional model simulations (Chen et al., 2006; Mao et al., 2006). These are shown in Tables IV.4 and IV.5, respectively. In order to simulate SOA formation in MPMPO, total POA concentrations (fractions of individual POA species are consistent between the two scenarios and are based on those used in Chen et al. (2006)), aerosol water content, and aerosol pH for both scenarios were assumed to be constant at 1.0 μg m^{-3}, 30 μg m^{-3}, and

83

Table IV.4. Twenty-four-hour average emission rates (moles m^{-2} sec^{-1}) for two scenarios used in zero-dimensional model simulations

Species	Emissions for Scenario 1	Emissions for Scenario 2
NO	1.36e-9	3.27e-8
NO_2	1.42e-10	3.63e-9
CO	1.33e-8	3.40e-7
HCHO	1.33e-11	6.73e-10
ALD1 [a]	2.63e-10	1.06e-9
OLEL [a]	1.38e-9	1.49e-9
AROL [a]	5.56e-11	7.18e-10
AROH [a]	6.60e-11	1.33e-9
ISOP [a]	2.64e-9	1.83e-9
TERP [a]	8.30e-10	1.87e-11
ALKL [a]	3.04e-9	1.11e-8
SO_2	5.06e-11	6.38e-9

[a]: ALD1: lumped small-carbon-number aldehydes; OLEL: lumped alkenes C_3-C_6; AROL: lumped low-SOA-yield aromatic species; AROH: lumped high-SOA-yield aromatic species; ISOP: isoprene; TERP: monoterpenes; ALKL: lumped alkanes C_2-C_6.

Table IV.5. Twenty-four-hour average dry deposition velocities (dm sec^{-1}) for two scenarios used in zero-dimensional model simulations

Species	Dry Deposition (urban)	Dry deposition (rural)
NO	9.08e-4	2.52e-3
NO_2	7.45e-4	2.03e-3
O_3	1.46e-3	2.71e-3
H_2O_2	4.77e-3	7.41e-3
NO_3	3.26e-2	1.48e-2
HNO_3	3.41e-2	1.75e-2
HONO	3.94e-3	6.88e-3
N_2O_5	3.00e-2	1.56e-2
CO	1.26e-3	2.83e-3
SO_2	3.82e-3	6.28e-3
HCHO	3.20e-3	6.67e-3
ALD [a]	2.03e-3	4.03e-3
ORA [a]	3.63e-3	6.06e-3
PAN [a]	8.89e-4	1.95-e3

[a]: ALD for general aldehydes, ORA for general organic acids, and PAN for general peroxy acetyl nitrates.

3.0, respectively. This simplified treatment omits considerations of emission, deposition, and size distribution of aerosols. In addition, the zero-dimensional model simulations

84

were performed for four days for each scenario. The first two days were used as initialization days, while the last two days were used for analysis.

Three-dimensional Model Simulation

AqChem was incorporated into the Community Multiscale Air Quality (CMAQ) model version 4.4 with CACM and MPMPO (Chen et al., 2006). In addition, the computationally efficient version of the MPMPO module (Tulet et al., 2006) was used. CMAQ originally employed the RADM aqueous-phase chemistry mechanism, mainly for the purpose of predicting aqueous-phase sulfate formation in grid resolved clouds and/or sub-grid convective clouds (Byun and Ching, 1999). In the CMAQ model, the aqueous-phase chemistry mechanism is called when the liquid water content of clouds exceeds 10^{-5} kg m^{-3}. Cloud droplet diameter was assumed to be 10 μm (Lim et al., 2005). In addition, CMAQ assumes that accumulation mode particles serve as cloud condensation nuclei and Aitken mode particles form interstitial aerosol that can be scavenged by clouds. Therefore, all accumulation mode particles and some fraction of Aitken mode particles are included in the resulting aqueous phase of the hydrometeors. Chemical species (e.g., nitrate, oxalic acid, S3, S5, S7, and S10) of cloud-incorporated particles are also subject to aqueous-phase chemistry. SOA formation due to both the gas-phase oxidation and the aqueous-phase oxidation is distributed between accumulation and Aitken mode particles using the proportion of preexisting OA in these two modes.

CMAQ with CACM and MPMPO was applied previously to an episode (August 3-4, 2004 with spin-up days of August 1-2, 2004) over the eastern United States (Chen et al., 2006). In this study, CMAQ with CACM and MPMPO and with the newly developed AqChem was applied to the same episode to study the significance of SOA

85

formation from the consideration of irreversible aqueous-phase organic chemistry in clouds. Model inputs (e.g., emissions and meteorological fields) and model configurations (e.g., model domain and vertical layers) for this episode are described in Mao et al. (2006) and Chen et al. (2006).

Results

Zero-dimensional Model Simulations

Figure IV.3a shows the SOA predictions from the zero-dimensional model simulation for Scenario 1, which features strong monoterpene emissions for a rural area. Averaged over 48 hours, total SOA prediction considering SOA formation from cloud-phase organic reactions is 5.7 μg m^{-3}, which is approximately 27% higher than the prediction without considering aqueous-phase chemistry in clouds. At the end of simulation, total SOA prediction with aqueous-phase chemistry in clouds is 8.7 μg m^{-3}, which is 32% more than that from the simulation without clouds. Compared to the SOA prediction without consideration of the aqueous-phase chemistry, total SOA prediction with aqueous-phase chemistry increases substantially during the hours 13-16 and hours 37-40, during which clouds are present. This suggests substantial rapid processing of organic compounds in cloud droplets and that such processing leads to formation of SOA.

As shown in Fig. IV.3a, the increase of SOA prediction from aqueous-phase chemistry is due primarily to the increase of SOA formation from S4 and S5 of MPMPO, which is attributed to the oxidation of S5 to form S5PD (lumped to S4) and the oxidation of S10 to form S10PD (lumped to S5) in AqChem, respectively. Because S4 and S5 are less volatile and more soluble than S5 and S10, respectively, more SOA is formed. Both S5 and S10 are surrogates for oxidation products of monoterpenes.

86

a.)

b.)
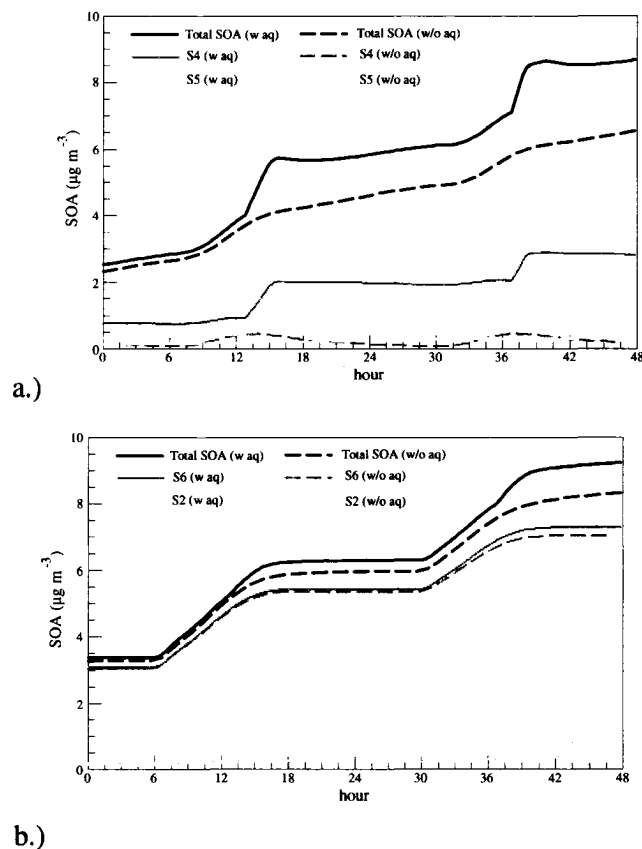
Figure IV.3. SOA predictions from zero-dimensional model simulations: a.) Scenario 1 (S4: SOA of surrogate species 4 of MPMPO; S5: SOA of surrogate species 5 of MPMPO) b.) Scenario 2 (S2: SOA of surrogate species 2 of MPMPO; S6: SOA of surrogate species 6 of MPMPO). "w aq" indicates simulation with consideration of the aqueous-phase organic chemistry in clouds; "w/o aq" indicates simulation without consideration of the aqueous-phase organic chemistry in clouds.

Figure IV.3b shows the SOA production from Scenario 2 using the same zero-dimensional model. Scenario 2 represents an urban environment with strong anthropogenic emissions (e.g., nitrogen oxides (NO_x) and aromatic compounds). If aqueous-phase chemistry in clouds is considered, the SOA concentrations predicted at the end of the simulation period and averaged over 48 hours are 9.23 $\mu g\ m^{-3}$ and 6.33 $\mu g\ m^{-3}$, respectively, which are 11% and 7% higher than that from simulation without

87

consideration of cloud chemistry. Individually, the increase of SOA prediction by considering aqueous-phase organic chemistry is due to the increase of SOA contributions from S2, S6, and, to a smaller extent, S1, which is then attributed to the aqueous-phase conversion of S3, S7, and organic compounds of carbon number less than four. S2, S6, and the majority of S1 are surrogates for oxidation products from aromatic compounds. Based on the aqueous-phase organic chemistry proposed in this study, the effect of aqueous-phase chemistry in clouds on SOA formation is less important for aromatic compounds than it is for monoterpene species.

Three-dimensional Model Simulation

Figure IV.4 shows the difference between 24-hour average SOA predictions at the surface for August 3-4, 2004 (UTC) when the SOA formation from aqueous-phase organic chemistry in cloud droplets is considered and not. In addition, the absolute values of SOA predictions at the surface layer for these two days are also shown if the SOA formation from aqueous-phase organic chemistry in clouds is considered. Consideration of SOA formation from aqueous-phase organic chemistry increases 24-hour average SOA predictions. The maximum difference in 24-hour average SOA predictions within the domain is 0.28 $\mu g/m^3$ for both days. Averaged over the entire domain, the relative increases of 24-hour average SOA predictions with consideration of SOA formation from aqueous-phase organic chemistry in clouds are 8.7% and 8.5% for August 3 and August 4, 2004, respectively.

88
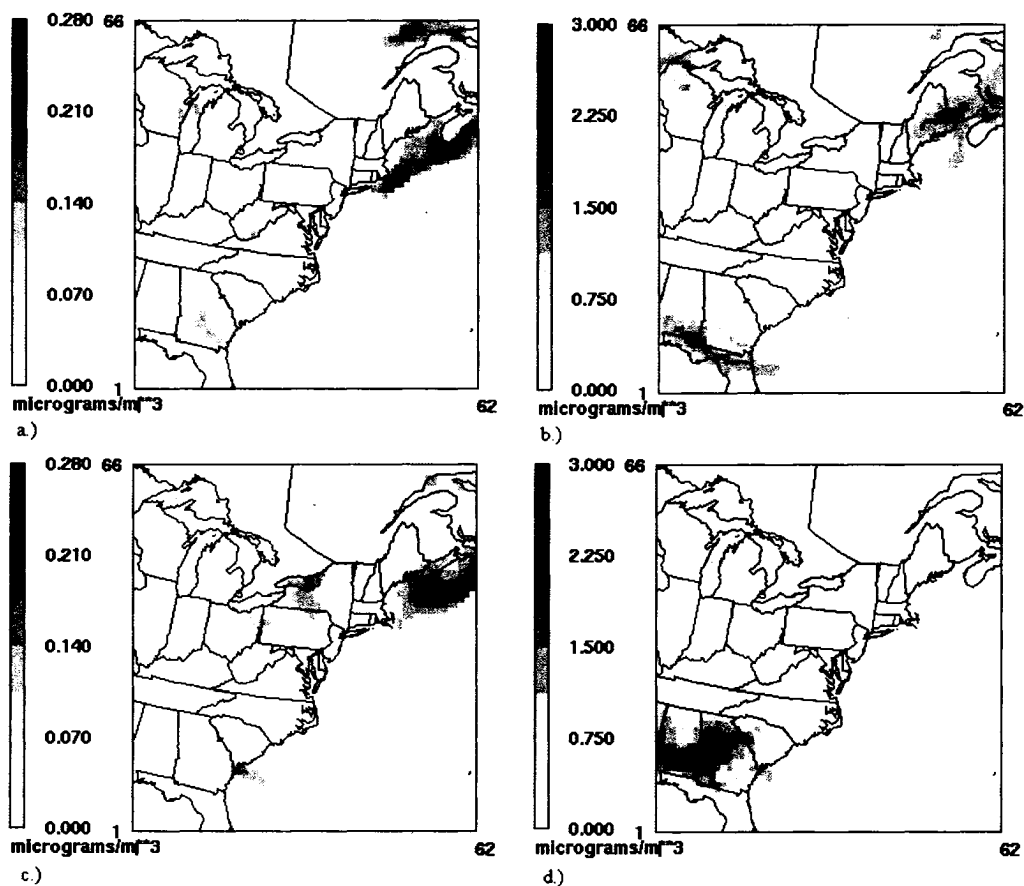
Figure IV.4. Spatial distribution of surface SOA predictions: a.) difference between 24-hour average SOA prediction on August 3, 2004, with/without SOA from aqueous-phase organic chemistry simulation in clouds; b.) 24-hour average SOA prediction on August 3, 2004, with SOA from aqueous-phase organic chemistry simulation in clouds; c.) difference between 24-hour average SOA prediction on August 4, 2004, with/without SOA from aqueous-phase organic chemistry simulation in clouds; d.) 24-hour average SOA prediction on August 4, 2004, with SOA from aqueous-phase organic chemistry simulation in clouds.

The increase of SOA predictions if aqueous-phase organic chemistry is considered is due mainly to the cloud processing of S5 and S10, which leads to the formation of less volatile products. Both S5 and S10 are lumped species for oxidation products of monoterpenes. This is consistent with the fact that the majority of SOA predicted within the domain is from biogenic monoterpenes (Chen et al., 2006).

89

The average relative increase across the domain is smaller than that from the zero-dimensional model simulation for Scenario 1 in which strong monoterpene emissions are considered. This is expected because the zero-dimensional model simulation represents an ideal situation in which a site is influenced by biogenic monoterpene emissions and is exposed to clouds for three hours in the afternoon (12.5% of the time of each day). Examination of the meteorological inputs for the chosen episode indicates that resolved clouds occupy approximately 10-20% of surface area during the episode. In addition, CMAQ internally calculates sub-grid convective clouds. Therefore, on average, each grid has the probability of 10-20% of being exposed to cloud processing, which is close to the cloud exposure time used in the zero-dimensional model. However, locations influenced strongly by monoterpene emissions may not be necessarily exposed to cloud processing. This is believed to be the major reason for a smaller relative SOA increase in the three-dimensional model simulation compared to the zero-dimensional model simulations if SOA formation from aqueous-phase organic chemistry in clouds is considered.

Figure IV.5 indicates the time series of the SOA predictions with or without consideration of SOA formation from the aqueous-phase organic chemistry in clouds at the two sites which have the maximum difference in 24-hour average SOA predictions for August 3 and August 4, 2004, respectively. At these two sites, the relative difference in SOA prediction with or without consideration of SOA formation from aqueous-phase organic chemistry are as high as 36% and 43%, respectively, indicating that accounting

90
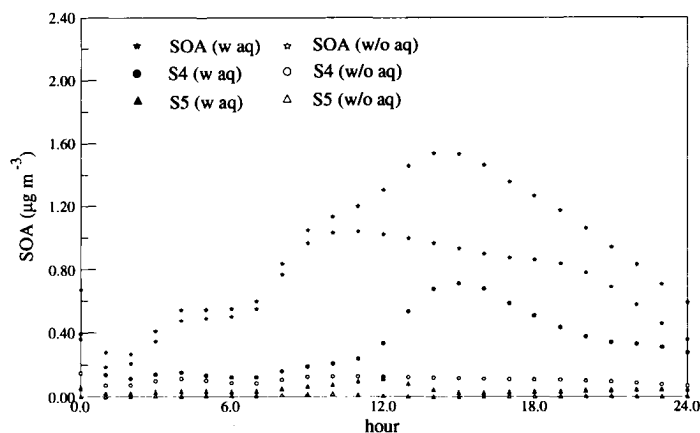
a.)
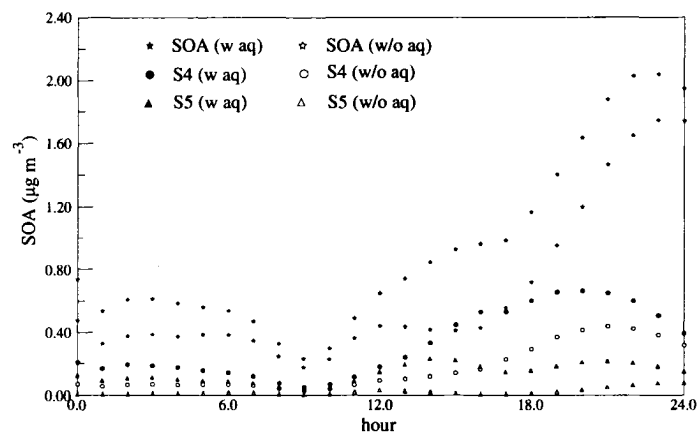
b.)

Figure IV.5. Time profiles of SOA predictions at sites with maximum difference in 24-hour averaged SOA predictions with or without consideration of aqueous-phase organic chemistry in clouds on August 3, 2004 in the northern Gulf of Maine (a.) and August 4, 2004 in the northern Gulf of Maine (b.).

for SOA formation from aqueous-phase organic chemistry in clouds could be important

at these locations. As shown in Fig. IV.5, the increase of SOA formation by considering

aqueous-phase organic chemistry is due mainly to the increase of SOA formation from

S4 and S5, which is again attributed to the aqueous-phase oxidation of S5 and S10, which

91

are surrogates for oxidation products of monoterpenes. This implies that the increase of SOA formation with consideration of aqueous-phase organic chemistry in clouds is due to the cloud processing of monoterpene oxidation products. These two sites are influenced by transport of monoterpene or monoterpene oxidation products from the New England region. In addition, these two sites are also exposed to resolved clouds almost throughout the entire episode. Therefore, SOA formation from aqueous-phase organics can be important when a site is influenced by biogenic monoterpene emissions or products and also exposed to cloud processing for significant time periods.

Figure IV.6 indicates additional SOA formation due to the in-cloud organic chemistry at layer 14 of the modeling domain. In addition, for comparative purposes, the total SOA predictions from the simulations with consideration of SOA formation from aqueous-phase organic chemistry are also shown for layer 14. The CMAQ modeling domain includes 21 vertical layers using a σ-pressure system extending from the surface to 10,000 Pa. Although the actual altitude for layer 14 varies, according to the U.S. standard atmosphere, layer 14 corresponds to the altitude between 1,800 – 2,300 meters. Layer 14 thus roughly represents the lower free troposphere. The maximum additional SOA formation due to aqueous-phase organic chemistry in clouds is 0.25 $\mu g\ m^{-3}$ for both days, only slightly smaller than the maximum difference at the surface. Similar to the surface layer, the increase of SOA predictions is due primarily to cloud processing of gas-phase monoterpene oxidation products, indicating the potential of SOA formation from an aqueous-phase mechanism involving biogenic precursors as suggested by Heald et al. (2006).

92
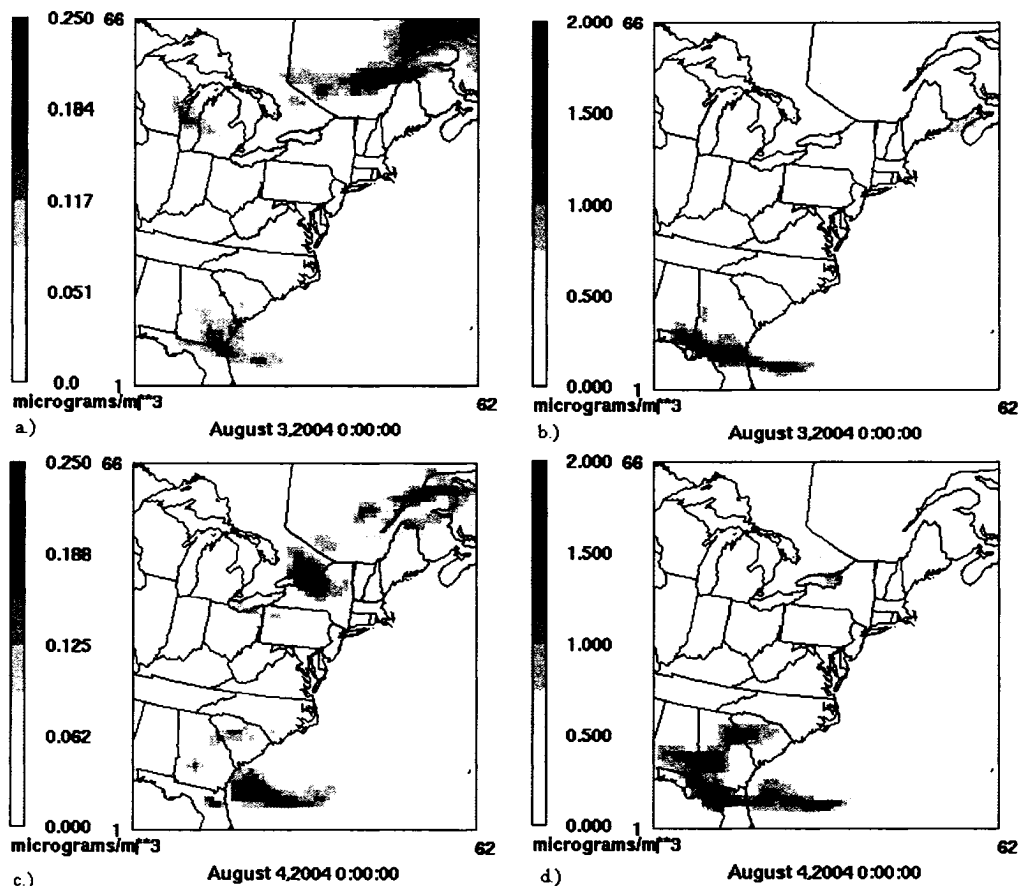
Figure IV.6. Spatial distribution of SOA predictions of layer 14: a.) difference in 24-hour average SOA prediction on August 3, 2004, with/without aqueous-phase organic chemistry simulation in clouds; b.) 24-hour average SOA prediction on August 3, 2004, with aqueous-phase organic chemistry simulation in clouds; c.) difference in 24-hour average SOA prediction on August 4, 2004, with/without aqueous-phase organic chemistry simulation in clouds; d.) 24-hour average SOA prediction on August 4, 2004, with aqueous-phase organic chemistry simulation in clouds.

Averaged across the modeling domain for layer 14, the relative difference in SOA predictions is 18.8% and 15.3 %, respectively for August 3 and August 4, which is much larger than the relative difference at the surface layer. This is due to the fact that less SOA is predicted to form from gas-phase oxidation of organic compounds in the free troposphere (Heald et al., 2005).

93

Discussion

An aqueous-phase chemistry mechanism was developed to study the potential of SOA formation in cloud droplets. The AqChem mechanism incorporates a compact treatment of hydrogen-oxygen and sulfur chemistry but treats in more detail organic chemistry based on recent work of Aumont et al. (2000), Ervens et al. (2004), and Lim et al. (2005) in an effort to represent the potential irreversible organic reactions that may lead to low-volatility products. AqChem was coupled to the existing CACM mechanism and MPMPO module. Zero-dimensional model simulations indicated that consideration of SOA formation from organic chemistry in cloud droplets could lead to increases of SOA prediction by approximately 27% and 7% for a rural scenario with strong monoterpene emissions and an urban scenario with strong aromatic compound emissions, respectively. Three-dimensional simulations showed an average of 8-9% increase in the SOA predictions at the surface when the aqueous-phase organic chemistry in clouds is considered. However, the relative increase of SOA prediction at certain locations could be much higher than the domain-wide, averaged surface increase. Overall, based on the proposed AqChem, the modeling work in this study suggests that SOA formation due to aqueous-phase organic chemistry in clouds could be important at locations that are strongly influenced by monoterpene emissions and where clouds are present for significantly long time, especially in the afternoon when photochemistry is strongest.

A key limitation of this study is the simple treatment of organic reactions in the aqueous phase for organic compounds of carbon number greater than four. Herrmann et al. (2005) presented a much more detailed treatment of organic chemistry in their aqueous-phase chemistry mechanism, although such a mechanism is probably too

94

complex for incorporation into three-dimensional models. More laboratory studies are also needed to characterize the mechanism of aqueous-phase reactions, especially for intermediate gas-phase oxidation products, which are soluble in water and have the potential to lead to low-volatility products.

Another limitation is the lack of treatment of potentially reversible oligomerization processes, especially for small molecules like glyoxal and methyl glyoxal (Hastings et al., 2005; Loeffler et al., 2006). These processes are not included because of a current lack of a quantitative description.

In addition, future studies need to consider the aqueous-phase processing of organic compounds in deliquescent particles. Unlike short-lived clouds, deliquescent particles provide additional time for processing organic compounds and could be more likely to lead to SOA, despite having significantly smaller water contents (Claeys et al., 2004). Such treatment would need to consider the interactions of different ions and molecules in the particles, which poses significantly more difficulty than processes in the cloud droplets.

Despite these limitations, the method used in this study provides a framework to study SOA formation due to aqueous-phase processing of organic compounds and underscores the potential of SOA formation via cloud processing of organic compounds. New findings of aqueous-phase organic chemistry should be incorporated into this framework when such quantitative information becomes available.

95

CHAPTER V

CONCLUSIONS AND FUTURE RESEARCH

Conclusions

In this thesis, CACM and MPMPO were updated with new chemistry for α-pinene, β-pinene, and d-limonene. The updated CACM and MPMPO were incorporated into the CMAQ model, and the CMAQ model with CACM and MPMPO was applied for the eastern US for August 3-4, 2004. In addition, the aqueous-phase chemistry mechanism AqChem was developed. AqChem allows certain organic compounds to undergo irreversible reactions with OH in cloud droplets to form less volatile products. AqChem was also incorporated into CMAQ with CACM and MPMPO and applied to the eastern US for August 3-4, 2004.

The main conclusions of thesis are:

1.) CMAQ with CACM and MPMPO predicted similar levels of SOA formation on average when compared to CMAQ with CB-IV and SORGAM. Both models predicted that SOA formation in the eastern US during August 3-4, 2004 was dominated by that from monoterpenes. Compared with measurements, both models significantly under predicted OA in the atmosphere, indicating missing sources of SOA in both models. Despite the similarity, the response of SOA formation to domain-wide NO_x emissions and temperature variations differs between CMAQ with CACM/MPMPO and CMAQ with CB-IV/SORGAM. The response from CMAQ with CACM/MPMPO is

96

more similar to that observed in chamber experiments. In addition, the spatial and temporal distributions of SOA from CMAQ with CACM/MPMPO are less varied than those from CMAQ with CB-IV/SORGAM.

2.) Simulation of the same episode using CMAQ with CACM, MPMPO, and AqChem indicated that the maximum contribution of SOA formation from irreversible reactions of organics in clouds was 0.28 $\mu g/m^3$ for 24-hour average concentrations and 0.60 $\mu g/m^3$ for one-hour average concentrations at certain surface locations. On average, domain-wide surface SOA predictions during August 3-4, 2004 are increased by 8.6% when irreversible, in cloud processing of organics is considered. At an upper layer corresponding to an altitude of approximately 1800 ~ 2300 meters in the lower free troposphere, the SOA predictions are increased by approximately 17% if irreversible reactions of organics in clouds is accounted for. The increase of SOA predictions within the domain is due to the cloud processing of oxidation products from monoterpenes. Contribution from irreversible cloud processing of isoprene oxidation products is negligible.

Future Research

During the course of conducting the research presented in this thesis, several new experimental and modeling studies appeared in the literature showing new data and/or mechanisms for SOA formation. The CACM (Griffin et al., 2002), MPMPO (Griffin et al., 2003), and AqChem modules provide a good framework to incorporate new experimental findings on SOA formation pathways. Future research should be targeted to update the CACM, MPMPO, and AqChem modules to improve their predicative capability on SOA formation. Potential research endeavors could include:

97

1.) SOA formation from isoprene. Isoprene was thought not to lead to SOA formation a decade ago (Pandis et al., 1992). New isoprene photooxidation experiments, however, showed that SOA yields are 1-2% at high NO_x levels (Kroll et al., 2005a) and ~3% at low NO_x levels (Kroll et al., 2006). Incorporation of such SOA yield data into global air quality models showed clearly the importance of SOA formation from isoprene (Henze and Seinfeld, 2006; Donkelaar et al., 2007; Liao et al., 2007). The current version of CACM includes a gas-phase chemistry mechanism for isoprene that does not lead to significant SOA. This mechanism should be updated to include products that contribute to SOA; corresponding updates to MPMPO will be necessary.

2.) SOA formation from sesquiterpenes. Although SOA formation from sesquitepenes has been recognized widely (Hoffmann et al., 1997; Griffin et al., 1999; Bonn and moortgat, 2003; Jaoui and Kamens, 2003; Jaoui et al., 2004; Vizuete, et al., 2004), a lack of emission inventory for sesquiterpenes prohibited realistic consideration of SOA formation from sesquiterpenes in three-dimensional air quality models. Fortunately, the latest development of a biogenic VOC emissions model (Model of Emissions of Gases and Aerosols from Nature, MEGAN (Guenther et al., 2006)) allows calculation of sesquiterpene emissions from pine trees (Helmig et al., 2007). Pine trees have significant sesquiterpene emissions (Helmig et al., 2007) and cover ~18% of contiguous US forest areas, which is more than any other genus (Smith et al., 2004). Sesquiterpene emissions from other biogenic sources are likely to be added to MEGAN in the near future. The availability of sesquiterpene emissions provides an opportunity to incorporate SOA formation from sesquiterpenes in three-dimensional air quality models.

98

CACM as well as MPMPO should be upgraded to describe SOA formation from representative sesquiterpene species.

3.) Incorporation of new SOA yield data from photooxidation experiments under low-NO$_x$ conditions. New chamber photooxidation experiments showed that SOA formation increases when the ratio of VOC to NO$_x$ decreases (Presto et al., 2005; Song et al., 2005). Ng et al. (2007) provided a comprehensive dataset regarding SOA formation under low-NO$_x$ conditions for major aromatic compounds (i.e., m-xylene, toluene, and benzene). Compared with previous data for these species (e.g., Odum et al., 1996; 1997), SOA yield under low-NO$_x$ conditions was found to be substantially higher. CACM and MPMPO should be upgraded to reflect this new development.

4.) SOA formation from small carbonyls. Although the exact mechanism for SOA formation from small carbonyls (e.g., glyoxal) is still not known, laboratory experiments and field measurements have already suggested the possibility of SOA formation from these compounds (e.g., Kroll et al., 2005b; Liggio et al., 2005; Matsunaga et al., 2005; Volkamer et al., 2006). It is likely that SOA formation from small carbonyls is related to potential polymerization processes that lead to enhanced SOA formation (Jang et al., 2002; Kalberer et al., 2004). Given the unknown mechanism, an empirical parameterization of SOA formation from potential oligermization and/or polymerization of small carbonyls could be pursued within the CACM, MPMPO, and AqChem modules as in Morris et al. (2006).

5.) Improvement of POA emission inventory. The ultimate goal of improving SOA modeling is to improve the prediction of OA in the atmosphere. POA is a substantial part of OA in the atmosphere. In addition, SOA formation also depends on

99

the availability of POA in the atmosphere through the absorptive mechanism. It is known that emission inventories are associated with the largest uncertainties in current three-dimensional air quality models (Seigneur et al., 1997; Russell and Dennis, 2000). In addition, recent work from Robinson et al. (2007) calls for a redefinition of POA and semi-volatile organic emissions because POA itself is often semivolatile. Upon being emitted, species associated with POA can evaporate partially with atmospheric dilution, creating substantial amounts of low-volatility gas-phase material. Photochemical processing of these materials provides an additional SOA formation pathway (Robinson et al., 2007). If this phenomenon is validated and widely accepted, MPMPO should be revised to reflect this because in the current MPMPO module, POA is assumed to be non-volatile.

In summary, understanding and modeling of SOA and OA in the atmosphere is an ongoing challenging research topic and will remain so in the coming years. It is recommended that the CACM, MPMPO, and AqChem modules are constantly updated in the future to reflect new developments in the understanding of SOA formation in the atmosphere.

LIST OF REFERENCES

Arey, J., S.M. Aschmann, E.S.C. Kwok, and R. Atkinson (2001), Alkyl nitrate, hydoxyalkyl nitrate, and hydroxycarbonyl formation from the NO_x-air photooxidations of C_5-C_8 n-alkanes, *Journal of Physical Chemistry A*,105, 1020–1027.

Atkinson, R. (1997), Gas-phase tropospheric chemistry of volatile organic compounds: 1. Alkanes and alkenes, *Journal of Physical Chemistry Reference Data*, 26, 215-290.

Atkinson, R., and J. Arey (2003), Gas-phase tropospheric chemistry of biogenic volatile organic compounds: A review, *Atmospheric Environment*, 37, S197-S219.

Atkinson, R., and S.M. Aschmann (1993), Atmospheric chemistry of the monoterpene reaction products nopinone, camphelinone, and 4-acetyl-1-methylcyclohexene, *Journal of Atmospheric Chemistry*, 16, 337-348.

Aumont, B., S. Madronich, I. Bey, and G.S. Tyndall (2000), Contribution of secondary VOC to the composition of aqueous atmospheric particles: A modeling approach, *Journal of Atmospheric Chemistry*, 35, 59-75.

Barthelmie, R.J., and S.C. Pryor (1999), A model mechanism to describe oxidation of monoterpenes leading to secondary organic aerosol: 1.α-pinene and β-pinene, *Journal of Geophysical Research*, 104, 23,657-23,699.

Blando, J.D., R.J. Porcja, T.H. Li, D. Bowman, P.J. Lioy, and B.J. Turpin (1998), Secondary formation and the Smoky Mountain organic aerosol: An examination of aerosol polarity and functional group composition during SEAVS, *Environmental Science & Technology*, 32, 604-613.

Blando, J.D., and B.J. Turpin (2000), Secondary organic aerosol formation in cloud and fog droplets: A literature evaluation of plausibility, *Atmospheric Environment*, 34, 1623-1632.

Bond, T.C., D.G. Streets, K.F. Yarber, S.M. Nelson, J.H. Woo, and Z. Klimont (2004), A technology-based global inventory of black and organic carbon emissions from combustion, *Journal of Geophysical Research*, 109, D14203, doi:10.1029/2003JD003697.

101

Bonn, B., and G.K. Moortgat (2003), Sesquiterpene ozonolysis: Origin of atmospheric new particle formation from biogenic hydrocarbons, *Geophysical Research Letters*, 30, 1585, doi:10.1029/2003GL017000.

Bonn, B., G. Schuster, and G.K. Moortgat (2002), Influence of water vapor on the process of new particle formation during monoterpene ozonolysis, *Journal of Physical Chemistry A*, 106, 2869-2881.

Byun, D.W., and J.K.S. Ching (1999), *Science algorithms of the EPA Models-3 Community Multi-scale Air Quality (CMAQ) modeling system*, Report EPA/600/R-99/030, Office of Research and Development, United States Environmental Protection Agency, Washington, D.C.

Cabada, J.C., S.N. Pandis, R. Subramanian, A.L. Robinson, A. Polidori, and B.J. Turpin (2004), Estimating the secondary organic aerosol contribution to $PM_{2.5}$ using the EC tracer method, *Aerosol Science and Technology*, 38, S1, 140-155.

Cai, X., and R.J. Griffin (2005), The size-dependent influence of surface tension on the absorptive partitioning of semi-volatile organic compounds, *Journal of Atmospheric Chemistry*, 50, 139-158.

Calogirou, A., N.R. Jensen, C.J. Nielsen, D. Kotzias, and J. Hjorth (1999), Gas-phase reactions of nopinone, 3-isopropenyl-6-oxo-heptanal, and 5-methyl-5-vinyl-tetrahydrofuran-2-ol with OH, NO_3 and ozone, *Environmental Science and Technology*, 33, 453-460.

Carlton, A.G., B.J. Turpin, H.J. Lim, K.E. Altieri, and S. Seitzinger (2006), Link between isoprene and secondary organic aerosol (SOA): Pyruvic acid oxidation yields low volatility organic acids in clouds, *Geophysical Research Letters*, 33, L06822, doi:10.1029/2005GL025374.

Carter, W.L. (1990), A detailed mechanism for gas-phase atmospheric reactions of organic compounds, *Atmospheric Environment*, 24A, 481-518.

Chameides, W.L., R.W. Lindsay, J. Richardson, and C.S. Kiang (1988), The role of biogenic hydrocarbons in urban photochemical smog - Atlanta as a case study, *Science*, 241,1473-1475.

Charlson, R.J., S.E. Schwartz, J.M. Hales, R.D. Cess, J.A. Jr. Coakley, J.E. Hansen, and D.J. Hofmann (1992), Climate forcing by anthropogenic aerosols, *Science*, 255, 423-430.

Chen, J., and R.J. Griffin (2005), Modeling secondary organic aerosol formation from oxidation of α-pinene, β-pinene, and d-limonene, *Atmospheric Environment*, 39, 7731-7744.

Chen, J., H. Mao, R.W. Talbot, and R.J. Griffin (2006), Application of the CACM and MPMPO modules using the CMAQ model for the eastern United States, *Journal of Geophysical Research*, 111, D23S25, doi:10.1029/2006JD007603.

Chen, J., R.J. Griffin, A. Grini, and P. Tulet (2007), Modeling secondary organic aerosol formation through cloud processing of organic compounds, *Atmospheric Chemistry and Physics Discussion*, 7, 8951-8982.

Chow, J.C., J.G. Watson, E.M. Fujita, Z. Lu, D.R. Lawson, and L.L. Ashbaugh (1994), Temporal and spatial variations of $PM_{2.5}$ and PM_{10} aerosol in the Southern California Air Quality Study, *Atmospheric Environment*, 28, 2061 − 2080.

Claeys, M., W. Wang, A.C. Ion, I. Kourtchev, A. Gelencser, and W. Maenhaut (2004), Formation of secondary organic aerosols from isoprene and its gas-phase oxidation products through reaction with hydrogen peroxide, *Atmospheric Environment*, 38, 4093-4098.

Code of Federal Register, 2006 Title 40 Part 50, National Ambient Air Quality Standards for Particulate Matter.

Colville, C.J., and R.J. Griffin (2004a), The roles of individual oxidants in secondary organic aerosol formation from Δ^3-carene: 1. Gas-phase chemical mechanism, *Atmospheric Environment*, 38, 4001-4012.

Colville, C.J., and R.J. Griffin (2004b), The roles of individual oxidants in secondary organic aerosol formation from Δ^3-carene: 2. SOA formation and oxidant contribution, *Atmospheric Environment*, 38, 4013-4023.

Cordes, W., and J. Rarey (2002), A new method for the estimation of the normal boiling point of nonelectrolyte organic compounds, *Fluid Phase Equilibria*, 201, 409-433.

Cottrell, L.D., R.J. Griffin, L.D. Ziemba, P.J. Beckman, B.C. Sive, R.W. Talbot, J.L. Jimenez, J.T. Jayne, D.R. Worsnop, and Q. Zhang (2007), Submicron particles at Thompson Farm during ICARTT measured using aerosol mass spectrometry: Organic aerosol and relationships to estimates of photochemical age, *Journal of Geophysical Research*, submitted.

Daescu, D., A. Sandu, and G.R. Carmichael (2003), Direct and adjoint sensitivity analysis of chemical kinetic systems with KPP: II Numerical validations and applications, *Atmospheric Environment*, 37, 5097-5114.

Damian, V., A. Sandu, M. Damian, F. Potra and G.R. Carmichael (2002), The Kinetic preprocessor KPP – A software environment for solving chemical kinetics, *Computers & Chemical Engineering*, 26, 1567-1579.

Decesari, S., M.C. Facchini, S. Fuzzi, and E. Tagliavini (2000), Characterization of water-soluble organic compounds in atmospheric aerosol: A new approach, *Journal of Geophysical Research*, 105, 1481-1489.

DeGouw, J.A., et al. (2005), The budget of organic carbon in a polluted atmosphere: Results from the New England Air Quality Study in 2002, *Journal of Geophysical Research*, 110, D16305, doi:10.1029/2004JD005623.

Dennis, R.L., D.W. Byun, J.H. Novak, K.J. Galluppi, C.J. Coats, and M.A. Vouk (1996), The next generation of integrated air quality modeling: EPA's Models-3, *Atmospheric Environment*, 30, 1925-1938.

Docherty, K.S., and P.J. Ziemann (2003), Effects of stabilized Criegee intermediate and OH radical scavengers on aerosol formation from reactions of β-pinene with O_3, *Aerosol Science and Technology*, 37, 877-891.

Donkelaar, A.V., R.V. Martin, R.J. Park, C.L. Heald, T.M. Fu, H. Liao, and A. Guenther (2007), Model evidence for a significant source of secondary organic aerosol from isoprene, *Atmospheric Environment*, 41, 1267-1274.

104

Dutot, A., J. Rude, and B. Aumont (2003), Neural network method to estimate the aqueous rate constants for the OH reactions with organic compounds, *Atmospheric Environment*, 37, 269-276.

EPA (2005), *Technical support document for the final Clean Air Interstate Rule: Air quality modeling*, US EPA Office of Air Quality Planning and Standards, RTP, NC. Available at http://www.epa.gov/air/interstateairquality/pdfs/finaltech02.pdf

Ervens, B., et al. (2003), CAPRAM 2.4 (MODAC mechanism): An extended and condensed tropospheric aqueous phase mechanism and its application, *Journal of Geophysical Research*, 108, 4426, doi:10.1029/2002JD002202.

Ervens B., G. Feingold, G. J. Frost, and S. M. Kreidenweis (2004), A modeling study of aqueous production of dicarboxylic acids: 1. Chemical pathways and speciated organic mass production, *Journal of Geophysical Research*, 109, D15205, doi:10.1029/2003JD004387.

Fredenslund, A., J. Gmehling, and P. Rasmussen (1977), *Vapor-Liquid Equilibrium Using UNIFAC*, Elsevier, New York.

Gelencser, A., and Z. Varga (2005), Evaluation of the atmospheric significance of multiphase reactions in atmospheric secondary organic aerosol formation, *Atmospheric Chemistry and Physics*, 5, 2823-2831.

Gery, M.W., G.Z. Whitten, J.P. Killus, and M.C. Dodge (1989), A photochemical kinetics mechanism for urban and regional scale computer modeling, *Journal of Geophysical Research*, 94, 12,925-12,956.

Glasius M., A. Calogirou, N.R. Jensen, J. Hjorth, and C.J. Nielsen (1997), Kinetic study of gas-phase reactions of pinonaldehyde and structurally related compounds, *International Journal of Chemical Kinetics*, 29, 527-533.

Glasius, M., M. Lahaniati, A. Calogirou, D. Di Bella, A.R. Jensen, J. Hjorth, D. Kotzias, and B.R. Larsen (2000), Carboxylic acids in secondary aerosols from oxidation of cyclic monoterpenes by ozone, *Environmental Science & Technology*, 23, 1001-1010.

Griffin, R.J., D.R. Cocker III, R.C. Flagan, and J.H. Seinfeld (1999a), Organic aerosol formation from the oxidation of biogenic hydrocarbons, *Journal of Geophysical Research*, 104, 3555-3567.

Griffin, R.J., D.R. Cocker III, J.H. Seinfeld, and D. Dabdub (1999b), Estimate of global atmospheric organic aerosol from oxidation of biogenic hydrocarbons, *Geophysical Research Letters*, 26, 2721-2724.

Griffin, R.J., D. Dabdub, M.J. Kleeman, M.P. Fraser, G.R. Cass, and J.H. Seinfeld (2002a), Secondary organic aerosol, 3. Urban/regional scale model of size-and composition-resolved aerosols, *Journal of Geophysical Research*, 107, D17, 4334, doi:10.1029/2001JD000544.

Griffin, R.J., D. Dabdub, and J.H. Seinfeld (2005), Development and initial evaluation of a dynamic species-resolved model for gas-phase chemistry and size-resolved gas/particle partitioning associated with secondary organic aerosol formation, *Journal of Geophysical Research*, 110, D05304, doi:10.1029/2004JD005219.

Griffin, R.J., D. Dabdub, and J.H. Seinfeld (2002b), Secondary organic aerosol, 1. Atmospheric chemical mechanism for production of molecular constituents, *Journal of Geophysical Research*, 107, 4332, doi: 10.1029/2001JD000541.

Griffin, R.J., C.A. Johnson, R.W. Talbot, H. Mao, R.S. Russo, Y. Zhou, and B.C. Sive (2004), Quantification of ozone formation metrics at Thompson Farm during the New England Air Quality Study (NEAQS) 2002, *Journal of Geophysical Research*, 109, D24302, doi:10.1029/2004JD005344.

Griffin, R. J., K. Nguyen, D. Dabdub, and J.H. Seinfeld (2003), A coupled hydrophobic-hydrophilic model for predicting secondary organic aerosol formation, *Journal of Atmospheric Chemistry*, 44, 171-190.

Guenther, A., C. Geron, T. Pierce, B. Lamb, P. Harley, and R. Fall (2000), Natural emissions of non-methane volatile organic compounds, carbon monoxide, and oxides of nitrogen from North America, *Atmospheric Environment*, 34, 2205-2230.

Guenther, A., T. Karl, P. Harley, C. Wiedinmyer, P.I. Palmer, and C. Geron (2006), Estimate of global terrestrial isoprene emissions using MEGAN (Model of Emissions of Gases and Aerosols from Nature), *Atmospheric Chemistry and Physics*, 6, 3181-4055.

Hakola, H., J. Arey, S.M. Aschmann, and R. Atkinson (1994), Product formation from the gas-phase reactions of OH radicals and O_3 with a series of monoterpenes, *Journal of Atmospheric Chemistry*, 18, 75-102.

Hallquist, M., I., Wangberg, and E. Ljungstrom (1997), Atmospheric fate of carbonyl oxidation products originating from α-pinene and Δ^3-carene: Determination of rate of reaction with OH and NO_3 radicals, UV absorption cross sections, and vapor pressures, *Environmental Science & Technology*, 31, 3166-3172.

Hallquist, M., I. Wangberg, E. Ljungstrom, I. Barnes, K. Becker (1999), Aerosol and product yields from NO_3 radical-initiated oxidation of selected monoterpenes, *Environmental Science & Technology*, 33, 553-559.

Hansen, D.A., E.S. Edgerton, B.E. Hartsell, J.J. Jansen, N. Kandasamy, G.M. Hidy, and C.L. Blanchard (2003), The Southeastern Aerosol Research and Characterization Study: Part 1 – Overview, *Journal of Air & Waste Management Association*, 53, 1460-1471.

Hastings, W.P., C.A. Koehler, E.L. Bailey, and D.O. DeHaan (2005), Secondary organic aerosol formation by glyoxal hydration and oligomer formation: Humidity effects and equilibrium shifts during analysis, *Environmental Science & Technology*, 39, 8728-8735.

Heald, C.L., et al. (2006), Concentrations and sources of organic carbon aerosols in the free troposphere over North America, *Journal of Geophysical Research*, 111, D23S47, doi: 1029/2006JD007705.

Heald, C.L., D.J. Jacob, R.J. Park, L.M. Russell, B.J. Huebert, J.H. Seinfeld, H. Liao, and R.J. Weber (2005), A large organic aerosol source in the free troposphere missing from current models, *Geophysical Research Letters*, 32, L18809, doi: 10.1029/2005GL023831.

Helmig, D., J. Ortega, T. Duhl, D. Tanner, A. Guenther, P. Harley, C. Wiedinmyer, J. Milford, and T. Sakulyanontvittaya (2007), Sesquiterpene emissions from pine trees – identifications, emission rates and flux estimates for the contiguous United States, *Environmental Science & Technology*, 41, 1545-1553.

Henze, D.K., and J.H. Seinfeld (2006), Global secondary organic aerosol from isoprene oxidation, *Geophysical Research Letters*, 33, L09812, doi:10.1029/2006GL025976.

Herrmann, H., A. Tilgner, P. Barzaghi, Z. Majdik, S. Gligorovski, L. Poulain, and A. Monod (2005), Towards a more detailed description of tropospheric aqueous phase organic chemistry: CAPRAM 3.0, *Atmospheric Environment*, 39, 4351-4363.

Hoffmann, T., R. Bandur, U. Marggraf, and M. Linscheid (1998), Molecular composition of organic aerosols formed in the α-pinene/O_3 reaction: Implication for new particle formation processes, *Journal of Geophysical Research*, 103, 25,569-25,578.

Hoffmann, T., J.R. Odum, F. Bowman, D. Collins, D. Klockow, R.C. Flagan, and J.H. Seinfeld (1997), Formation of organic aerosols from the oxidation of biogenic hydrocarbons, *Journal of Atmospheric Chemistry*, 26, 189-222.

Jacobson, M.Z. (2001), Global direct radiative forcing due to multicomponent anthropogenic and natural aerosols, *Journal of Geophysical Research*, 106, D2, 1551-1568.

Jang, M., N.M. Czoschke, S. Lee, and R.M. Kamens (2002), Heterogeneous atmospheric aerosol production by acid-catalyzed particle-phase reactions, *Science*, 298, 814-817.

Jaoui, M., and R.M. Kamens (2001), Mass balance of gaseous and particulate products analysis from α-pinene/NO_x/air in the presence of natural sunlight, *Journal of Geophysical Research*, 106, 12541-12558.

Jaoui, M., and R.M. Kamens (2003), Gas and particulate distribution from the photooxidation of α-humulene in the presence of NO_x, natural atmospheric air and sunlight, *Journal of Atmospheric Chemistry*, 46, 29-54.

Jaoui, M., K.G. Sexton, and R.M. Kamens (2004), Reaction of α-cedrene with ozone: mechanism, gas and particulate products distribution, *Atmospheric Environment*, 38, 2709-2725.

Jayne, J.T., D.C. Leard, X. Zhang, P. Davidovits, K.A. Smith, C.E. Kolb, and D.R. Worsnop (2000), Development of an Aerosol Mass Spectrometer for size and composition analysis of submicron particles, *Aerosol Science and Technology*, 33, 49-70.

108

Jenkin, M.E. (2004), Modeling the formation and composition of secondary organic aerosol from α- and β-pinene ozonolysis using MCM v3, *Atmospheric Chemistry and Physics*, 4, 1741-1757.

Jenkin, M.E., S.M. Saunders, and M.J. Pilling (1997), The tropospheric degradation of volatile organic compounds: A protocol for mechanism development, *Atmospheric Environment*, 31, 81-104.

Jenkin, M.E., S.M. Saunders, V. Wagner, and M.J. Pilling (2003), Protocol for the development of the master chemical mechanism, MCMv3 (part B): Tropospheric degradation of aromatic volatile organic compounds, *Atmospheric Chemistry and Physics*, 3, 181-193.

Jenkin, M.E., D.E. Shallcross, J.N. Harvey (2000), Development and application of a possible mechanism for the generation of *cis*-pinic acid from the ozonolysis of α- and β-pinene, *Atmospheric Environment*, 34, 2837-2850.

Johnson, D., S.R. Utembe, and M.E. Jenkin (2006), Simulating the detailed chemical composition of secondary organic aerosol formed on a regional scale during the TORCH 2003 campaign in the southern UK, *Atmospheric Chemistry and Physics*, 6, 419-431.

Jones, A., L. Roberts, and A. Slingo (1994), A climate model study of indirect radiative forcing by anthropogenic sulphate aerosols, *Nature*, 370, 450-453.

Kalberer, M., et al. (2004), Identification of polymers as major components of atmospheric organic aerosols, *Science*, 303, 1659-1662.

Kamens, R., and M. Jaoui (2001), Modeling aerosol formation from α-pinene + NO_x in the presence of natural sunlight using gas-phase kinetics and gas-particle partitioning theory, *Environmental Science & Technology*, 35, 1394-1405.

Kamens, R., M. Jang, C. Chien, and K. Leach (1999), Aerosol formation from the reaction of α-pinene and ozone using a gas-phase kinetics-aerosol partitioning model, *Environmental Science & Technology*, 33, 1430-1438.

Kanakidou, M., et al. (2005), Organic aerosol and global climate modeling: A review, *Atmospheric Chemistry and Physics*, 5, 1053-1123.

109

Kanakidou, M., K. Tsigaridis, F.J. Dentener, and P.J. Crutzen (2000), Human-activity-enhanced formation of organic aerosols by biogenic hydrocarbon oxidation, *Journal of Geophysical Research*, 105, 9243-9254.

Kawamura, K., and K. Ikushima (1993), Seasonal changes in the distribution of dicarboxylic acids in the urban atmosphere, *Environmental Science & Technology*, 27, 2227-2235.

Kelly, N.A., and R.F. Gunst (1990), Response of ozone to changes in hydrocarbon and nitrogen oxide concentrations in outdoor smog chambers filled with Los Angeles air, *Atmospheric Environment*, 24A, 2991-3005.

Keywood, M.D., V. Varutbangkul, R. Bahreini, R.C. Flagan, and J.H. Seinfeld (2004), Secondary organic aerosol formation from the ozonolysis of cycloalkenes and related compounds, *Environmental Science & Technology*, 38, 4157-4164.

Koch, S., R. Winterhalter, E. Uherek, A. Kolloff, P. Neeb, and G.K. Moortgat (2000), Formation of new particles in the gas-phase ozonolysis of monoterpenes, *Atmospheric Environment*, 34, 4031-4042.

Kroll, J. H., N. L. Ng, S. M. Murphy, R. C. Flagan, and J. H. Seinfeld (2005a), Secondary organic aerosol formation from isoprene photooxidation under high-NO_x conditions, *Geophysical Research Letters*, 32, L18808, doi:10.1029/2005GL023637.

Kroll, J. H., N. L. Ng, S. M. Murphy, R. C. Flagan, and J. H. Seinfeld (2006), Secondary organic aerosol formation from isoprene photooxidation, *Environmental Science & Technology*, 40, 1869–1877.

Kroll, J.H., N.L. Ng, S.M. Murphy, V. Varutbangkul, R.C. Flagan, and J.H. Seinfeld (2005b), Chamber studies of secondary organic aerosol growth by reactive uptake of simple carbonyl compounds, *Journal of Geophysical Research*, 110, D23207, doi:10.1029/2005JD006004.

Kwok, E.S.C., and R. Atkinson (1995), Estimation of hydroxyl radical reaction rate constants for gas-phase organic compounds using a structure-reactivity relationship: an update, *Atmospheric Environment*, 29, 1685-1695.

110

Lamb, B., D. Gay, T. Pierce (1993), A biogenic hydrocarbon emission inventory for the U.S.A using a simple forest canopy model, *Atmospheric Environment A*, 27, 1673-1690.

Larsen, B.R., D. Di Bella, M. Glasius, R. Winterhalter, N.R. Jensen, J. Hjorth (2001), Gas-phase OH oxidation of monoterpenes: gaseous and particulate products, *Journal of Atmospheric Chemistry*, 38, 231-276.

Liao H., D.K. Henze, J.H. Seinfeld, S. Wu, and L.J. Mickley (2007), Biogenic secondary organic aerosol over the United States: Comparisons of climatological simulations with observations, *Journal of Geophysical Research*, 112, D06201, doi:10.1029/2006JD007813.

Liggio, J., S.M. Li, and R. McLaren (2005), Heterogeneous reactions of glyoxal on particulate matter: Identification of acetals and sulfate esters, *Environmental Science & Technology*, 39, 1532-1541.

Lim H.J., A.G. Carlton, and B. J. Turpin (2005), Isoprene forms secondary organic aerosol through cloud processing: Model simulations, *Environmental Science & Technology*, 39, 4441 – 4446.

Liousse, C., J.E. Penner, C. Chuang, J.J. Walton, H. Eddleman, and H. Cachier (1996), A global three-dimensional study of carbonaceous aerosols, *Journal of Geophysical Research*, 101, 19411-19432.

Loeffler, K.W., C.A. Koehler, N.M. Paul, and D.O. DeHaan (2006), Oligomer formation in evaporating aqueous glyoxal and methyl glyoxal solutions, *Environmental Science & Technology*, 40, 6318-6323.

Malm, W.C. (1989), Atmospheric haze: Its sources and effects on visibility in rural areas of the continental United States, *Environmental Monitoring and Assessment*, 12, 203-225.

Malm, W.C., J.F. Sisler, D. Huffman, R.A. Eldred, and T.A. Cahill (1994), Spatial and seasonal trends in particle concentration and optical extinction in the United States, *Journal of Geophysical Research*, 99, 1347-1370.

Mao, H., R. Talbot, D. Troop, R. Johnson, S. Businger, and A.M. Thompson (2006), Smart balloon observations over the North Atlantic: Part II — O_3 data analysis and modeling, *Journal of Geophysical Research*, 111, D23S56, doi:10.1029/2005jd006507.

Martin, L.R., and T.W. Good (1991), Catalyzed oxidation of sulfur dioxide in solution: the iron-manganese synergism, *Atmospheric Environment*, 25A, 2395-2399.

Matsunaga, S.N., C. Wiedinmyer, A.B. Guenther, J.J. Orlando, T. Karl, D.W. Toohey, J.P. Greenberg, and Y. Kajii (2005), Isoprene oxidation products are a significant aerosol component, *Atmospheric Chemistry and Physics Discussion*, 5, 11143-11156.

McDonald, J.D., B. Zielinska, E.M. Fujita, H.C. Sagebiel, J.C. Chow, and J.G. Watson (2000), Fine particle and gaseous emission rates from residential wood combustion, *Environmental Science & Technology*, 34, 2080-2091.

Morris, R.E., B. Koo, A. Guenther, G. Yarwood, D. McNally, T.W. Tesche, G. Tonnesen, J. Boylan, and P. Brewer (2006), Model sensitivity evaluation for organic carbon using two multi-pollutant air quality models that simulate regional haze in the southeastern United States, *Atmospheric Environment*, 40, 4960-4972.

Myrdal, P.B., and S.H. Yalkowsky (1997), Estimating pure component vapor pressures of complex organic molecules, *Industrial and Engineering Chemistry Research*, 36, 2494-2499.

Murphy, D.M., D.S. Thomson, and M.J. Mahoney (1998), In situ measurements of organics, meteoritic material, mercury, and other elements in aerosols at 5 to 19 kilometers, *Science*, 282, 1664-1669.

NARSTO (2004), *Particulate Matter Assessment for Policy Makers: A NARSTO Assessment*, edited by P. McMurry, M. Shepherd, and J. Vickery, Cambridge University Press, Cambridge, England.

Nenes, A., S.N. Pandis, and C. Pilinis (1998), ISORROPIA: a new thermodynamic equilibrium model for multiphase multi-component inorganic aerosol, *Aquatic Geochemistry*, 4, 123-152.

112

Ng, N.L., J.H. Kroll, A.W.H. Chan, P.S. Chhabra, R.C. Flagan, and J.H. Seinfeld (2007), Secondary organic aerosol formation from m-xylene, toluene, and benzene, *Atmospheric Chemistry and Physics Discussions*, 7, 4085-4126.

Noziere, B., and I. Barnes (1998), Evidence for the formation of a PAN analogue of pinonic structure and investigation of its thermal stability, *Journal of Geophysical Research*, 103, 25,587 – 25,597.

Noziere, B., I. Barnes, and K. Becker (1999), Product study and mechanisms of the reactions of α-pinene and of pinonaldehyde with OH radicals, *Journal of Geophysical Research*, 104, 23,645 – 23,658.

Odum, J.R., T. Hoffmann, F. Bowman, D. Collins, R.C. Flagan, and J.H. Seinfeld (1996), Gas/particle partitioning and secondary organic aerosol yields, *Environmental Science & Technology*, 30, 2580-2585.

Odum, J.R., T.P. Jungkamp, R.J. Griffin, R.C. Flagan, and J.H. Seinfeld (1997), The atmospheric aerosol-forming potential of whole gasoline vapor, *Science*, 276, 96-99.

Pandis, S.N., R.A. Harley, G.R. Cass, and J.H. Seinfeld (1992), Secondary organic aerosol formation and transport, *Atmospheric Environment*, Part A, 26A, 2269-2282.

Pankow, J.F. (1994a), An absorption model of the gas/aerosol partitioning of organic compounds in the atmosphere, *Atmospheric Environment*, 28, 185-188.

Pankow, J.F. (1994b), An absorption model of the gas/aerosol partitioning involved in the formation of secondary organic aerosol, *Atmospheric Environment*, 28, 189-193.

Pankow, J.F., J.H. Seinfeld, W.E. Asher, and G.B. Erdakos (2001), Modeling the formation of secondary organic aerosol. 1. Application of theoretical principles to measurements obtained in the α-pinene/, β-pinene/, sabinene/, Δ3-carene/, and cyclohexene/ozone systems, *Environmental Science & Technology*, 35, 1164-1172.

Pope, C.A., and D.W. Dockery (2006), Health effects of fine particulate air pollution: Lines that connect, *Journal of Air and Waste Management Association*, 56, 709-742.

Presto, A.A., K.E. Huff Hartz, and N.M. Donahue (2005), Secondary organic aerosol production from terpene ozonolysis: 2. Effect of NO_x concentrations, *Environmental Science & Technology*, *39*, 7046-7054.

Pun, B.K., R.J. Griffin, C. Seigneur, and J.H. Seinfeld (2002), Secondary organic aerosol: II. Thermodynamic model for gas/particle partitioning of molecular constituents, *Journal of Geophysical Research*, 107, 4333, doi: 10.1029/2001JD000542.

Pun, B.K., S.Y. Wu, C. Seigneur, J.H. Seinfeld, R.J. Griffin, and S.N. Pandis (2003), Uncertainties in modeling secondary organic aerosols: Three-dimensional modeling studies in Nashville/Western Tennessee, *Environmental Science & Technology*, 37, 3647-3661.

Robinson, A.L., N.M. Donahue, M.K. Shrivastava, E.A. Weitkamp, A.M. Sage, A.P. Grieshop, T.E. Lane, J.R. Pierce, and S.N. Pandis (2007), Rethinking organic aerosols: Semivolatile emissions and photochemical aging, *Science*, 315, 1259-1262.

Russell, A., and R. Dennis (2000), NARSTO critical review of photochemical models and modeling, *Atmospheric Environment*, 34, 2283-2324.

Salcedo, D., et al. (2005), Characterization of ambient aerosols in Mexico City during the MCMA-2003 campaign with Aerosol Mass Spectrometry: Results from the CENICA supersite, *Atmospheric Chemistry and Physics*, 6, 925-946.

Sandu, A., D. Daescu, and G.R. Carmichael (2003), Direct and adjoint sensitivity analysis of chemical kinetic systems with KPP: I – Theory and software tools, *Atmospheric Environment*, 37, 5083-5096.

Sandu, A., J.G. Verwer, J.G. Blom, E.J. Spee, G.R. Carmichael, and F.A. Potra (1997), Benchmarking stiff ODE solvers for atmospheric chemistry problems II: Rosenbrock methods, *Atmospheric Environment*, 31, 3459-3472.

Saunders, S.M., M.E. Jenkin, R.G. Derwent, and M.J. Pilling (2003), Protocol for the development of the Master Chemical Mechanism, MCM v3 (Part A): Tropospheric degradation of non-aromatic volatile organic compounds, *Atmospheric Chemistry and Physics*, 3, 161-180.

Saxena, P., and L.M. Hildemann (1996), Water-soluble organics in atmospheric particles: A critical review of the literature and application of thermodynamics to identify candidate compounds, *Journal of Atmospheric Chemistry*, 24, 57-109.

Schell, B., I. J. Ackermann, H. Hass, F. S. Binkowski, and A. Ebel (2001), Modeling the formation of secondary organic aerosol within a comprehensive air quality model system, *Journal of Geophysical Research*, 106, 28,275-28,294.

Schwartz, S.E. (1986), Mass-transport considerations pertinent to aqueous-phase reactions of gases in liquid-water clouds, in *Chemistry of Multiphase Atmospheric Systems*, edited by W. Jaeschke, Springer, New York, 1986.

Seigneur, C. (2001), Current status of air quality models for particulate matter, *Journal of Air & Waste Management Association*, 51, 1508-1521.

Seinfeld, J.H., G.B. Erdakos, W.E. Asher, J.F. Pankow (2001), Modeling the formation of secondary organic aerosol (SOA). 2. The predicted effects of relative humidity on aerosol formation in the α-pinene/, β-pinene/, sabinene/, Δ^3-carene/, and cyclohexene-ozone systems, *Environmental Science & Technology*, 35, 1806-1817.

Seinfeld, J.H., and S.N. Pandis (1998), *Atmospheric Chemistry and Physics From Air Pollution to Climate Change*, John Wiley, New York.

Seinfeld, J.H., and J.F. Pankow (2003), Organic atmospheric particulate material, *Annual Review Physical Chemistry*, 54, 121-140.

Shah, S.D., D.R. Cocker III, J.W. Miller, and J.M. Norbeck (2004), Emission rates of particulate matter and elemental and organic carbon from in-use diesel engines, *Environmental Science & Technology*, 38, 2544-2550.

Smith, W.B., P. Miles, J. Vissage, and S. Pugh (2004), *Forest resources of the United States, 2002*, General technical report, NC-241; U.S. Forest Service North Central Research Station, St. Paul, MN.

Song, C., K. Na, and D.R. Cocker III (2005), Impact of the hydrocarbon to NO_x ratio on secondary organic aerosol formation, *Environmental Science & Technology*, 39, 3143-3149.

115

Stockwell, W.R., P. Middleton, J.S. Chang, and X. Tang (1990), The second generation regional acid deposition model chemical mechanism for regional air quality modeling, *Journal of Geophysical Research*, 95, 16,343-16,367.

Streets, D. G. et al. (2007), Air quality during the 2008 Beijing Olympic Games, *Atmospheric Environment*, 41, 480-492.

Sullivan, A.P., R.J. Weber, A.L. Clements, J.R. Turner, M.S. Bae, and J.J. Schauer (2004), A method for on-line measurement of water-soluble organic carbon in ambient aerosol particles: Results from an urban site, *Geophysical Research Letters*, 31, L13105, doi:10.1029/2004GL019681.

Takekawa, H., H. Minoura, and S. Yamazaki (2003), Temperature dependence of secondary organic aerosol formation by photo-oxidation of hydrocarbons, *Atmospheric Environment*, 37, 3413-3424.

Talbot, R., H. Mao, and B. Sive (2005), Diurnal characteristics of surface level O_3 and other important trace gases in New England, *Journal of Geophysical Research*, 110, D09307, doi:10.1029/2004JD005449.

Tanner, R.L., W.J. Parkhurst, M.L. Valente, and W.D. Philips (2004), Regional composition of $PM_{2.5}$ aerosols measured at urban, rural, and "background" sites in the Tennessee valley, *Atmospheric Environment*, 38, 3143-3153.

Tulet, P., A. Grini, R.J. Griffin, and S. Petitcol (2006), ORILAM-SOA: A computationally efficient model for predicting secondary organic aerosols in 3D atmospheric models, *Journal of Geophysical Research*, D23208, doi:10.1029/2006JD007152.

Turpin, B.J., and H.J. Lim (2001), Species contributions to $PM_{2.5}$ mass concentrations: revisiting common assumptions for estimating organic mass, *Aerosol Science and Technology*, 35, 602-610.

Turpin, B.J., P. Saxena, and E. Andrews (2000), Measuring and simulating particulate organics in the atmosphere: Problems and prospects, *Atmospheric Environment*, 34, 2983-3013.

116

Vizuete, W., V. Junquera, and D.T. Allen (2004), Sesquiterpene emissions and secondary organic aerosol formation potentials for Southeast Texas, *Aerosol Science and Technology*, 38, 167-181.

Volkamer, R., J.L. Jimenez, F. S. Martini, K. Dzepina, Q. Zhang, D. Salcedo, L.T. Molina, D.R. Worsnop, and M.J. Molina (2006), Secondary organic aerosol formation from anthropogenic air pollution: Rapid and higher than expected, *Geophysical Research Letters*, 33, L17811, doi:10.1029/2006GL026899.

Vutukuru, S., R.J. Griffin, and D. Dabdub (2006), Simulation and analysis of secondary organic aerosol dynamics in the South Coast Air Basin of California, *Journal of Geophysical Research*, 111, D10S12, doi: 10.1029/2005JD006139.

Wangberg, I., I. Barnes, and K.H. Becker (1997), Product and mechanistic study of the reactions of NO_3 radicals with α-pinene, *Environmental Science & Technology*, 31, 2130-2135.

Warneck, P. (1999), The relative importance of various pathways for the oxidation of sulfur dioxide and nitrogen dioxide in sunlit continental fair weather clouds, *Physical Chemistry Chemical Physics*, 1, 5471-5483.

Warneck, P. (2003), In-cloud chemistry opens pathway to the formation of oxalic acid in the marine atmosphere, *Atmospheric Environment*, 37, 2423-2427.

Winterhalter, R., P. Neeb, D. Grossmann, A. Kolloff, O. Horie, and G. Moortgat (2000), Products and mechanism of the gas-phase reaction of ozone with β-pinene, *Journal of Atmospheric Chemistry*, 35, 165-197.

Yao, X., M. Fang, and C.K. Chan (2002), Size distributions and formation of dicarboxylic acids in atmospheric particles, *Atmospheric Environment*, 36, 2099-2107.

Yu, J., D.R. Cocker III, R.J. Griffin, R.C. Flagan, and J.H. Seinfeld (1999), Gas-phase ozone oxidation of monoterpenes: Gaseous and particulate products, *Journal of Atmospheric Chemistry*, 34, 207-258.

117

Yu, S.C., R. Dennis, P.V. Bhave, and B.K. Eder (2004), Primary and secondary organic aerosols over the United States: estimates on the basis of observed organic carbon (OC) and elemental carbon (EC), and air quality modeled primary OC/EC ratios, *Atmospheric Environment*, 38, 5257-5268.

Zaveri, R. (1997), Development and evaluation of a comprehensive tropospheric chemistry model for regional and global application, dissertation, Virginia Polytechnic Institute and State University, Blacksburg, Virginia.

Zhang, Y., B. Pun, K. Vijayaraghavan, S.-Y. Wu, C. Seigneur, S. Pandis, M. Jacobson, A. Nenes, and J.H. Seinfeld (2004a), Development and application of the Model of Aerosol Dynamics, Reaction, Ionization, and Dissolution (MADRID), *Journal of Geophysical Research*, 109, D01202, doi:10.1029/2003JD003501.

Zhang, Y., B. Pun, S. Wu, K. Vijayaraghavan, and C. Seigneur (2004b), Application and evaluation of two air quality models for particulate matter for a Southeastern U.S. episode, *Journal of Air & Waste Management Association*, 54, 1478-1493.

Ziemann, P.J. (2002), Evidence for low-volatility diacyl peroxides as a nucleating agent and major component of aerosol formed from reactions of O_3 with cyclohexene and homologous compounds, *Journal of Physical Chemistry A*, 106, 4390-4402.

Ziemba, L.D., E.V. Fischer, R.J. Griffin, and R.W. Talbot (2007), Aerosol acidity in northern New England: Temporal trends and source region analysis, *Journal of Geophysical Research*, 112, D10S22, doi:10.1029/2006JD007605.

APPENDICES

APPENDIX A

GAS-PHASE OXIDATION MECHANISMS FOR α-PINENE, β-PINENE, AND d-LIMONENE

Table A.1. Oxidation mechanism for α-pinene (k_i refers to the rate constant of reaction i)

Num.	Reactants	Products	Rate constant [b] $(cm^3 \ molecule^{-1} \ s^{-1})$	Ref./ Note
1A	APIN + OH	$RO_2101 + RO_2T$	1.21E-11 × EXP(444/T)	1
2A	APIN + NO₃	$RO_2102 + RO_2T$	1.19E-12 × EXP(490/T)	1
3A	APIN + O₃	$0.2RO_2103 + 0.2CO + 0.8OH + 0.05UR101 + 0.15PINA + 0.15H_2O_2 + 0.33RO_2104 + 0.27RO_2105 + 0.8 RO_2T$	1.01E-15 × EXP(-732/T)	1
4A	APIN + O	0.75UR103 + 0.25NOPI	3.2E-11	1
5A	$RO_2101 + NO$	$0.2AP101 + 0.6PINA + 0.8NO_2 + 0.8HO_2 + 0.2KETH + 0.2HCHO$	8.8E-13 × EXP(180.2/T)	2
6A	$RO_2101 + RO_2T$	$0.7PINA + HO2 + 0.3UR107 + RO_2T + O_2$	1.82E-13 × EXP(416/T)	2
7A	$RO_2101 + HO_2$	0.8PINA + 0.2KETH + 0.2HCHO + OOH1	4.1E-13 × EXP(790/T)	2
8A	$RO_2102 + NO$	$0.6PINA + 1.825NO_2 + 0.175AP102 + 0.225KETH + 0.225HCHO + 0.4HO_2$	k_5	
9A	$RO_2102 + RO_2T$	$0.795PINA + 0.795NO_2 + 0.135AP101 + 0.07AP102 + RO_2T +O_2$	k_6	
10A	$RO_2102 + HO_2$	$0.6PINA + 0.825NO_2 + 0.175AP102 + 0.225KETH + 0.225HCHO + 0.225HO_2 + 0.175OOH1 + 0.825OOH2$	k_7	
11A	$RO_2103 + NO$	$CF(101)AP103 + CF(102)NRPA + CF(102)HO_2 + CF(102)NO_2$	1.05E-12 × EXP(180.2/T)	2,a
12A	$RO_2103 + RO_2T$	$NRPA + HO_2 + RO_2T + O_2$	k_6	
13A	$RO_2103 + HO_2$	NRPA + OOH1	k_7	
14A	$RO_2104 + NO$	$NO_2 + RO_2108 + RO_28 + 2RO_2T$	k_5	
15A	$RO_2104 + RO_2T$	$0.7RO_2108 + 0.7RO_28 + 0.3RP102 + 2.4RO_2T + O_2$	k_6	
16A	$RO_2104 + HO_2$	$RO_2108 + RO_28 + OOH2 + 2RO_2T$	k_7	

120

Table A.1. Continued

17A	$RO_2105 + NO$	$HCHO + NO_2 + RO_2109 + RO_2T$	k_5	
18A	$RO_2105 + RO_2T$	$0.8HCHO + 0.8RO_2109 + 0.10UR105 + 0.05RP103 + 0.05UR108 + 1.8RO_2T + O_2$	k_6	
19A	$RO_2105 + HO_2$	$HCHO + RO_2109 + OOH2 + RO_2T$	k_7	
20A	$PINA + hv$	$CO + HO_2 + RO_2103$	$=J_{ALD2}$	3
21A	$PINA + OH$	$0.8RO_2106 + 0.2 RO_2104 + H_2O + RO_2T$	9.1E-11	4
22A	$PINA + NO_3$	$RO_2106 + HNO_3 + RO_2T$	5.4E-14	4
23A	$RO_2106 + NO$	$RO_2103 + NO_2 + CO_2 + RO_2T$	$1.11E-11 \times EXP(180.2/T)$	2
24A	$RO_2106 + NO_2 + M$	$PAN101 + M$	Refer to reference	3
25A	$PAN101$	$RO_2106 + NO_2 + RO_2T$	Refer to reference	3
26A	$RO_2106 + RO_2T$	$0.2UR101 + 0.8RO_2103 + 0.8CO_2 + 1.8RO_2T + O_2$	5.0E-12	2
27A	$RO_2106 + HO_2$	$UR101 + O_3$	$4.3E-13 \times EXP(1040/T)$	2
28A	$NRPA + hv$	$CO + HO_2 + RO_2108 + RO_2T$	$=J_{ALD2}$	3
29A	$NRPA + OH$	$0.8RO_2107 + 0.2RO_2104 + RO_2T + H_2O$	k_{21}	
30A	$NRPA + NO_3$	$RO_2107 + RO_2T + HNO_3$	k_{22}	
31A	$RO_2107 + NO$	$NO_2 + CO_2 + RO_2108 + RO_2T$	k_{23}	
32A	$RO_2107 + NO_2 + M$	$PAN102 + M$	k_{24}	
33A	$PAN102$	$RO_2107 + NO_2 + RO_2T$	k_{25}	
34A	$RO_2107 + RO_2T$	$0.2UR102 + 0.8CO_2 + 0.8RO_2108 + 1.8RO_2T + O_2$	k_{26}	
35A	$RO_2107 + HO_2$	$UR102 + O_3$	k_{27}	
36A	$RO_2108 + NO$	$CF(103)AP104 + CF(104)KETH + CF(104)NO_2 + CF(104)HO_2$	$1.24E-12 \times EXP(180.2/T)$	2,a
37A	$RO_2108 + RO_2T$	$KETH + HO_2 + RO_2T + O_2$	k_6	
38A	$RO_2108 + HO_2$	$KETH + OOH1$	k_7	
39A	$RO_2109 + NO$	$CO_2 + NO_2 + RO_2108 + RO_2T$	k_{23}	
40A	$RO_2109 + NO_2 + M$	$PAN103 + M$	k_{24}	
41A	$PAN103$	$RO_2109 + NO_2 + RO_2T$	k_{25}	

121

Table A.1. Continued

42A	$RO_2109 + RO_2T$	$0.3RP101 + 0.1UR104 + 0.6CO_2 + 0.6RO_2108 + 1.6RO_2T + O_2$	k_{26}	
43A	$RO_2109 + HO_2$	$UR104 + O_2$	k_{27}	
44A	$AP101 + OH$	$PINA + NO_2 + H_2O$	5.63E-12	5
45A	$AP102 + OH$	$RO_2108 + NO_2 + H_2O + RO_2T$	6.86E-12	5
46A	$AP103 + OH$	$NRPA + NO_2 + H_2O$	2.53E-12	5
47A	$AP104 + OH$	$KETH + NO_2 + H_2O$	2.02E-12	5
48A	$RP101 + OH$	$UR104 + O_3 - HO_2$	2.62E-11	5
49A	$RP102 + OH$	$UR106 + O_3 - HO_2$	2.36E-11	5
50A	$RP103 + OH$	$UR105 + O_3 - HO_2$	2.66E-11	5

[a]CF(101) – CF(104) are calculated based on Arey et al. (2001). [b]Rate constant references: 1. Atkinson (1997); 2. Jenkin et al. (1997); 3. Griffin et al. (2002a); 4. Glasius et al. (1997); 5. Kwok and Atkinson (1995).

Table A.2. Chemical species in the α-pinene oxidation mechanism.

Term	Description
	Reactive, fully integrated species
APIN	α-pinene
PINA	Pinonaldehyde
NRPA	Norpinonaldehyde
AP101	2-nitrato-3-hydroxy-pinane
AP102	2-nitrato-3-oxo-pinane
AP103	2,2-dimethyl-3-acetyl-cyclobutyl-methyl-nitrate
AP104	2,2-dimethyl-3-acetyl-cyclobutyl-nitrate
PAN101	peroxy 2,2-dimethyl-3-acetyl-cyclobutyl-acetyl-nitrate
PAN102	peroxy 2,2-dimethyl-3-acetyl-cyclobutyl-formyl-nitrate
PAN103	peroxy 2,2-dimethyl-3-formylmethyl-cyclobutyl-formyl-nitrate
RP101	pinalic-3-acid
RP102	1-hydroxy-pinonaldehyde
RP103	10-hydroxy-pinonaldehyde
	Nonreacting, fully integrated species
UR101	pinonic acid
UR102	norpinonic acid
UR103	2,3-pinane-epoxide
UR104	pinic acid
UR105	10-hydroxy-pinonic acid
UR106	1-hydroxy-pinonic acid
UR107	2,3-dihydroxy-pinane
UR108	2-(2,2-dimethyl-3-formylmethyl-cyclobutyl)-2-keto-acetaldehyde
	Reactive, organic pseudo-steady species
RO$_2$101	hydroxy alkyl peroxy radical from oxidation of α-pinene (2-peroxy-3-hydroxy-pinane)
RO$_2$102	nitrato alkyl peroxy radical from oxidation of α-pinene (65% is 2-peroxy-3-nitrato-pinane, 35% is 2-nitrato-3-peroxy-pinane)
RO$_2$103	cyclic keto alkyl peroxy radical from oxidation of α-pinene (C$_4$ cycle, 1-methyl peroxy, 2,2-dimethyl, 3-acetyl)
RO$_2$104	cyclic keto aldehydic peroxy radical from oxidation of α-pinene (C$_4$ cycle, 1-peroxy, 1-acetyl, 2,2-dimethyl, 3-formylmethyl)
RO$_2$105	cyclic keto alkyl peroxy radical from oxidation of α-pinene (C$_4$ cycle, 1-(1-keto-ethyl peroxy), 2,2-dimethyl, 3-formylmethyl)
RO$_2$106	acyl peroxy radical from aldehydic H abstraction of pinonaldehyde
RO$_2$107	acyl peroxy radical from aldehydic H abstraction of norpinonaldehyde
RO$_2$108	cyclic keto alkyl peroxy radical from oxidation of α-pinene and β-pinene (C$_4$ cycle, 1-peroxy, 2,2-dimethyl, 3-acetyl)
RO$_2$109	acyl peroxy radical from oxidation of α-pinene and β-pinene (C$_4$ cycle, 1-formyl peroxy, 2,2-dimethyl, 3-formylmethyl)

Table A.3. Oxidation mechanism for β-pinene. (k_i refers to the rate constant of reaction i)

Num.	Reactants	Products	Rate constant [b] $(cm^3\ molecule^{-1}\ s^{-1})$	Ref./ Note
1B	BPIN + OH	$RO_2201 + RO_2T$	2.38E-11 × EXP(357/T)	1
2B	BPIN + NO$_3$	$RO_2202 + RO_2T$	2.51E-12	1
3B	BPIN + O$_3$	$0.51NOPI + 0.11ACID + 0.03CO + 0.03H_2O + 0.84HCHO + 0.35H_2O_2 + 0.33RO_2203 + 0.33OH + 0.16 ALKM + 0.16CO_2 + 0.33\ RO_2T$	1.5E-17	1
4B	BPIN + O	$0.75UR201 + 0.25\ NOPI$	2.7E-11	1
5B	$RO_2201 + NO$	$CF(201)AP201 + CF(202)NOPI + CF(202)HO_2 + CF(202)HCHO + CF(202)NO_2$	8.8E-13 × EXP(180.2/T)	2,a
6B	$RO_2201 + RO_2T$	$0.3UR202 + 0.7NOPI + 0.7HO_2 + 0.7HCHO + RO_2T + O_2$	1.82E-13 × EXP(416/T)	2
7B	$RO_2201 + HO_2$	$NOPI + HCHO + OOH1$	4.1E-13 × EXP(790/T)	2
8B	$RO_2202 + NO$	$0.57NOPI + 1.31NO_2 + 0.57HCHO + 0.17AP202 + 0.17HO_2 + 0.26UR203$	k_5	
9B	$RO_2202 + RO_2T$	$0.318NOPI + 0.058NO_2 + 0.318HCHO + 0.28AP201 + 0.142AP202 + 0.26UR203 + 0.102HO_2 + RO2T$	k_6	
10B	$RO_2202 + HO_2$	$0.83NOPI + 0.83NO_2 + 0.83HCHO + 0.17AP202 + 0.17OOH1 + 0.83OOH2$	k_7	
11B	NOPI + OH	$RO_2203 + H_2O + RO_2T$	1.43E-11	3
12B	$RO_2203 + NO$	$RO_2109 + NO_2 + RO_2T$	1.05E-12 × EXP (180.2/T)	2,c
13B	$RO_2203 + RO_2T$	$0.35UR204 + 0.3UR205 + 0.35RO_2109 + 1.35RO_2T$	k_6	
14B	$RO_2203 + HO_2$	$RO_2109 + OOH2 + RO_2T$	k_7	
15B	AP201 + OH	$NOPI + HCHO + NO_2 + H2O$	4.82E-12	4
16B	AP202 + OH	$NOPI + CO_2 + NO_2 + H2O$	6.92E-12	4

[a]CF(201) and CF(202) are calculated based on Arey et al. (2001). [b]Rate constant references: 1. Atkinson (1997); 2. Jenkin et al. (1997); 3. Atkinson and Aschmann (1993); 4. Kwok and Atkinson (1995); [c]See α-pinene oxidation mechanism (Table A.1) for reactions of RO$_2$109.

124

Table A.4. Chemical species in the β-pinene oxidation mechanism.

Term	Description
	Reactive, fully integrated species
BPIN	β-pinene
NOPI	nopinone
AP201	2-nitrato-10-hydroxy-pinane
AP202	2-formyl-2-nitrato-6-dimethyl-norpinane
	Nonreactive, fully integrated species
UR201	2,10-pinane-epoxide
UR202	2,10-hydroxy-pinane
UR203	2,10-dinitrato-pinane
UR204	3-hydroxy-nopinone
UR205	3-oxo-nopinone
	Reactive, pseudo-steady state species
RO_2201	hydroxy alkyl peroxy radical from oxidation of β-pinene (2-peroxy-10-hydroxy-pinane)
RO_2202	nitrato alkyl peroxy radical from oxidation of β-pinene (80% is 2-peroxy-10-nitrato-pinane; 20% is 2-nitrato-10-peroxy-pinane)
RO_2203	keto alkyl peroxy radical from oxidation of nopinone (3-peroxy-2-norpinone)

See Table A.2 for products formed from reactions of RO_2109.

125

Table A.5. Oxidation mechanism for d-limonene. (k_i refers to the rate constant of reaction i)

Num.	Reaction	Products	Rate constant [b] (cm^3 molecule^{-1} s^{-1})	Ref. Note
1L	DLMN + OH	0.6RO$_2$301 + 0.4 RO$_2$302 + RO$_2$T	1.71E-10	1
2L	DLMN + NO$_3$	0.6RO$_2$303 + 0.4 RO$_2$304 + RO$_2$T	1.22E-11	1
3L	DLMN + O$_3$	0.033EDLM + 0.069H$_2$O$_2$ + 0.134RO$_2$305 + 0.133RO$_2$306 + 0.033UR301+ 0.698OH + 0.267 RO$_2$307 + 0.431CO + 0.236LMKT+ 0.036ACID + 0.2HCHO + 0.164 RO$_2$308 + 0.698 RO$_2$T	2.00E-16	1
4L	DLMN + O	0.75UR302 + 0.25UR303	7.2E-11	1
5L	RO$_2$301 + NO	CF(301)AP301 + CF(302)EDLM + CF(302)NO$_2$ + CF(302)HO$_2$	8.8E-13 × EXP(180.2/T)	2,a
6L	RO$_2$301 + RO$_2$T	0.7EDLM + 0.7HO2 + 0.3UR313 + RO$_2$T + O$_2$	1.82E-13 × EXP(416/T)	2
7L	RO$_2$301 + HO$_2$	EDLM + OOH1	4.1E-13 × EXP(790/T)	2
8L	RO$_2$302 + NO	CF(303)AP302 + CF(304)LMKT + CF(304)NO$_2$ + CF(304)HCHO + CF(304)HO$_2$	k_5	a
9L	RO$_2$302 + RO$_2$T	0.7LMKT + 0.7HCHO + 0.7HO$_2$ + 0.3UR314 + RO$_2$T + O$_2$	k_6	
10L	RO$_2$302 + HO$_2$	LMKT + HCHO + OOH1	k_7	
11L	RO$_2$303 + NO	0.825EDLM + 1.825NO$_2$ + 0.175AP303 + 0.175HO$_2$	k_5	
12L	RO$_2$303 + RO$_2$T	0.56EDLM + 0.56NO$_2$ + 0.265AP301 + 0.175AP303 + 0.105HO$_2$ + RO$_2$T + O$_2$	k_6	
13L	RO$_2$303 + HO$_2$	0.825EDLM + 0.825NO$_2$ + 0.175AP303 + 0.175OOH1 + 0.825OOH2	k_7	
14L	RO$_2$304 + NO	0.83LMKT + 1.83NO$_2$ + 0.83HCHO + 0.17AP304 + 0.17HO$_2$	k_5	
15L	RO$_2$304 + RO$_2$T	0.578LMKT + 0.578NO$_2$ + 0.578HCHO + 0.28AP302 + 0.142AP304 + 0.102HO$_2$ + RO$_2$T + O$_2$	k_6	
16L	RO$_2$304 + HO$_2$	0.83LMKT + 0.83NO$_2$ + 0.83HCHO + 0.17AP304 + 0.17OOH1 + 0.83OOH2	k_7	

126

Table A.5. Continued

17L	$RO_2305 + NO$	$RO_28 + 0.8EDLM + NO_2 + RO_2T$	k_5	
18L	$RO_2305 + RO_2T$	$0.48EDLM + 0.6RO_28 + 0.2UR315 + 0.2UR316 + 1.6RO_2T + O_2$	k_6	
19L	$RO_2305 + HO_2$	$RO_28 + 0.8EDLM + OOH2 + RO_2T$	k_7	
20L	$RO_2306 + NO$	$NO_2 + RO_2309 + HCHO + RO_2T$	k_5	
21L	$RO_2306 + RO_2T$	$0.1UR307 + 0.1UR315 + 0.1UR316 + 0.7\ RO_2309 + 0.7HCHO + 1.7\ RO_2T$	k_6	
22L	$RO_2306 + HO_2$	$RO_2309 + HCHO + OOH2 + RO_2T$	k_7	
23L	$RO_2307 + NO$	$CF(305)AP305 + 0.9CF(306)RO_2305 + CF(306)NO_2 + 0.9CF(306)RO_2T$	$1.05E-12 \times EXP(180.2/T)$	2,a
24L	$RO_2307 + RO_2T$	$0.9RO_2305 + 1.9RO_2T + O_2$	k_6	
25L	$RO_2307 + HO_2$	$0.9RO_2305 + 0.9RO_2T + OOH2$	k_7	
26L	$RO_2308 + NO$	$RO_28 + 0.77LMKT + NO_2 + RO_2T$	k_{23}	
27L	$RO_2308 + RO_2T$	$RO_28 + 0.77LMKT + 2RO_2T + O_2$	k_6	
28L	$RO_2308 + HO_2$	$RO_28 + 0.77LMKT + RO_2T + OOH2$	k_7	
29L	$RO_2309 + NO$	$NO_2 + CO_2 + 0.88\ RO_2307 + 0.88\ RO_2T$	$1.11E-11 \times EXP(180.2/T)$	2
30L	$RO_2309 + NO_2 + M$	PAN301	Refer to Reference	3
31L	PAN301	$RO_2309 + NO_2$	Refer to Reference	3
32L	$RO_2309 + RO_2T$	$0.3UR308 + 0.2UR309 + 0.44\ RO_2309 + 0.5CO_2 + 1.44RO_2T$	$5.0E-12$	
33L	$RO_2309 + HO_2$	$UR309 + O_2$	$4.3E-13 \times EXP(1040/T)$	2
34L	$EDLM + OH$	$RO_2310 + RO_2T$	$1.10e-10$	4
35L	$EDLM + NO_3$	$RO_2311 + RO_2T$	$2.5e-13$	4
36L	$EDLM + O_3$	$0.59RP301 + 0.09ACID + 0.41CO + 0.41H_2O + 0.5HCHO + 0.09H_2O_2 + 0.41OH + 0.41RO_2312 + 0.41RO_2T$	$8.3e-18$	4
37L	$EDLM + hv$	$CO + HO_2 + RO_2307 + RO_2T$	$=J_{ALD2}$	3

127

Table A.5. Continued

38L	$RO_2310 + NO$	CF(307)AP306 + CF(308)HCHO + CF(308)RP301 + CF(308)NO$_2$ + CF(308)HO$_2$	k_5	a
39L	$RO_2310 + RO_2T$	0.7HCHO + 0.7RP301 + 0.7HO$_2$ + 0.3UR317 + RO$_2$T + O$_2$	k_6	
40L	$RO_2310 + HO_2$	HCHO + RP301 + OOH1	k_7	
41L	$RO_2311 + NO$	0.83HCHO + 0.83RP301 + 1.83NO$_2$ + 0.17AP307 + 0.17HO$_2$	k_5	
42L	$RO_2311 + RO_2T$	0.578HCHO + 0.578RP301 + 0.578NO$_2$ + 0.28AP306 + 0.142AP307 + 0.102HO$_2$ + RO$_2$T + O$_2$	k_6	
43L	$RO_2311 + HO_2$	0.83HCHO + 0.83RP301 + 0.83NO$_2$ + 0.17AP307 + 0.17OOH1 + 0.83OOH2	k_7	
44L	$RO_2312 + NO$	RP302 + RO$_2$8 + NO$_2$ + RO$_2$T	K_{23}	
45L	$RO_2312 + RO_2T$	0.7RP302 + 0.7RO$_2$8 + 0.3UR318 + 1.7RO$_2$T + O$_2$	k_6	
46L	$RO_2312 + HO_2$	RP302 + RO$_2$8 + OOH2 + RO$_2$T	k_7	
47L	LMKT + hv	RO$_2$8 + 0.77LMKT + RO$_2$T	$=J_{KETL}$	3
48L	LMKT + OH	RO$_2$313 + RO$_2$T	1.29E-10	4
49L	LMKT + NO$_3$	RO$_2$314 + RO$_2$T	1.05E-11	4
50L	LMKT + O$_3$	0.445RO$_2$315 + 0.445CO +0.89OH + 0.055UR304 + 0.055H$_2$O$_2$ + 0.055RP301 + 0.223RO$_2$316 + 0.222 RO$_2$317 + 0.89RO$_2$T	1.50E-16	4
51L	LMKT + O	0.75UR305 + 0.25UR306	$k_{47} \times k_4 / k_1$	
52L	$RO_2313 + NO$	CF(309)AP308 + CF(310)RP301 + CF(310)HO$_2$ + CF(310)NO$_2$	k_{23}	
53L	$RO_2313 + RO_2T$	0.7RP301 + 0.7HO$_2$ + 0.3UR320 + RO$_2$T + O$_2$	k_6	
54L	$RO_2313 + HO_2$	RP301 + OOH1	k_7	
55L	$RO_2314 + NO$	0.825RP301 + 1.825NO$_2$ + 0.175HO$_2$ + 0.175AP309	k_{23}	
56L	$RO_2314 + RO_2T$	0.56RP301 + 0.56NO$_2$ + 0.265AP308 + 0.175AP309 + 0.105HO$_2$ + RO$_2$T + O$_2$	k_6	

128

Table A.5. Continued

57L	$RO_2314 + HO_2$	$0.825RP301 + 0.825NO_2 + 0.175AP309 + 0.175OOH1 + 0.825OOH2$	k_7	
58L	$RO_2315 + NO$	$CF(311)AP310 + 0.88CF(312)RO_2316 + CF(312)NO_2 + 0.88CF(312)RO_2T$	$1.24E-12 \times EXP(180.2/T)$	2,a
59L	$RO_2315 + RO_2T$	$0.53RO_2316 + 0.2UR321 + 0.2UR322 + 1.53RO_2T + O_2$	k_6	
60L	$RO_2315 + HO_2$	$0.88RO_2316 + OOH2 + 0.88RO_2T$	k_7	
61L	$RO_2316 + NO$	$NO_2 + RO_28 + RP303 + RO_2T$	k_{23}	
62L	$RO_2316 + RO_2T$	$0.6RO_28 + 0.6RP303 + 0.2UR319 + 0.2UR323 + 1.6RO_2T + O_2$	k_6	
63L	$RO_2316 + HO_2$	$RO_28 + RP303 + OOH2 + RO_2T$	k_7	
64L	$RO_2317 + NO$	$NO_2 + RO_2318 + HCHO + RO_2T$	k_{23}	
65L	$RO_2317 + RO_2T$	$0.1UR310 + 0.1UR319 + 0.1UR323 + 0.7 RO_2318 + 0.7HCHO + 1.7 RO_2T + O_2$	k_6	
66L	$RO_2317 + HO_2$	$HCHO + RO_2318 + RO_2T + OOH2$	k_7	
67L	$RO_2318 + NO$	$0.875 RO_2315 + NO_2 + CO_2 + 0.875RO_2T$	$1.11E-11 \times EXP(180.2/T)$	2
68L	$RO_2318 + NO_2$	PAN302	Refer to Reference	3
69L	PAN	$RO_2318 + NO_2$	Refer to Reference	3
70L	$RO_2318 + RO_2T$	$0.3UR311 + 0.2UR312 + 0.4375 RO_2315 + 0.5CO_2 + 1.4375 RO_2T$	k_{32}	2
71L	$RO_2318 + HO_2$	$UR312 + O_2$	k_{33}	2
72L	AP301 + OH	$EDLM + NO_2 + H_2O$	6.00E-11	5
73L	AP302 + OH	$LMKT + HCHO + NO_2 + H_2O$	9.26E-11	5
74L	AP303 + OH	$RO_2307 + NO_2 + H_2O + RO_2T$	6.05E-11	5
75L	AP304 + OH	$LMKT + CO_2 + NO_2 + H2O$	1.07E-10	5
76L	AP305 + OH	$0.9EDLM + NO_2 + H_2O$	5.49E-11	5
77L	AP306 + OH	$RP301 + HCHO + NO_2 + H_2O$	2.63E-11	5
78L	AP307 + OH	$RP303 + CO_2 + NO_2 + H_2O$	3.25E-11	5
79L	AP308 + OH	$RP303 + NO_2 + H_2O$	8.10E-12	5
80L	AP309 + OH	$RO_2315 + NO_2 + H_2O + RO_2T$	9.30E-12	5

129

Table A.5. Continued

81L	AP310 + OH	$0.88RP301 + NO_2 + H_2O$	3.74E-12	5
82L	RP301 + OH	$0.1UR304 + 0.1O_3 + 0.8HO_2 + 0.8RP301 + 0.9CO_2 + NO_2 - NO$	2.72E-11	5
83L	RP302 + OH	$0.1UR324 + 0.1O_3 + 0.8HO_2 + 0.77RP302 + 0.9CO_2 + NO_2 - NO$	2.94E-11	5
84L	RP303 + OH	$0.1UR324 + 0.1O_3 + 0.8HO_2 + 0.77RP303 + 0.9CO_2 + NO_2 - NO$	4.65E-11	5

[a]CF(301) – CF(312) are calculated based on Arey et al. (2001); [b]Rate constant references: 1. Atkinson (1997); 2. Jenkin et al. (1997); 3. Griffin et al. (2002a); 4. Calogirou et al. (1999); 5. Kwok and Atkinson (1995).

130

Table A.6. Chemical species in the d-limonene oxidation mechanism.

Term	Description
	Reactive, fully integrated species
DLMN	d-limonene
EDLM	limonaldehyde (3-isopropenyl-6-keto-heptanal)
LMKT	limona ketone (1-methyl-4-acetyl-hexene)
AP301	1-methyl-1-nitrato-2-hydroxy-4-isopropenyl-cyclohexane
AP302	1-methyl-4-(1-methyl-1-nitrato-2-hydroxy-ethyl)-cyclohexene
AP303	1-methyl-1-nitrato-2-keto-4-isopropenyl-cyclohexane
AP304	2-methyl-2-nitrato-2-(4-methyl-4-cyclohexenyl)-acetaldehyde
AP305	2-isopropenyl-5-keto-hexylnitrate
AP306	1-hydroxy-2-methyl-2-nitrato-3-formylmethyl-6-keto-heptane
AP307	2-methyl-2-nitrato-3-formylmethyl-6-keto-heptanal
AP308	1-methyl-1-nitrato-2-hydroxy-4-acetyl-cyclohexane
AP309	1-methyl-1-nitrato-2-keto-4-acetyl-cyclohexane
AP310	2-acetyl-5-keto-hexylnitrate
RP301	keto-limonaldehyde (3-acetyl-6-keto-heptanal)
RP302	3,6-dioxo-heptanal
RP303	3-acetyl-pentadial
PAN301	peroxy 5-formyl-4-isopropenyl-pentionyl nitrate
PAN302	peroxy 5-formyl-4-acetyl-pentionyl nitrate
	Nonreactive, fully integrated organic species
UR301	limononic acid
UR302	1-methyl-4-isopropenyl-1,2-cyclohexane-epoxide
UR303	3-isopropenyl-6-methyl-cyclohexanone
UR304	keto-limononic acid
UR305	1-methyl-4-acetyl-1,2-cyclohexane-epoxide
UR306	3-acetyl-6-methyl-cyclohexanone
UR307	7-hydroxy-limononic acid
UR308	limonalic acid
UR309	limonic acid
UR310	7-hydroxy-keto-limononic acid
UR311	keto-limonalic acid
UR312	keto-limonic acid
UR313	1-methyl-1,2-dihydroxy-4-isopropenyl-cyclohexane
UR314	1-methyl-4-(1-methyl-1,2-dihydroxy-ethyl)-cyclohexene
UR315	5-keto-limonaldehyde
UR316	5-hydroxy-limonaldehyde
UR317	3-(1-methyl-1,2-dihydroxy-ethyl)-6-keto-heptanal
UR318	3-acetyl-3-hydroxy-6-keto-heptanal
UR319	3-acetyl-5-hydroxy-6-keto-heptanal
UR320	1-methyl-1,2-dihydroxy-4-acetyl-cyclohexane
UR321	3-hydroxymethyl-2,6-heptanedione
UR322	3-formyl-2,6-heptanedione

131

Table A.6. Continued

UR323	3-acetyl-5,6-dioxo-heptanal
UR324	3-acetyl-4-formyl-butanoic acid
Reactive, organic pseudo-steady state species
RO_2301	cyclic hydroxy alkenyl peroxy radical from oxidation of d-limonene (C_6 cycle, 1-methyl, 1-peroxy, 2-hydroxy, 4-isopropenyl)
RO_2302	cyclic hydoxy alkenyl peroxy radical from oxidation of d-limonene (C_6 cycle, 1-methyl, 1-ene, 4-(1-methyl-2-hydroxy-1-ethyl peroxy))
RO_2303	cyclic nitrato alkenyl peroxy radical from oxidation of d-limonene (65% is C_6 cycle, 1-methyl, 1-peroxy, 2-nitrato, 4-isopropenyl; 35% is C_6 cycle, 1-methyl, 1-nitrato, 2-peroxy, 4-isopropenyl)
RO_2304	cyclic nitrato alkenyl peroxy radical from oxidation of d-limonene (80% is C_6 cycle, 1-methyl, 1-ene, 4-(1-methyl-2-nitrato-1-ethyl peroxy); 20% is C_6 cycle, 1-methyl, 1-ene, 4-(1-methyl-1-nitrato-2-ethyl peroxy))
RO_2305	keto alkenyl aldehydic peroxy radical from oxidation of d-limonene (C_7 chain, 3-isopropenyl, 5-peroxy, 6-keto)
RO_2306	keto alkenyl aldehydic peroxy radical from oxidation of d-limonene (C_7 chain, 3-isopropenyl, 6-keto, 7-peroxy)
RO_2307	keto alkenyl peroxy radical from oxidation of d-limonene (C_6 chain, 1-peroxy, 2-isopropenyl, 5-keto)
RO_2308	cyclic alkenyl peroxy radical from oxidation of d-limonene (C_6 cycle, 1-methyl, 1-ene, 4-peroxy, 4-acetyl)
RO_2309	acyl radical from decomposition of RO_2306
RO_2310	keto hydroxy alkyl peroxy radical from oxidation of limonaldehyde (C_7 chain, 1-hydroxy, 2-peroxy, 2-methyl,3-formylmethyl, 6-keto)
RO_2311	keto nitrato alkyl peroxy radical from oxidation of limonaldehyde (80% C_7 chain, 1-nitrato, 2-peroxy, 2-methyl, 3-formylmethyl, 6-keto 20% C_7 chain, 1-peroxy, 2-nitrato, 2-methyl, 3-formylmethyl, 6-keto)
RO_2312	keto aldehydic peroxy radical from oxidation of limonaldehyde (C_7 chain, 3-peroxy, 3-acetyl, 6-keto)
RO_2313	cyclic hydroxy alkyl peroxy radical from oxidation of limona ketone (C_6 cycle, 1-methyl, 1-peroxy, 2-hydroxy, 4-acetyl)
RO_2314	cyclic nitrato alkyl peroxy radical from oxidation of limona ketone (65% C_6 cycle, 1-methyl, 1-peroxy, 2-nitrato, 4-acetyl; 35% C_6 cycle, 1-methyl, 1-nitrato, 2-peroxy, 4-acetyl)
RO_2315	keto alkyl peroxy radical from oxidation of limona ketone (C_6 chain, 1-peroxy, 2-acetyl, 5-keto)
RO_2316	keto aldehydic peroxy radical from oxidation of limona ketone (C_7 chain, 3-acetyl, 5-peroxy, 6-keto)
RO_2317	keto aldehydic peroxy radical from oxidation of limona ketone (C_7 chain, 3-acetyl, 6-keto, 7-peroxy)
RO_2318	acyl radical from decomposition of RO_2317

132

APPENDIX B

LIST OF ACRONYMS

AI:	Appledore Island
AMS:	Aerosol Mass Spectrometer
AqChem:	Aqueous-phase Chemistry Mechanism
BEIS:	Biogenic Emission Inventory System
CACM:	Caltech Atmospheric Chemistry Mechanism
CB-IV:	Carbon Bond – IV
CMAQ:	Community Multi-scale Air Quality Model
EC:	Elemental Carbon
EPA:	Environmental Protection Agency
HO_2:	Hydroperoxy radical
ICARTT:	International Consortium for Atmospheric Research on Transport and Transformation
IMPROVE:	Interagency Monitoring of Protected Visual Environment
KPP:	Kinetic Pre-Processor
MCM:	Master Chemical Mechanism
MNB:	Mean Normalized Bias
MNGE:	Mean Normalized Gross Error
MPMPO:	Model to Predict the Multiphase Partitioning of Organics
OA:	Organic Aerosol
OM:	Organic Matter

133

PILS:	Particle-into-liquid Sampler
PM:	Particulate Matter
POA:	Primary Organic Aerosol
RO_2:	Peroxy Radicals
SEARCH:	Southeastern Aerosol Research Characterization Study
SMOKE:	Sparse Matrix Operator Kernel Emissions
SOA:	Secondary Organic Aerosol
SoCAB:	South Coast Air Basin of California
SORGAM:	Secondary Organic Aerosol Model
SVOCs:	Semi-volatile Organic Compounds
TF:	Thompson Farm
VOCs:	Volatile Organic Compounds

134